

AD 72 6551

AD 72 6551

CSOL
R-655

DEVELOPMENT OF A MERCURY TILTMETER FOR SEISMIC RECORDING

Final Report on Design, Construction, and Installation
of an M. I. T. Tiltmeter at a Low Noise Site
July 1969 through March 1970

by

Seldon W. Buck, Frank Press, Dudley Shepard,
M. Nuri Toksoz, and Henry Trautham, Jr.

March 1971

Sponsored By
Advanced Research Projects Agency
ARPA Order No. 1481

NATIONAL TECHNICAL
INFORMATION SERVICE

Massachusetts Institute of Technology
Cambridge, Massachusetts 02139

Approved for public release
distribution unlimited.

D D C
RECEIVED
JUN 30 1971
RECEIVED

**BEST
AVAILABLE COPY**

UNCLASSIFIED

Security Classification

DOCUMENT CONTROL DATA - R & D

(Security classification of title, body of abstract and indexing annotation must be entered when the overall report is classified)

ORIGINATING ACTIVITY (Corporate author)

Massachusetts Institute of Technology
Cambridge, MA 02139

2a. REPORT SECURITY CLASSIFICATION

UNCLASSIFIED

2b. GROUP

3. REPORT TITLE

Development of a Mercury Tiltmeter for Seismic Recording

4. DESCRIPTIVE NOTES (Type of report and inclusive dates)

Scientific.....Final

5. AUTHOR(S) (First name, middle initial, last name)

Sheldon W. Buck, Frank Press, Dudley Shepard, M. Nafi Toksoz, and Hentry Trantham, Jr.

6. REPORT DATE

March 1971

7a. TOTAL NO. OF PAGES

126

7b. NO. OF REFS

0

8a. CONTRACT OR GRANT NO

F44620-69-C-0126

b. PROJECT NO.

9555

c.

62701D

d.

9a. ORIGINATOR'S REPORT NUMBER(S)

9b. OTHER REPORT NO(S) (Any other numbers that may be assigned this report)

AFOSR-TR-71-1826

10. DISTRIBUTION STATEMENT

Approved for public release; distribution unlimited.

11. SUPPLEMENTARY NOTES

TECH, OTHER

12. SPONSORING MILITARY ACTIVITY

AF Office of Scientific Research (NPG)
1400 Wilson Boulevard
Arlington, VA 22209

13. ABSTRACT

A seismic tiltmeter has been designed in a joint effort between the Charles Stark Draper Laboratory Division of MIT and the MIT Department of Earth and Planetary Sciences. A pair of ninety-foot mercury pendulums were constructed and installed in a low noise site near Eilat, Israel. (Specifications include @ a gap of 0.012"):

Length	- 27.4 meters
Natural (undamped) period	- 131 seconds
Damping Ratio	- 0.9
Tiltmeter Output @ DC	- 2.2 volt/micro radian
Sensitivity (OdB S/N Ratio)	- 3×10^{-11} radian

Department of Earth and Planetary Sciences
Massachusetts Institute of Technology
Cambridge, Massachusetts 02139

in collaboration with

Charles Stark Draper Laboratory
A Division of Massachusetts Institute of Technology
Cambridge, Massachusetts 02139

DEVELOPMENT OF A MERCURY TILTMETER FOR SEISMIC RECORDING

Final Report on Design, Construction, and Installation
of an M.I.T. Tiltmeter at a Low Noise Site
July 1969 through March 1970

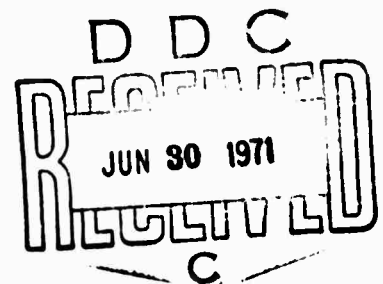
by

Sheldon W. Buck[†]
Frank Press*
Dudley Shepard[†]
M. Nafi Toksöz*
Henry Trantham, Jr.[†]

ARPA Order No. 1484
Project Code No. 9F10
Name of Contractor—M.I.T.
Date of Contract—1 July 1969
Contract Expiration Date—15 March 1971
Amount of Contract—\$90,000
Contract No. F 44620-69-C-0126
Principal Investigator—Frank Press, 617-864-6900, ext. 3382
Project Engineer—Sheldon W. Buck, 617-864-6900, ext. 821-531
Short Title of Work—Development of Mercury Tiltmeter

*Department of Earth and Planetary Sciences

[†]Charles Stark Draper Laboratory



ACKNOWLEDGMENT

This research was supported by the Advanced Research Projects Agency of the Department of Defense and was monitored by the Air Force Office of Scientific Research under Contract No. F44620-69-C-0126.

For their assistance, the following persons merit the Institute's appreciation. Professor C. L. Pekeris, Director of the Department of Applied Mathematics, at the Weizmann Institute of Science for his cooperation and use of the tunnels at the Weizmann Geophysical Observatory near Eilat, Israel and also to Professor Ari Ben-Menahem.

Dr. Hans Jarosch of the Weizmann Institute for his personal attention and assistance during the installation phase of this program.

Micha Cohen and Udi Schmir of Eilat, Israel for their helpful skills and eight weeks effort during the final assembly and installation of these underground instruments.

At MIT, particular credit must be given to Mr. George Keough, of the Seismology Laboratory of the Earth and Planetary Sciences Department, who was responsible for all electronic packaging design, circuit construction, electronic systems testing, and without whom these instruments would never have been assembled and installed.

R-655

DEVELOPMENT OF A MERCURY TILTMETER FOR SEISMIC RECORDING

Final Report on Design, Construction, and Installation of an MIT
Tiltmeter at a Low Noise Site - July 1969 through March 1970

ABSTRACT

A seismic tiltmeter has been designed in a joint effort between the Charles Stark Draper Laboratory Division of MIT and the MIT Department of Earth and Planetary Sciences. A pair of ninety-foot mercury pendulums were constructed and installed in a low noise site near Eilat, Israel. Specifications include (@ a gap of 0.012"):

Length	- 27.4 meters
Natural (undamped) Period	- 131 seconds
Damping Ratio	- 0.9
Tiltmeter Output @ DC	- 2.2 volt/micro radian
Sensitivity (0dB S/N Ratio)	- 3×10^{-11} radian

by Sheldon Buck
March, 1971

TABLE OF CONTENTS

<u>Chapter</u>		<u>Page</u>
1	INTRODUCTION	1
2	TILTMETER DESCRIPTION	2
3	RECORDING INSTRUMENTATION DESCRIPTION.	13
4	INSTALLATION.	19
5	PRELIMINARY PERFORMANCE	39
<u>APPENDICES</u>		
A-1	Adjustable and Fixed End Tank Design	43
A-2	Theoretical Response	45
A-3	Mechanical Drawings and List	57
B-1	Tiltmeter High-frequency Circuits	65
B-2	Special Electronics for the 4-mil Tiltmeter	71
B-3	Operation of Diode Ring Demodulator	81
B-4	Certain Nonlinearities and Errors in a Capacitive Bridge Tiltmeter	85
B-5	Study of Linearity Versus Capacitor Gap	91
B-6	Linearity Tests on 4-mil Tiltmeter Electronics	95
B-7	Circuit Diagrams.	111

LIST OF ILLUSTRATIONS

<u>Figure</u>		<u>Page</u>
2-1	MIT DL tiltmeter.	8
2-2	Block diagram — bridge electronics	9
2-3	Tiltmeter mechanical responses	10
2-4	Tilt mechanical gain	11
2-5	Displacement mechanical gain	12
3-1	MIT seismic station.	15
3-2	Data channel filters	16
3-3	Differential temperature bridge calibration	17
4-1	Plan of the Geophysical Observatory	22
4-2	Analog recording consoles.	23
4-3	Tiltmeter showing mercury lines.	24
4-4	Fixed end tank	25
4-5	Adjustable end tank	26
4-6	Electronic boxes	27
4-7	Bridge electronics — alignment panel.	28
4-8	Bridge electronics — differential capacitance	29
4-9	Oscillator, power supply, and differential temperature	30
4-10	Filter networks — offset trims.	31
4-11	Filter networks — control panel	32
4-12	Filter networks — tidal low pass filter	33
4-13	Filter networks — surface band pass filter	34
4-14	Filter networks — eigen low pass filter	35
4-15	Filter networks — eigen high pass filter	36
4-16	Tiltmeter installation with shields removed	37
5-1	Surface wave records.	40

<u>Figure</u>		<u>Page</u>
A. 2-1	Tiltmeter mechanical model.	46
A. 2-2	Oil-filled capacitor.	51
A. 2-3	Root locus plot.	54
A. 3-1	Seismic tiltmeter — Mod II — installation.	61
A. 3-2	Seismic tiltmeter — Mod II — layout	62
A. 3-3	Mercury chamber-fixed seismic tiltmeter — Mod II	63
A. 3-4	Mercury chamber-adjustable seismic tiltmeter — Mod II.	64
B. 1-1	Tiltmeter high-frequency circuits	65
B. 1-2	Current amplifier	66
B. 1-3	Demodulator.	68
B. 1-4	Capacitance bridge	69
B. 2-1	Differential capacitance bridge	72
B. 2-2	Current amplifier	74
B. 2-3	Signal amplifier	77
B. 2-4	AC reference amplifier.	78
B. 3-1(a)	Demodulator.	82
B. 3-1(b)	Demodulator.	82
B. 3-1(c)	Demodulator.	83
B. 3-1(d)	Demodulator.	83
B. 4-1	Capacitive bridge tiltmeter	85
B. 4-2	Bridge transformer	85
B. 5-1	Bridge output versus gap	93
B. 6-1	Test block diagram.	95
B. 6-2(a)	Bridge output	98
B. 6-2(b)	Bridge output	99
B. 6-2(c)	Bridge output	100
B. 6-2(d)	Bridge output	101
B. 6-2(e)	Bridge output	102
B. 6-2(f)	Bridge output	103
B. 6-3	System linearity test diagram	104
B. 6-4(a)	Linearity test bridge electronics.	105
B. 6-4(b)	Linearity test bridge electronics.	106
B. 6-4(c)	Linearity test bridge electronics.	107

<u>Figure</u>	<u>Page</u>
B. 6-4(d) Linearity test bridge electronics	108
B. 6-4(e) Linearity test bridge electronics	109
 B. 7-1 MIT seismic station.	 112
B. 7-2 System op-amps	113
B. 7-3 Mercury tiltmeter bridge electronics	114
B. 7-4 Bridge electronics — layout	115
B. 7-5 Eigen filter	116
B. 7-6 Eigen high pass — layout	117
B. 7-7 Eigen low pass -- layout	118
B. 7-8 Surface wave filter	119
B. 7-9 Surface wave filter — layout	120
B. 7-10 Surface wave filter — line driver	121
B. 7-11 Tidal filter.	122
B. 7-12 Tidal filter — layout	123
B. 7-13 Greenray crystal oscillator	124
B. 7-14 Differential thermometer — schematic	125
B. 7-15 Differential thermometer—layout	126

CHAPTER 1

INTRODUCTION

A seismic tiltmeter has been designed in a joint effort of the Charles Stark Draper Laboratory Division of MIT and the MIT Department of Earth and Planetary Sciences. The purpose was to redesign the Benioff tiltmeter¹ to exploit its capability more fully. The primary design goal was to decrease the tiltmeter sensitivity to temperature and pressure changes.

Initial operation of a pair of nineteen (19) foot mercury pendulums at a seismically-noisy location outside of Boston² showed the ability of the first MIT seismic tiltmeters to detect long-period waves from relatively small-magnitude earthquakes.

It was felt that a more sensitive version operated at a low-noise site, could open up opportunities for important contributions in seismological research. The spectral content in the range 50-100s of surface waves from small-magnitude events could be studied, and used to explore the source mechanism of earthquakes and explosions. Mantle surface waves and eigenvibrations from the more numerous small events could be used to improve precision in determining the relative amplitude and frequency of the earth's eigenvibrations. Long-period surface tilts corresponding to atmospheric and ocean loading, tectonic strain accumulation and release could be explored.

A second pair of tiltmeters (90-foot version) were constructed and installed at a low-noise site 500 feet inside a granite mountain near Eilat, Israel. A geophysical observatory had been constructed at this location by the Department of Applied Mathematics of the Weizmann Institute of Science of Rehovot, Israel. Professor C. L. Pekeris, Director of the department, agreed to the installation of the new instruments. The tiltmeters are installed in 100-foot trenches in two orthogonal 120-foot vaults located at the far end of a 500-foot tunnel.

These instruments were designed with capacitor gaps of 0.004 inches (0.1 mm), or about one-tenth the gap used in the first set of tiltmeters. This reduction in gap yielded the expected increase in sensitivity. However, an unanticipated degradation in frequency response occurred. This will be corrected by

widening the gap threefold. This change can be accomplished without loss of sensitivity since the gain can be recovered electronically.

At present, three output channels are producing data as follows:

1. Surface wave band, 16-120 seconds.
2. Mantle surface wave, eigenvibration band,
32-7200 seconds.
3. Permanent tilt and tidal band, 300 seconds to dc.

CHAPTER 2

TILTMETER DESCRIPTION

General

Referring to Fig. 2-1, we can see that, like the seismic tiltmeter designed by Hugo Benioff and William Giles of the Seismological Laboratory of California Institute of Technology, the MIT mercury pendulum is formed by two end tanks at opposite ends of the instrument and a connecting tube filled with mercury. An air line filled with dry nitrogen is used to equalize the pressure over the mercury. A differential-capacitance bridge with a capacitor plate over the mercury pool in each end tank forms a differential mercury-level transducer while rejecting common-mode changes in mercury level. An inert, stable transformer oil fills the gap between the mercury pool surface and both the fixed and adjustable capacitor plates. Besides providing additional protection against mercury oxidation, the oil prevents the mercury from wetting and, hence, sticking to a capacitor plate in case of accidental contact during assembly, adjustment, or instrument saturation due to very large nearby earthquakes. Recovery from these disturbances is immediate, except for the filter response. A second purpose of the insulating oil is to increase the dielectric constant in the capacitor gap; thereby greatly increasing the ratio between the transducers' capacitance and the line capacitance of the 44-foot-long, 2-1/2 inch OD coaxial cable. The 1/4-inch ID connecting tube is made of butyrate in order to approximately match the thermal coefficient of expansion of mercury and to provide a clear, transparent path between end tanks for checking the presence of dirt or gas bubbles. The end tank structures are made of quartz for insulation and mechanical stability. A differential screw-adjustment mechanism on one end tank permits equalization of the capacitor plate gaps. The end tanks rest on a three-point, non-redundant, strain-free base which prevents both stress and tilting of the end tanks due to differential thermal expansion between the pier and end tank.

The relative plate gaps of the end tank capacitors are detected by a differential capacitance bridge. The scale factor change normally caused by a common-mode gap change has been nearly eliminated by using a current source, instead of the original voltage source, to excite the capacitance bridge. A block-diagram of the bridge electronics is shown in Fig. 2-2. A 300-kHz crystal oscillator provides

the ac reference for the current amplifier driving the bridge transformer. A bridge transformer steps up the voltage from the current amplifier 10:1. One pair of secondaries forms two arms of an ac bridge circuit. The other two arms of the ac bridge are the capacitors of the adjustable and fixed end tanks, shunted by the capacity of the coaxial line. An auxiliary winding on the bridge transformer provides quadrature correction. The output of the ac bridge is amplified by an ac preamp having a feedback circuit tuned to the crystal oscillator for noise reduction. Amplified ac signals are converted to bipolar dc signals by a phase-sensitive demodulator which obtains its reference from the primary of the bridge transformer. The phase-sensitive (diode ring) demodulator will rectify only signals coherent with the reference signal, thereby eliminating stray ac pickup. The dc signal is filtered and passed through a signal-conditioning amplifier for gain normalization and low output impedance. Two of these signal-conditioning amplifiers were used so that the bridge output could be monitored without disturbing the seismic and tidal filter networks connected to the primary output. Since the tiltmeter constitutes an open-loop system, all components must have high precision and stability, and all amplifiers must have negative feedback, for both gain stability and linearity. For a more detailed discussion of the linearity of the differential capacitance bridge, refer to Appendix B.6. For linearity of the mercury pendulum, see Appendix A.2.

Sensitivity

The theoretical deadband of the mercury tiltmeter is zero, equivalent to infinite tilt sensitivity. Useable sensitivity, however, is limited by site noise and the electronic signal-to-noise ratios at the recorder outputs. Assuming zero site noise, at a S/N ratio of 1:1 (0 dB), the tilt sensitivities of the three channels are:

Surface wave	(16- 120 seconds)	$\sim 3 \times 10^{-''}$ radians
Eigenperiod	(32-7200 seconds)	$\sim 3 \times 10^{-''}$ radians
Tidal	(dc- 300 seconds)	$< 1 \times 10^{-''}$ radians

Tiltmeter Response

Appendix A.2 is a detailed analysis of the tiltmeter system response to two independent ground-motion variables: absolute tilt (θ_0) and absolute horizontal displacement (X_0). Tiltmeters prior to the one described here have all been operated with large capacitor gaps ($H \geq 40$ mil), and have conformed to a simple second-order dynamic model. After installation of the Israel tiltmeter ($H = 4$ mil), it became apparent that the response was not as predicted. A subsequent lengthy and detailed analysis of the system dynamics, taking into account the mercury /oil/ capacitor plate interactions (Appendix A.2), accurately predicts the observed response. The two tiltmeter responses are:

$$\text{TILT} \quad \frac{z_o}{\frac{l}{2} \theta_o} = \frac{-1}{(j\omega\tau + 1) \left[1 + j 2 \zeta \frac{\omega}{\omega_n} - \left(\frac{\omega}{\omega_n} \right)^2 \right]} \quad 2.1$$

$$\text{HORIZONTAL DISPLACEMENT} \quad \frac{y_o}{X_o} = \frac{\frac{3a}{4A} \left(\frac{\omega}{\omega_n} \right)^2}{(j\omega\tau + 1) \left[1 + j 2 \zeta \frac{\omega}{\omega_n} - \left(\frac{\omega}{\omega_n} \right)^2 \right]} \quad 2.2$$

where:

- z_o = capacitor gap change (linear with bridge output)
- X_o = absolute horizontal displacement
- θ_o = absolute tilt
- A = reservoir cross-sectional area
- a = mercury tube cross-sectional area
- l = total tiltmeter length
- ζ = damping ratio
- $\tau \approx 1.75 \times 10^{-4} \text{ H}^{-3}$ for gap $H > 3 \times 10^{-2} \text{ cm}$
- ω_n = tiltmeter natural frequency

These responses differ from previous models in the term involving τ , a time constant associated with the mercury/oil subsystem. The two amplitude-response functions are plotted in Fig. 2-3 for three different values of gap H : 0.004", 0.012", and ∞ . From Eq 2.1 and 2.2, we see that, as the gap H is increased, the transfer function degenerates into the accustomed second order form. Values of τ , ζ , and ω_n for differing gaps, H , are given in Table II-1.

H (in.)	ζ	τ (s)	$f_b = \frac{1}{2\pi\tau}$ (Hz)	ω_n ($\frac{\text{rad}}{\text{s}}$)	$f_n = \frac{\omega_n}{2\pi}$ (Hz)
0	0.35	∞	0	0.061	0.00971
0.004	0.68	348	0.00046	0.073	0.0117
0.012	0.9	7.5	0.0213	0.048	0.00765
0.040	0.7	0.175	0.90	0.043	0.00684
∞	0.7	0	∞	0.043	0.00685

The effect of τ is easily seen from the plots of Fig. 2-3. At small values of H , the time constant τ becomes large enough to affect the dynamic response in the region of interest. The response becomes third-order with the introduction of a breakpoint, and first-order rolloff at $f_b = \frac{1}{2\pi\tau}$, in addition to the usual second-order break at $f_n = \frac{\omega_n}{2\pi}$.

At a gap H of 0.004 in., both the tilt and displacement responses are down > 20 dB ($\div 10$) in the region 0.01 - 1 Hz. In addition, the response becomes increasingly sensitive to common-mode changes in H . This is clearly undesirable in terms of instrument gain. From dynamic-response considerations alone, a gap of $H = \infty$ would seem to be the ideal. However, both bridge sensitivity and bridge linearity are inverse functions of H . In view of all effects, the gap is being lowered to what seems a best compromise, 0.012 in.

Mechanical Gain

Mechanical gain is an expression of recorder pen motion versus input ground motion. A tiltmeter responds to two independent ground-motion variables, absolute tilt (θ_0) and absolute horizontal displacement (X_0). We must therefore, define two mechanical gains: tilt gain (in./rad) and displacement gain (in./in.).

The mechanical gains in each data channel are found by the product:

$$\text{tiltmeter response} \times \text{filter response} \times \text{recorder scale factor}$$

The tiltmeter responses are shown in normalized form in Fig. 2-3.

The un-normalized responses for any specific gap, H , are determined by assigning a precise number to a single point on the curves. This is easily and precisely done by introducing a known tilt through the adjustable end tank and observing the steadystate bridge output change. For the Israel tiltmeter, this number has been determined as 6.67 volt/microradian @ $H = 0.004$ in. The mechanical gain figures given below assume this figure. For different values of H , the tiltmeter scale factor changes, but it is assumed that this change will be balanced by a complementary recorder scale-factor change.

The data channel filter responses and recorder scale factors are described in more detail in Chapter 3. The filter amplitude responses are given in Fig. 3-2.

Tilt Gain

Tilt mechanical gain is shown in Fig. 2-4. The most serious degradation due to the 4-mil gap is in the surface wave channel where response is down ~ 18 dB from the ideal throughout the band. The eigenresponse is down approximately 3 dB ($\times 0.7$) at an 18-minute period. The tidal band is not seriously affected. By

increasing the gap to 0.012 in. , we approach the ideal to within 2 dB($\times 0.8$) over all regions of interest.

Displacement Gain

Displacement mechanical gain is shown in Fig. 2-5. The percentage degradations in the various frequency bands are identical to those in tilt gain. This is a result of the identical tilt and displacement transfer function denominators. One significant improvement which would result from opening the gap to > 0.012 in. would be a flatter amplitude response in the surface wave band of 16 - 120 seconds.

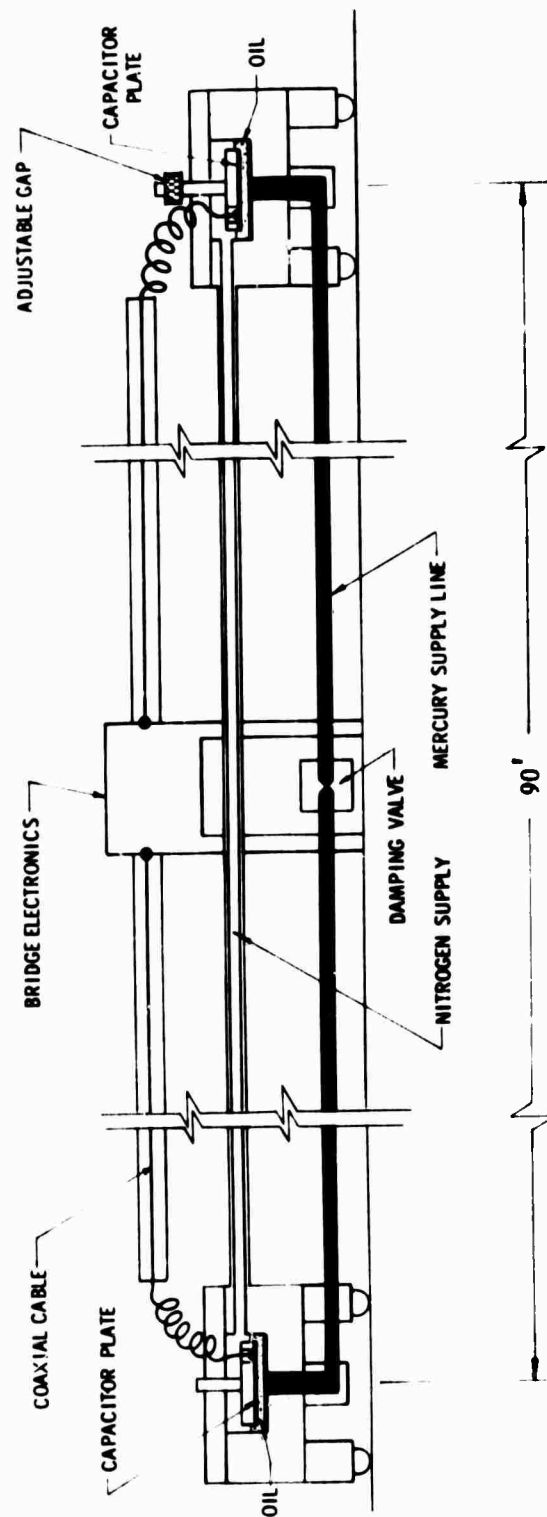


Fig. 2-1 MIT/DL tiltmeter.

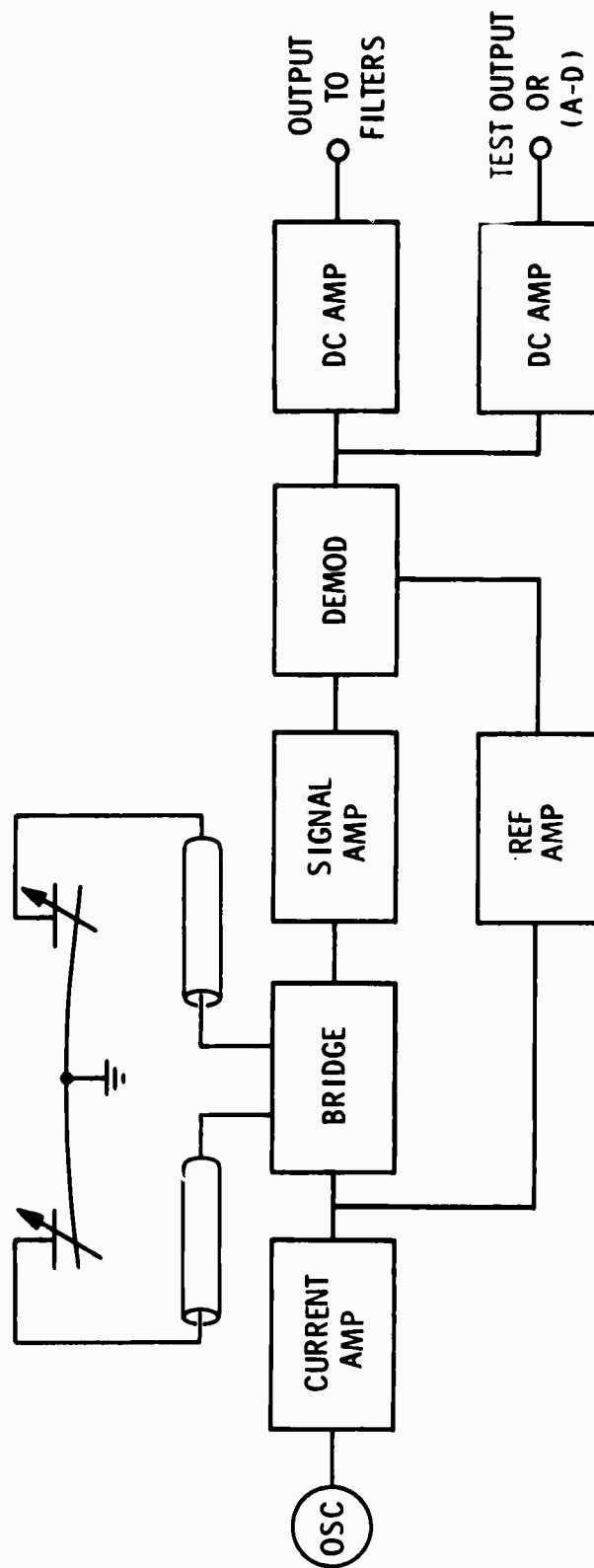


Fig. 2-2 Block diagram -- bridge electronics.

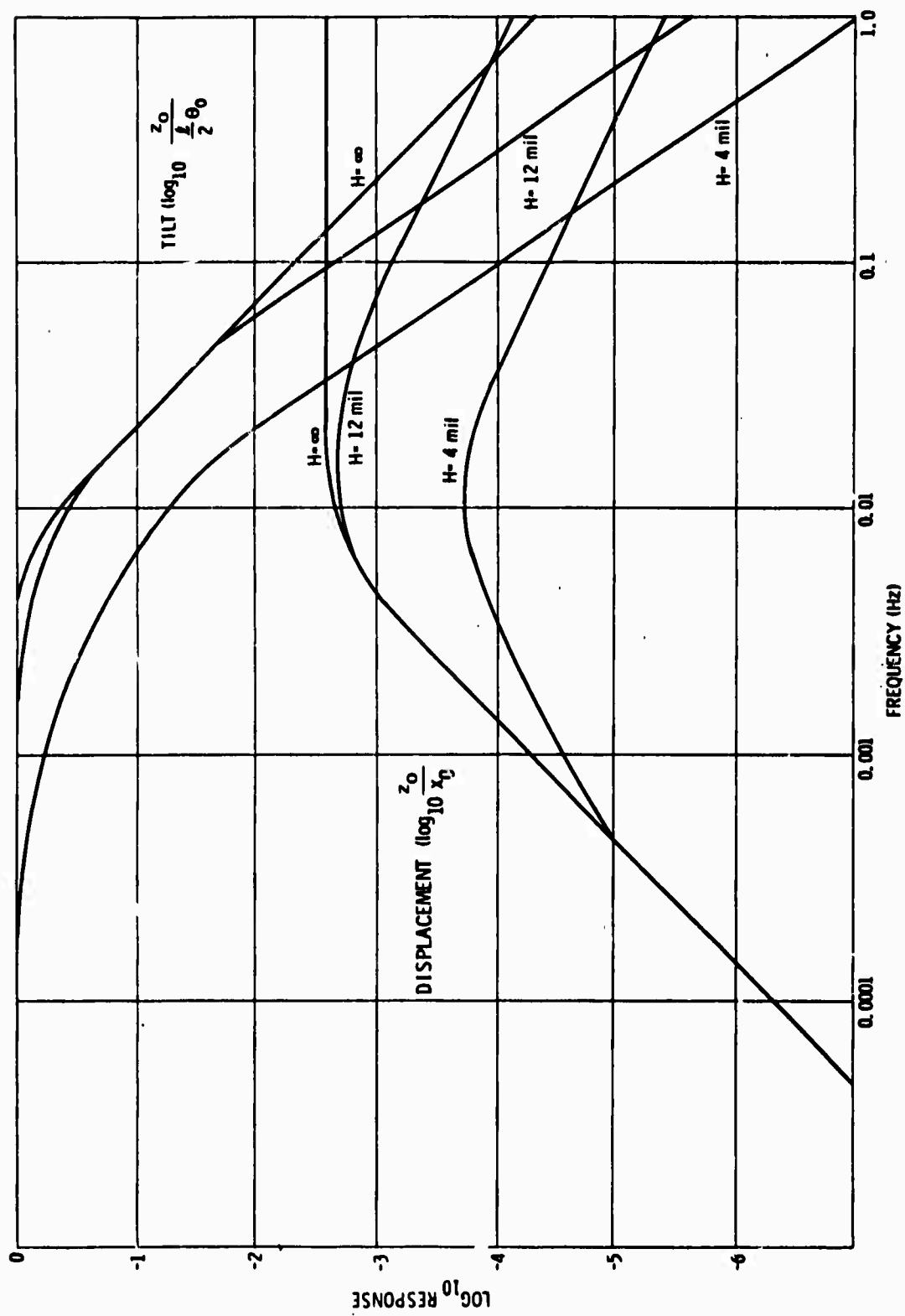


Fig. 2-3 Tiltmeter mechanical responses.

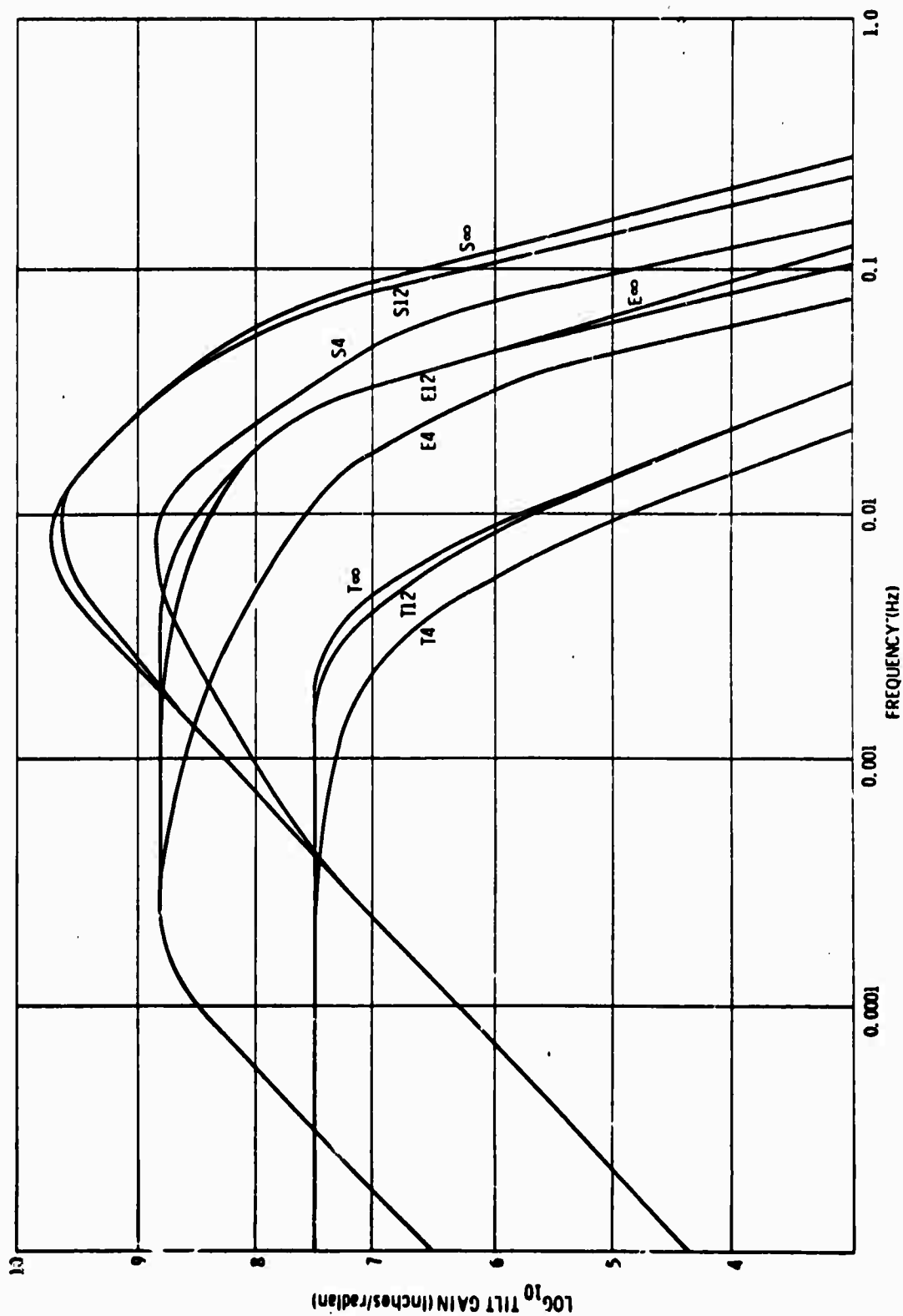


Fig. 2-4 Tilt mechanical gain.

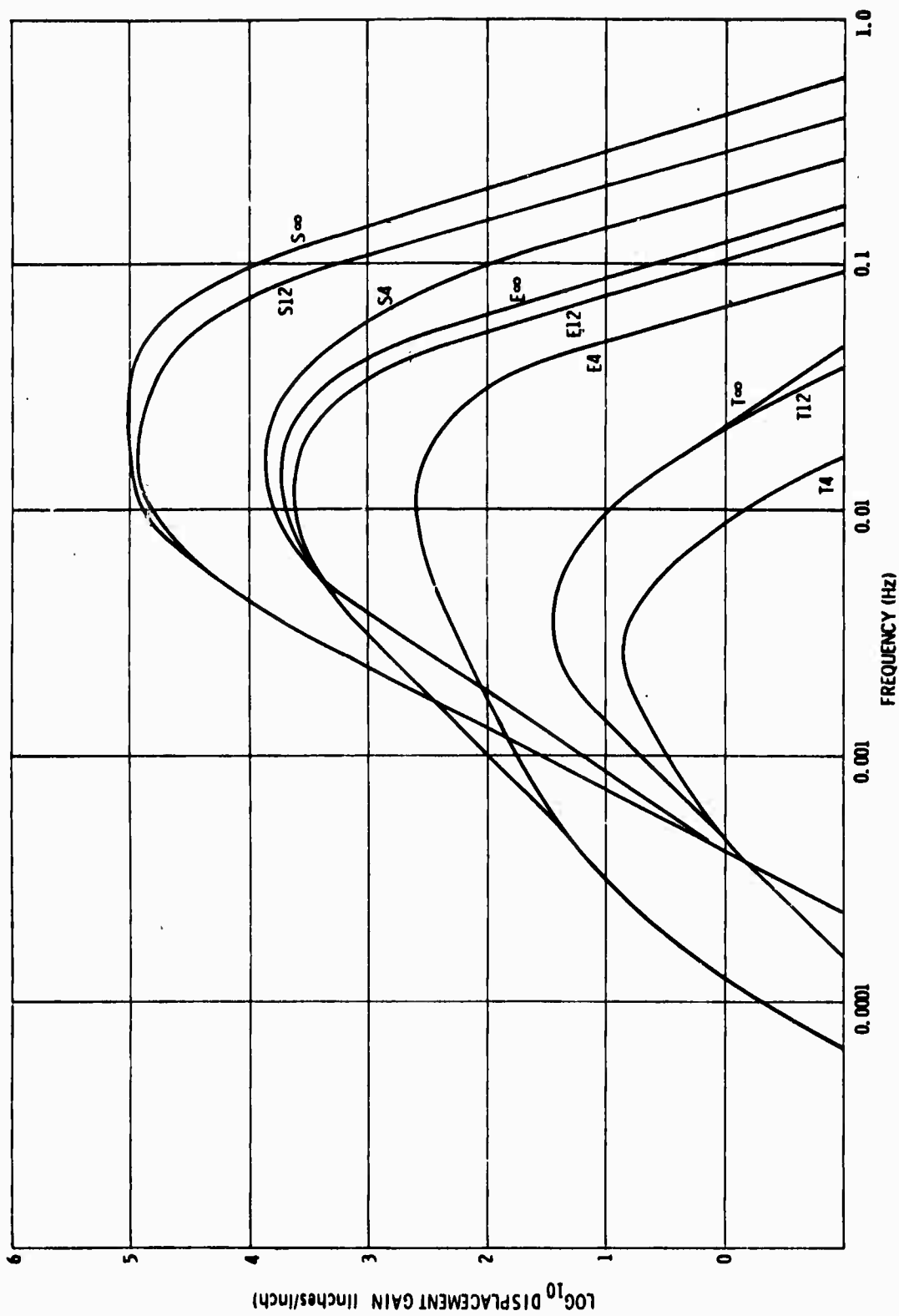


Fig. 2-5 Displacement mechanical gain.

CHAPTER 3

RECORDING INSTRUMENTATION DESCRIPTION

Outputs of the MIT seismic tiltmeters are recorded on both chart and drum analog recorders. The output of each tiltmeter passes through one low-pass and two bandpass filters. A block diagram of the recording instrumentation at the Weizmann Geophysical Observatory is shown in Fig. 3-1. Figure 3-2 gives the amplitude responses of the three filter channels.

The low-pass filter was designed to isolate earth tides and long-term drift. The two bandpass filters were designed for emphasis of (a) eigenperiod on free-mode oscillations of the earth, and (b) surface waves in the region 0.5 - 4 cycles per minute for explosion versus earthquake discrimination.

The tidal filter is an active third-order Butterworth low-pass with a breakpoint at 300 seconds and a rolloff of -18 dB/octave. It has unity gain in the pass-band and an optimally flat amplitude response.

The eigenperiod filter consists of an active second-order high-pass section with a breakpoint at 7200 seconds and rolloff of -12 dB/octave and two cascaded third-order Butterworth low-pass sections with breakpoints at 32 seconds and combined rolloff of -36 dB/octave.

The surface-wave filter consists of an active second-order high-pass section with a 120-second breakpoint and -12 dB/octave rolloff, followed by a chopper-stabilized preamp with a gain of 500, followed by two cascaded active third-order Butterworth low-pass sections with breakpoints at 16 seconds and combined rolloff of -36 dB/octave.

Leeds and Northrup Speedomax W/L 2 pen, 10-inch chart recorders are used to record the outputs of the earth tide and eigenperiod filter networks. The earth tide recorder runs at a chart speed of 4 inches per hour and a full-scale span of 2 volts. The eigenperiod recorder runs at a chart speed of 15 inches per hour and a full-scale span of 100 millivolts.

The L&N chart recorders have built-in AZAR units for zero pen position (bias) and full-scale span (range or scale factor) adjustments.

Geotech drum recorders (Model RV301-1 Helicorder) are used for recording surface waves. The drum speed is 1 revolution per hour, and the stylus traverses the drum at the rate of 3/8 in. per hour. The helicorders have been modified with rectilinear pens which, when driven with Geotech AR311 amplifiers, have a scale factor of 0.05 volts/in. @ 0dB. The solid-state helicorders are very stable and have a good signal-to-noise ratio.

Line buffers or drive amplifiers were incorporated in all filter output channels. Besides providing low output impedance, these line buffers incorporated special feedback compensation for stable operation with 800-foot signal cables with a 2000-pF capacitance. The signal cables were shielded, twisted-pair, two-conductor microphone cables.

Differential Temperature Bridges

Since the tiltmeter is sensitive to horizontal ambient temperature gradients, differential temperature bridges were provided for each tiltmeter, with the resistive probes located at the end tanks. Compensation for gradients was originally contemplated, but the effects of such gradients in the Weizman Observatory have thus far been insignificantly small. Figure 3-3 is a calibration of the two bridges.

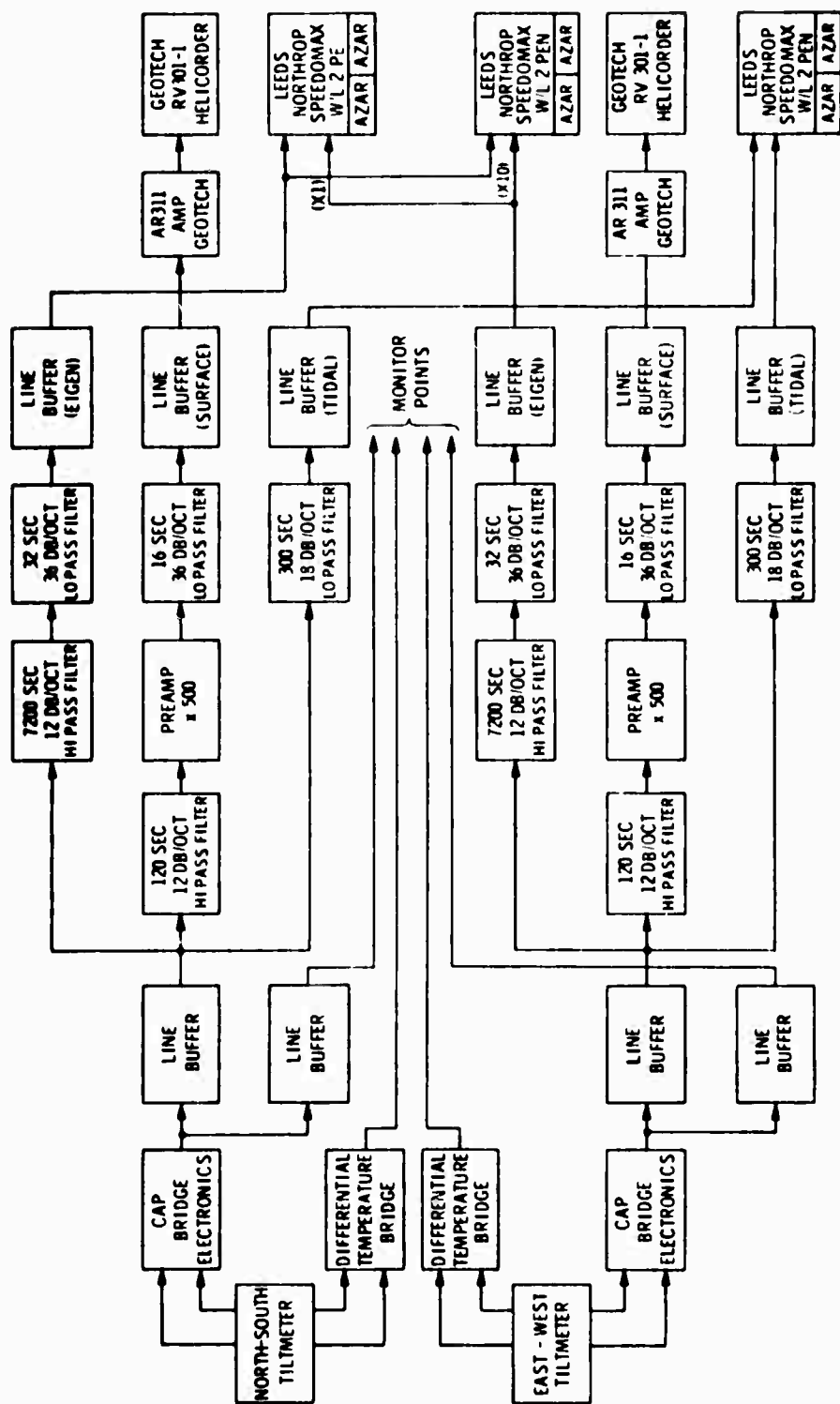


Fig. 3-1 MIT seismic station

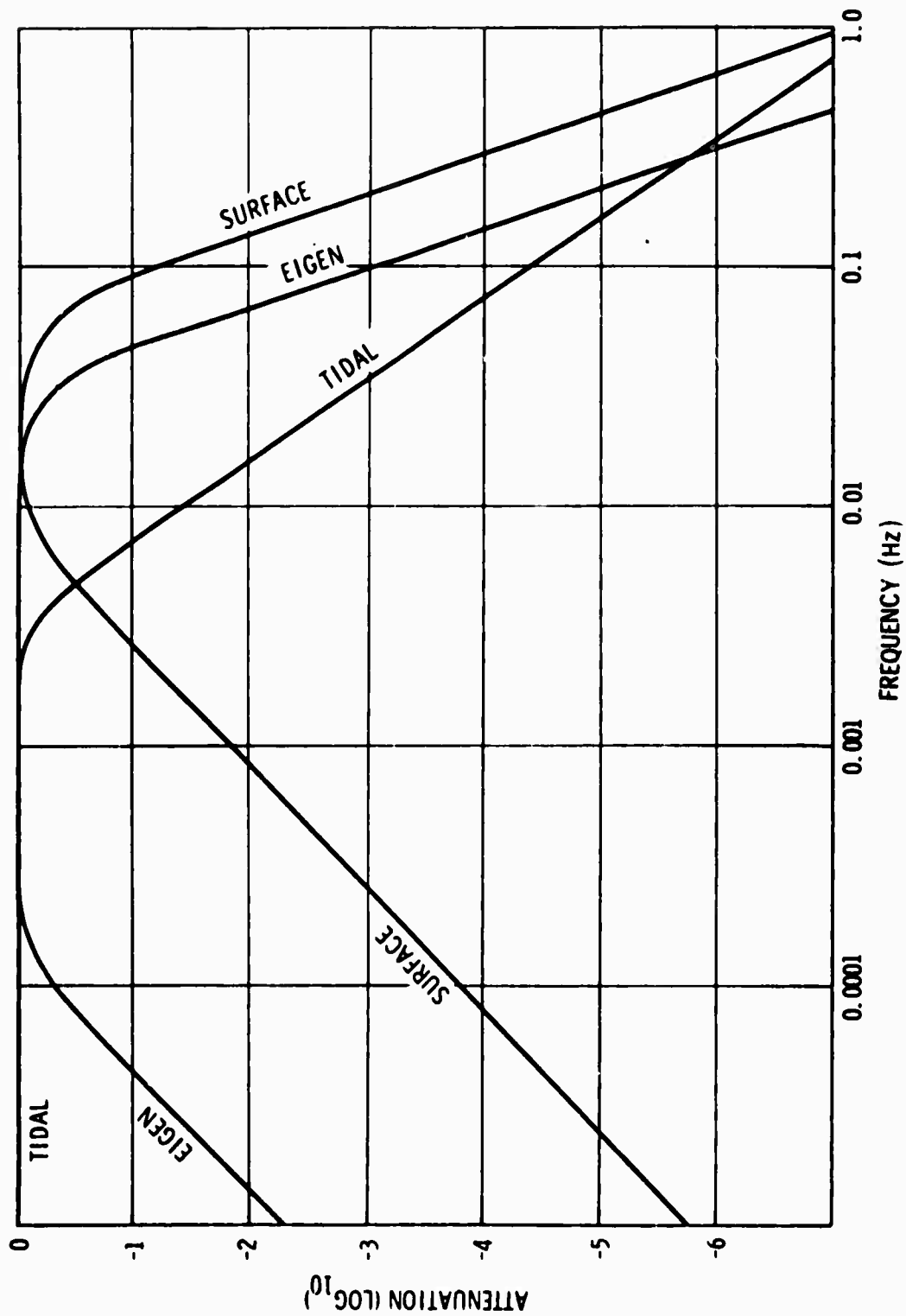


Fig. 3-2 Data channel filters.

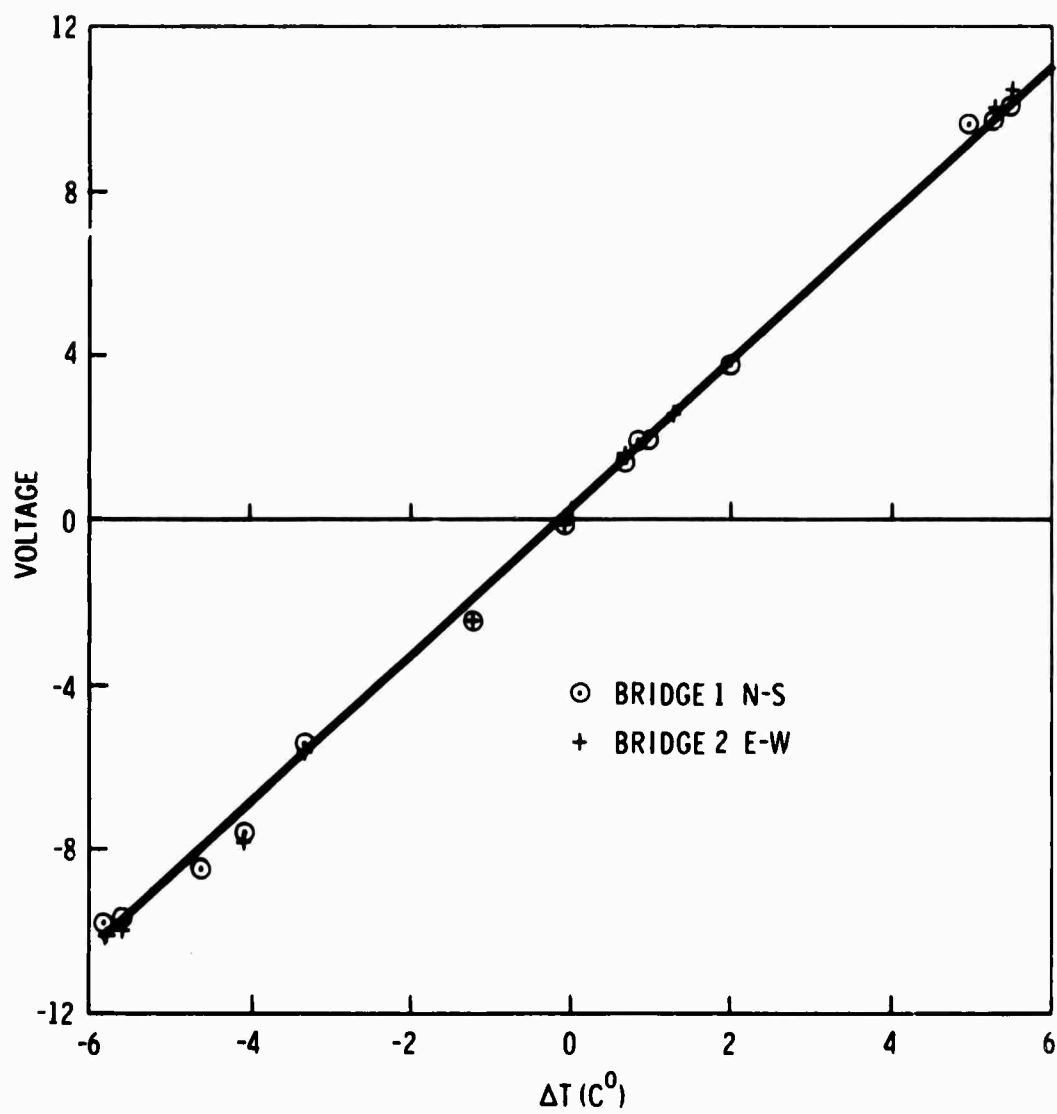


Fig. 3-3 Differential temperature bridge calibration.

BLANK PAGE

CHAPTER 4

INSTALLATION

Installation of the Model II MIT seismic tiltmeter took place near Eilat, Israel, during the months of May and June, 1970. After completing the instrument fabrication work, the end tank subassemblies, electronic field cases, recording consoles, and other equipments were crated and otherwise prepared for air freight to Lod airport near Tel Aviv, Israel. On April 22, 4,800 pounds of equipment, working tools and test instruments left the United States for Israel.

The 90-foot mercury pendulums are installed in orthogonal trenches located over 500 feet inside a granite mountain just north of Eilat, near the Timna copper mines. A plan of this geophysical observatory of the Weizmann Institute of Science is shown in Fig. 4-1. The instrument tunnels are lined with gunite or shotcrete, and are pressure-sealed with bulkhead doors. The environment of these sealed tunnels is nearly a constant 118°F , or 48°C , with a relative humidity varying from 90 to 100%.

The first installation task was the installation of recording equipment. One of the Leeds & Northrop servo amplifiers burned out because of a heat-sink bracket which loosened during shipment, causing a short circuit. The three L & N W/L II 10-inch chart recorders are installed in an enclosed 19-inch console along with three AZAR (adjustable zero/adjustable range) units. Initially, one of these two channel recorders was used for recording earth tides, one for eigenperiods, and one for differential temperature. Eventually, two recorders will be used for eigenperiods at different gain settings.

The drum "Helicorders", along with their drive amplifiers, were mounted in a second 19-inch console. Initially, there was a problem with the pen heater control circuit because of the elevated operating temperatures.

Timing signals for both recording consoles were derived from the observatory's time standard, which is checked each day and synchronized whenever necessary. An air conditioner is now providing cool air in the recording room; this has greatly reduced overheating of the recording equipment electronics and motors. Fig. 4-2 is a photograph of the drum and chart recording consoles.

The next task was to prepare the trenches for installation of the tiltmeters. Four sets of three conical holes were drilled in the trench end tank piers. These precisely-located conical holes were made with special carbide drills and counter-sinks, and held the one-inch stainless steel balls used to support the end tank assemblies. Then, the bases of the aluminum end tank shields were grouted in place.

The four 45-foot, 2 1/2-inch diameter, coaxial lines were assembled, using 12-foot sections except for the end. A continuous length of #18 Teflon-coated wire was used as a center conductor, while 2 1/2-inch diameter copper tubing was used as an outer conductor. Brass couplings with O-ring seals were used to join the 12-foot sections. Problems were encountered because of damage and distortion of the copper tubing during shipment. The assembly of the coaxial lines, including the installation in the trenches and fitting with the junction boxes, took about one week.

Aluminum heat shields were installed to protect the 1/4"-ID, 3/8"-OD butyrate plastic tubing used as a mercury line between end tanks. Butyrate tubing was selected because it was clear, semi-rigid, and approximately matched the thermal expansion of mercury. However, the matching of thermal expansion with mercury, which worked out well at the Agassiz (Harvard, Mass.) installation, did not hold for the Weizmann installation. Apparently, at the higher operating temperature (118°F) the plastic expands even more than the mercury. Also, the increase in nitrogen pressure with temperature in the completely sealed instrument added to the problem. A photograph of a tiltmeter with the mercury line exposed is shown in Fig. 4-3.

The nitrogen lines (1/8" ID, 1/4" OD) between end tanks were installed next, and secured to and supported by the coaxial lines.

The adjustable and fixed end tanks were installed and leveled. The requirement for a better leveling fixture became apparent, and has since been designed and built. The end tank leveling and relative elevation is controlled by adjustment shims in the end tank supports. The leveling procedure proved very time-consuming, but seems to provide for very stable end tanks once adjusted.

The two tiltmeters were filled with mercury. Trouble was immediately encountered with the first instrument (North-South) because of mercury oxidation. This mercury surface contamination may have been caused by dirt in the mercury floating to the surface, or oxidation caused by lack of proper purging of the instrument with nitrogen before filling. The South end tank was opened, drained, cleaned, and refilled. Mercury from a new shipment was used in filling the East-West tiltmeter, along with continuous nitrogen purging. A different filling technique

helped prevent bubbles from entering the mercury lines. No trouble was encountered in filling the East-West instrument, and the end tank surfaces appeared very clean.

The fixed end tank capacitor plates were adjusted to 0.004-inch, or 0.1-millimeter gap, by the use of shims. At this small clearance, a short circuit occurred in the South end tank, which was then opened for inspection. No suspected floating metal particle was found. The South end tank was reassembled. Capacitance readings of 2000 picofarads were obtained, indicating the proper 0.004-inch gap, but a high dissipation factor would occasionally show. Again, no trouble whatsoever was found in the West end tank. One of the fixed end tanks is shown in Fig. 4-4.

The adjustable end tank gaps were made equal to the fixed end tank gaps by means of the differential screw adjustment. One turn of the screw equals 0.0009 inches, or 0.023 mm, so no trouble was encountered in achieving a balanced capacitor plate clearance. A tapered collet nut provided a means of eliminating the backlash on each of the two threads on the differential screw. Some backlash remained after final tightening, but it was small enough to be compensated for. One of the adjustable end tanks is shown in Fig. 4-5.

As the room temperature rose after sealing the tunnel, the mercury level dropped in the end tanks, i.e., the capacitor plate gaps increased. This change in mercury level was easily compensated by injecting more mercury into the mercury line with a syringe. The mercury-level syringe is adjusted with a micrometer located at the center of each instrument, in front of the junction box. A photograph of the syringe/micrometer, junction box, bridge electronics, and filter network field cases is shown as Fig. 4-6.

The bridge electronics box was installed and the differential capacitance bridge nulled, quadrature trimmed, and amplifiers tuned after the capacitor plates were adjusted. The bridge circuits are described and analyzed in detail in Appendix B.2. Photographs of the differential capacitance bridge, along with its oscillator or ac reference and power supply, and the differential temperature bridge are shown in Fig. 4-7, 8, 9. No trouble was encountered in tuning or trimming after power supply warmup.

Next, the filter networks were installed, adjusted and calibrated before connection to the bridge electronics. The input voltage bias trim to the gain-of-500 amplifier between the high-and low-pass sections of the surface-wave filter required readjustment due to the great temperature change. Otherwise, all circuits showed low noise, stable outputs, and performance as expected. Photographs of the tidal, surface, and eigennetworks, including detailed construction, are shown in Fig. 4-10, 11, 12, 13, 14, and 15. The completed tiltmeter, with end tank shields removed, is shown in Fig. 4-16.

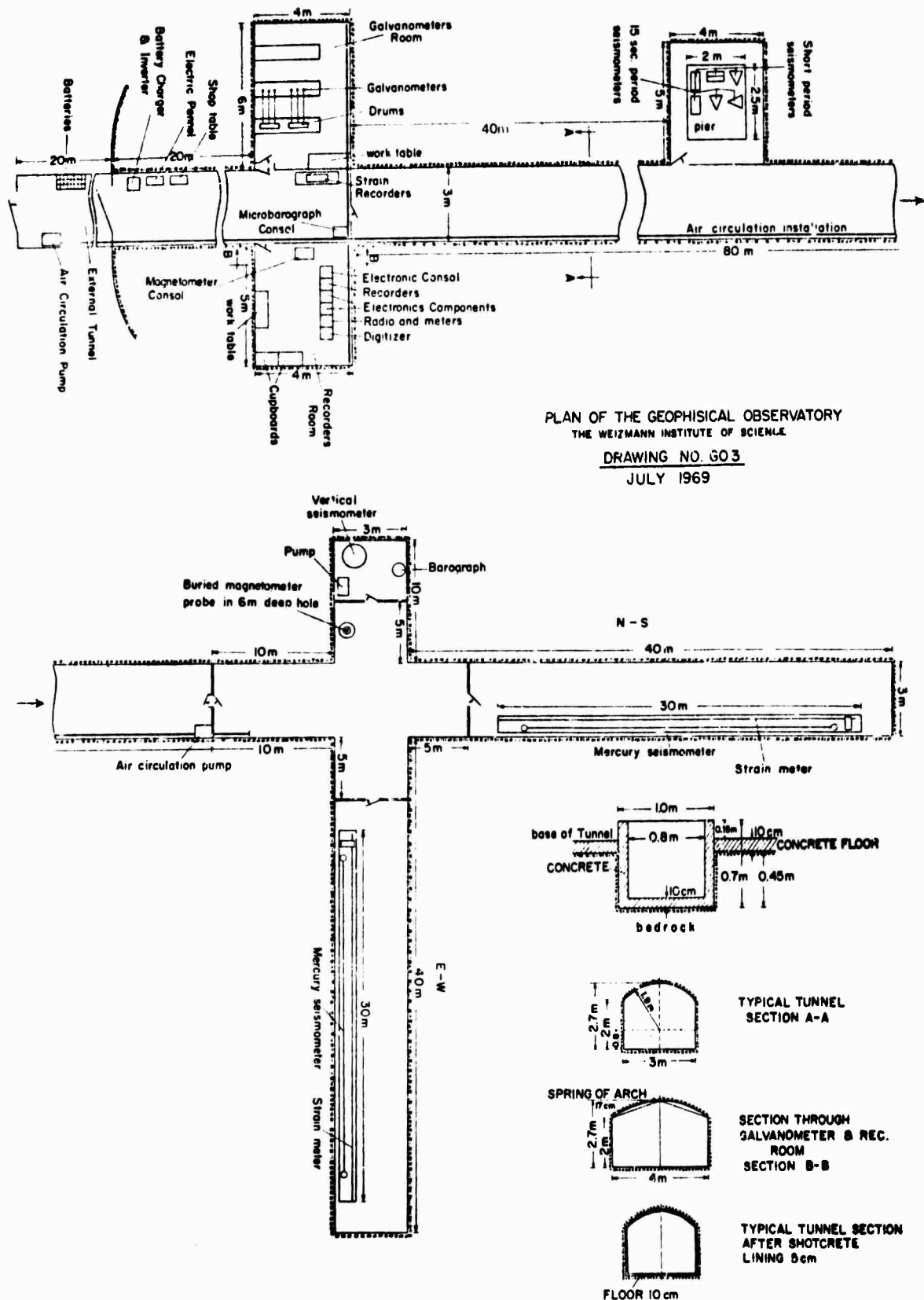


Fig. 4-1 Plan of the geophysical observatory.

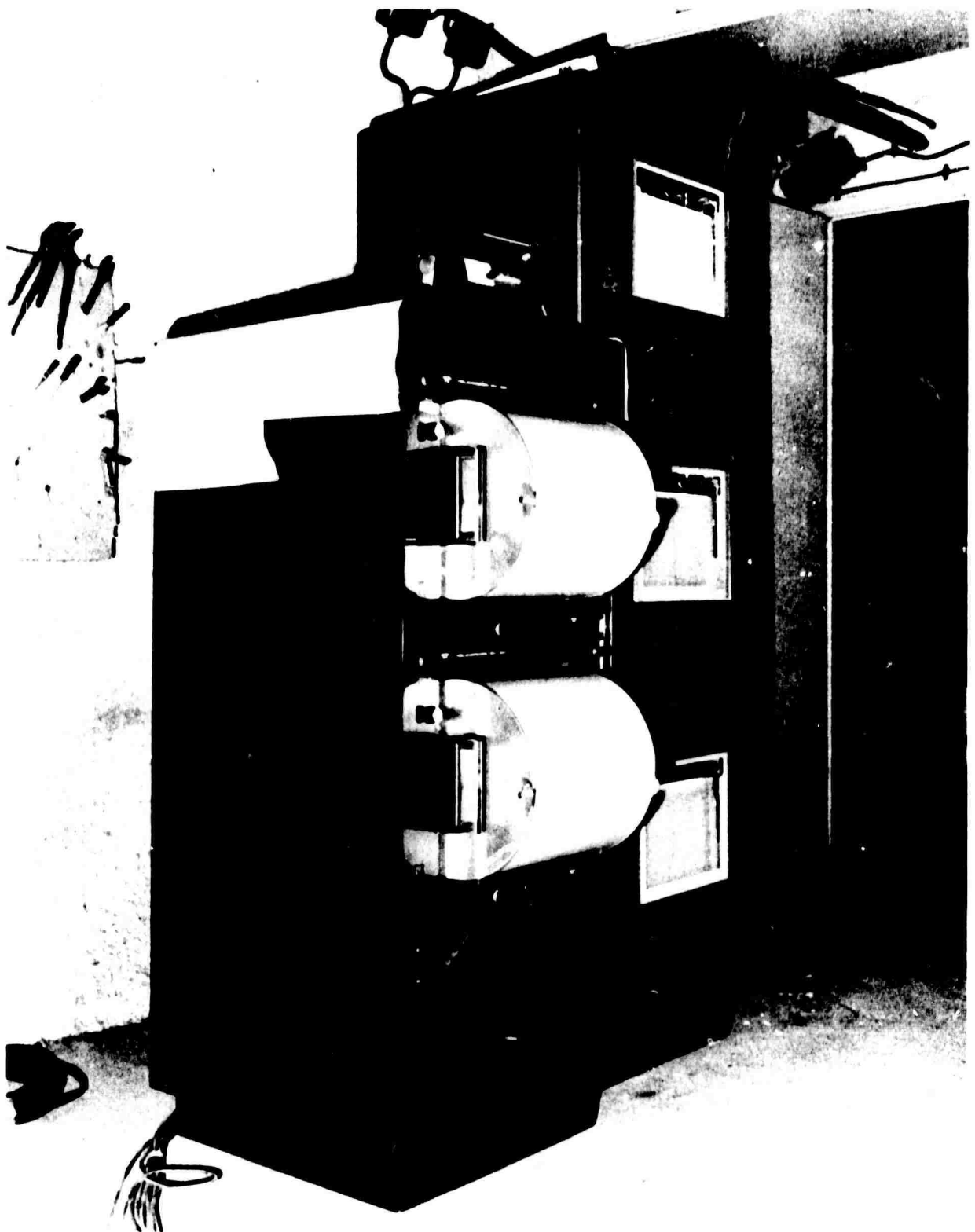


Fig. 4-2 Analog recording consoles.

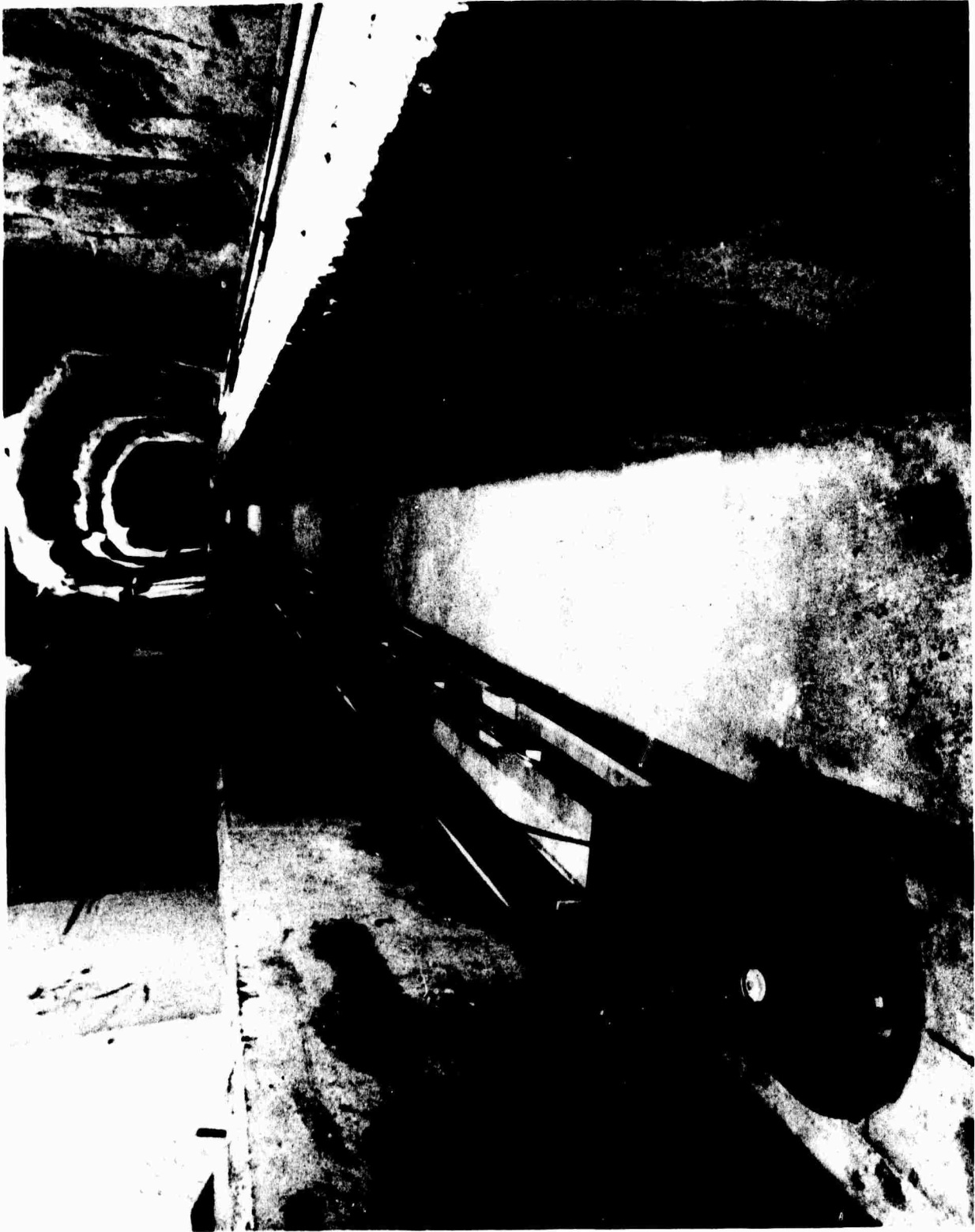


Fig. 4-3 Tiltmeter showing mercury lines.

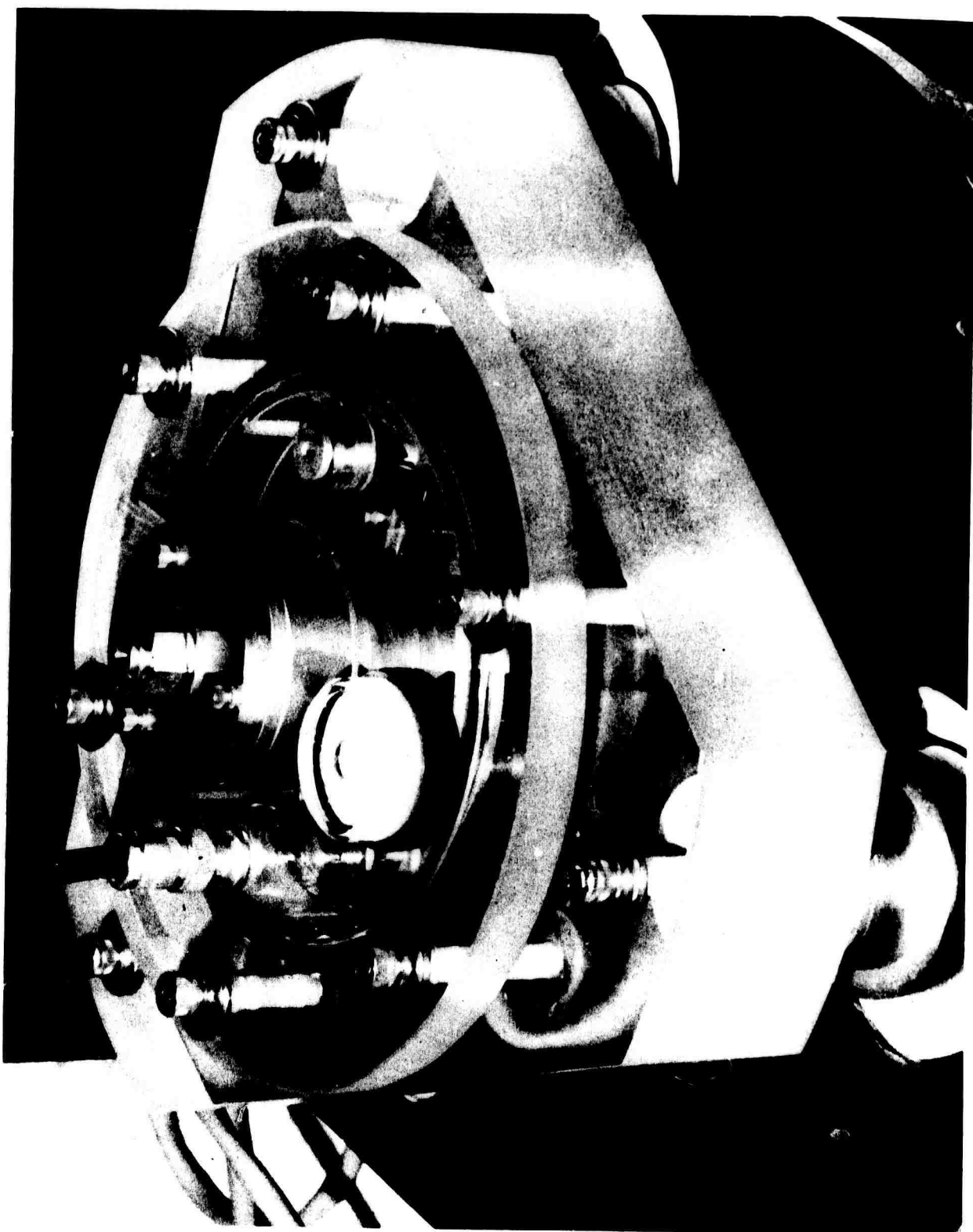


Fig. 4-4 Fixed end tank.

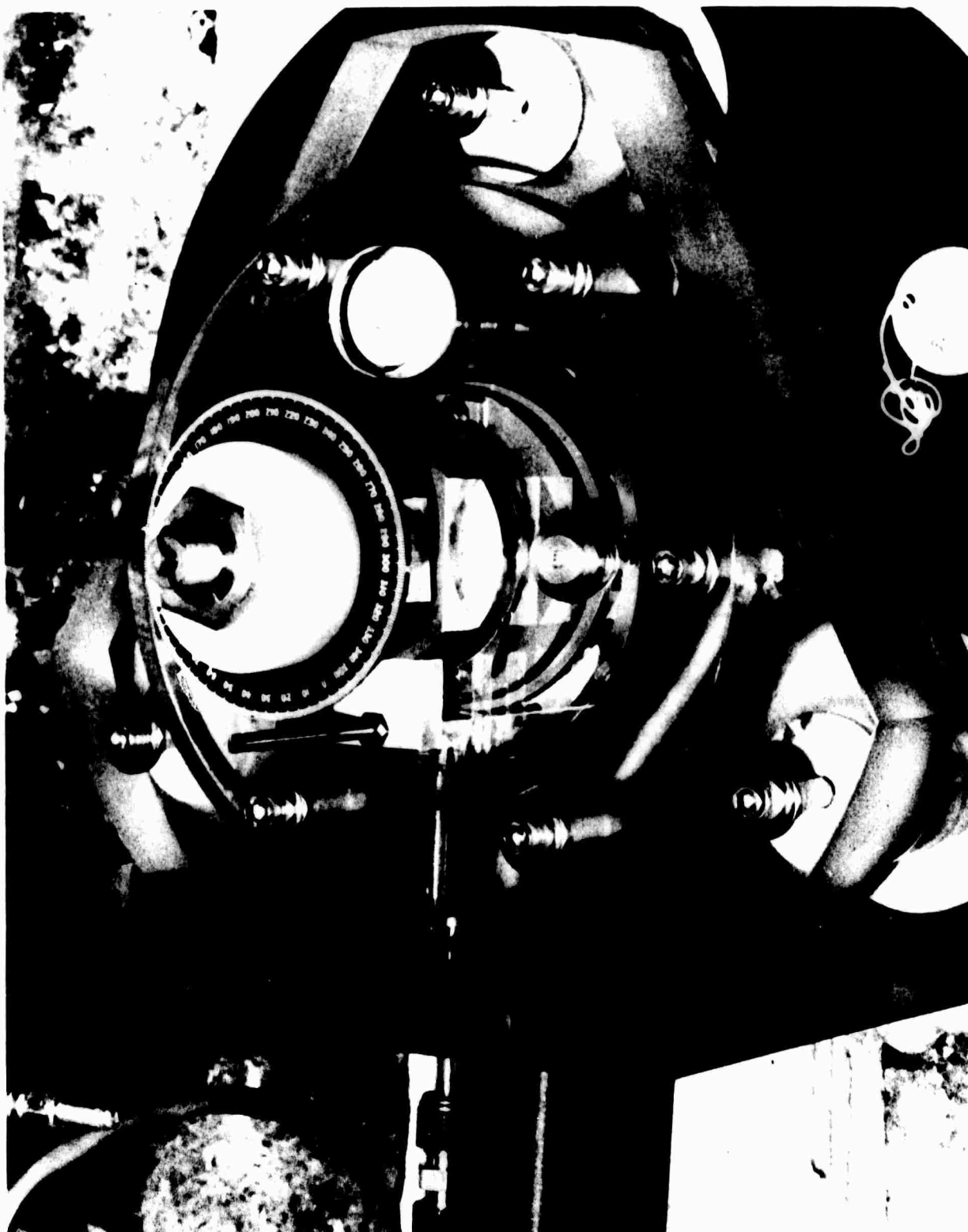


Fig. 4-5 Adjustable end tank.

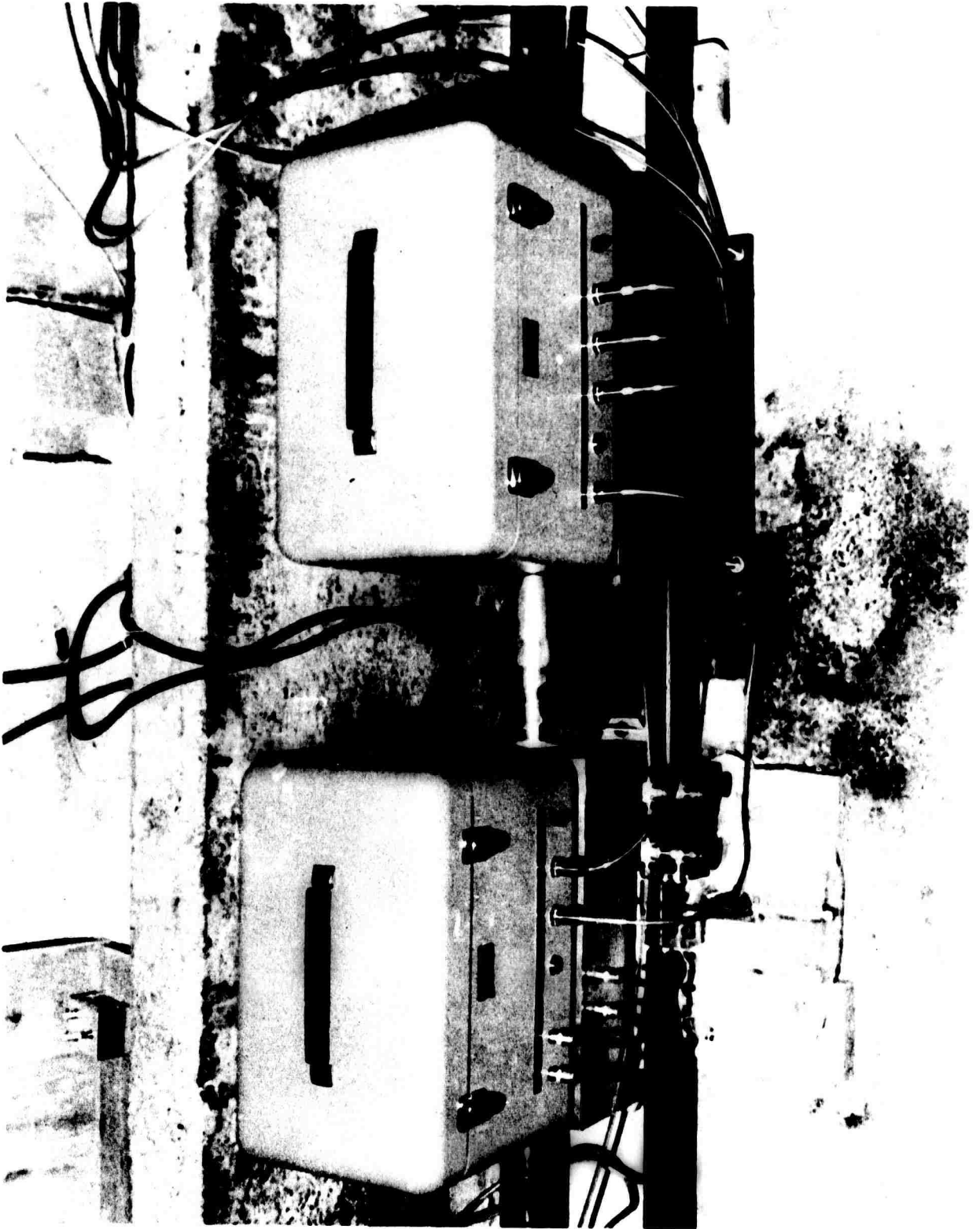


Fig. 4-6 Electronic boxes.

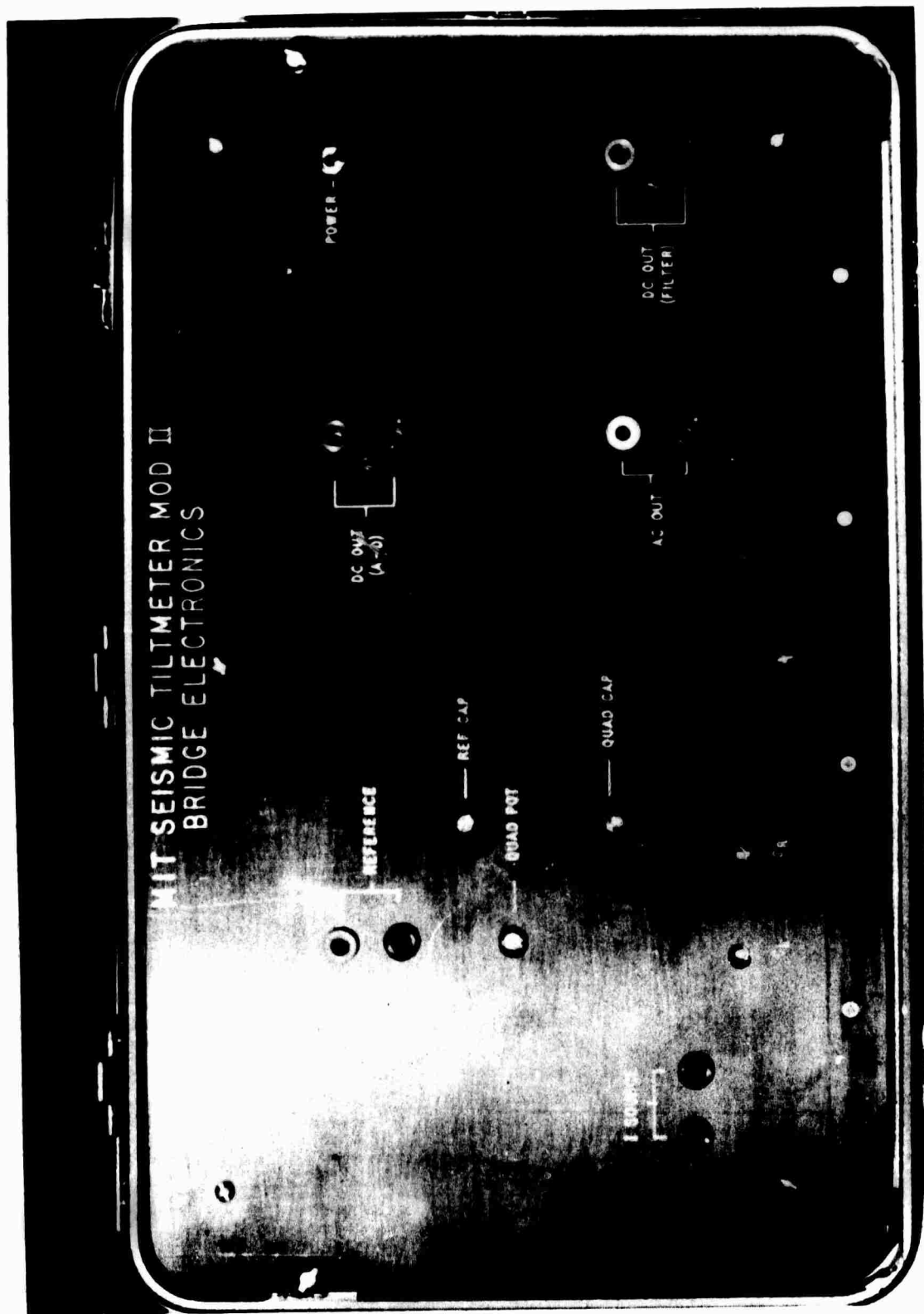


Fig. 4-7 Bridge electronics—alignment panel.

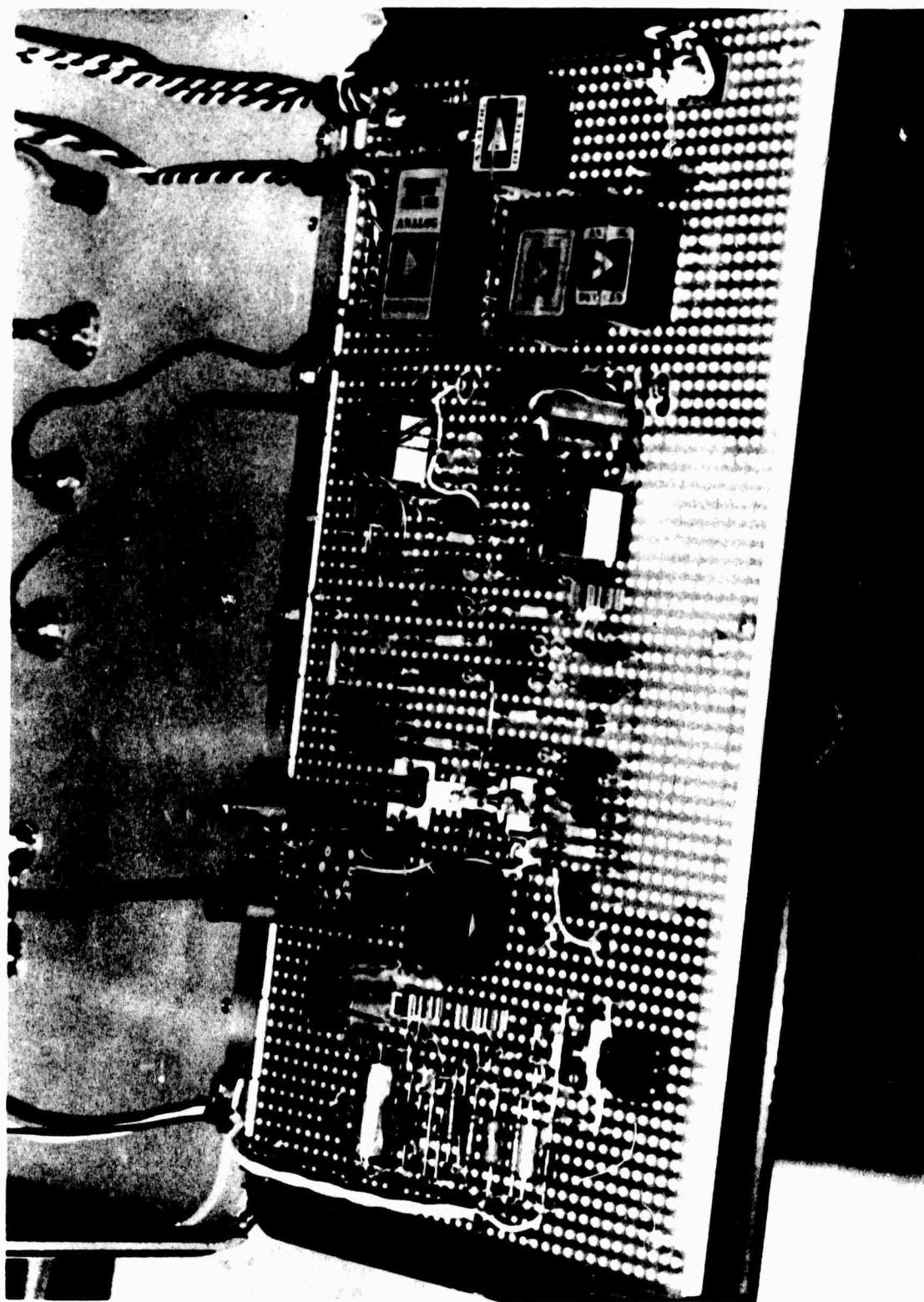


Fig. 4-8 Bridge electronics—differential capacitance.

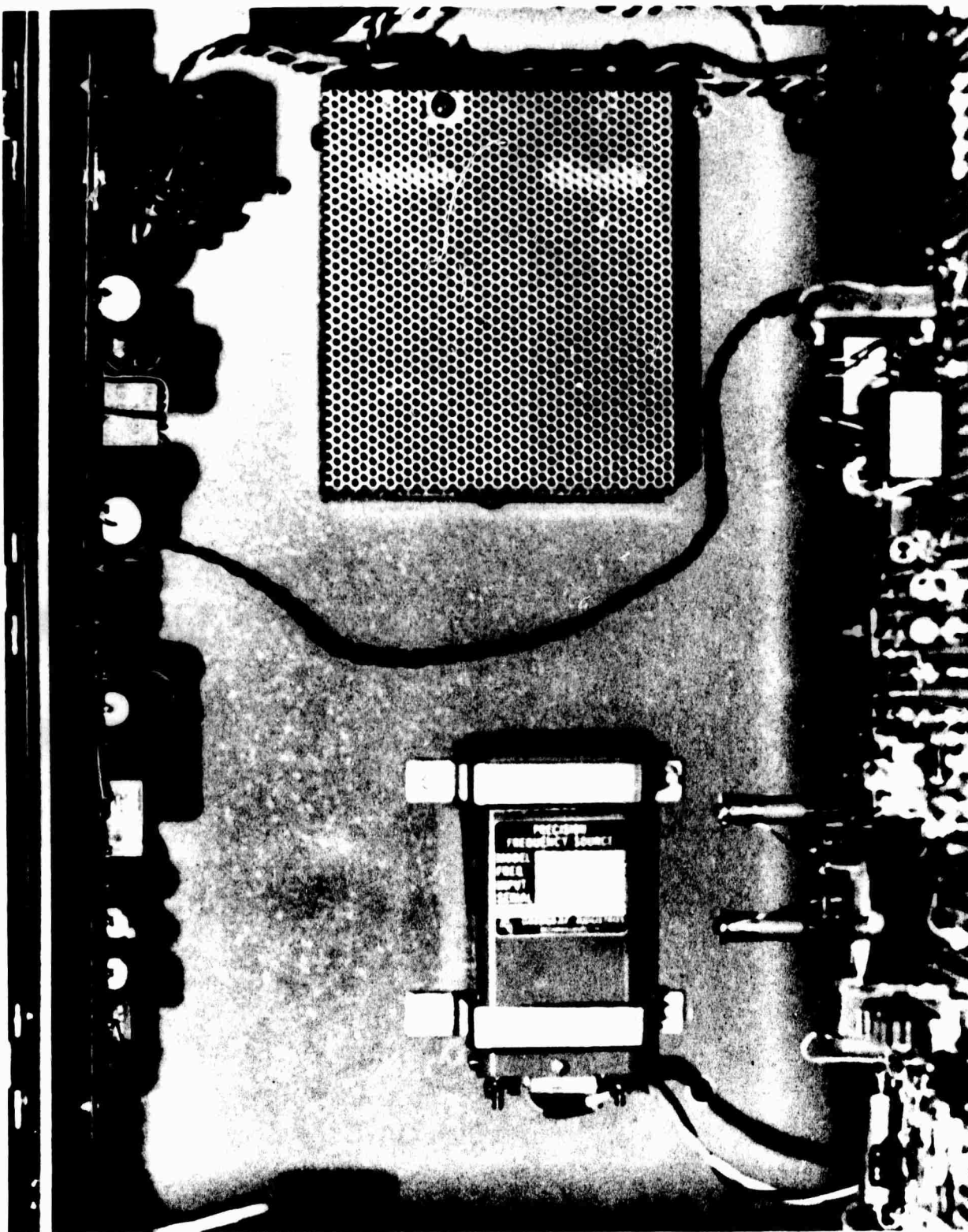


Fig. 4-9 Oscillator, power supply, and differential temperature.



Fig. 4-10 Filter networks—offset trims.

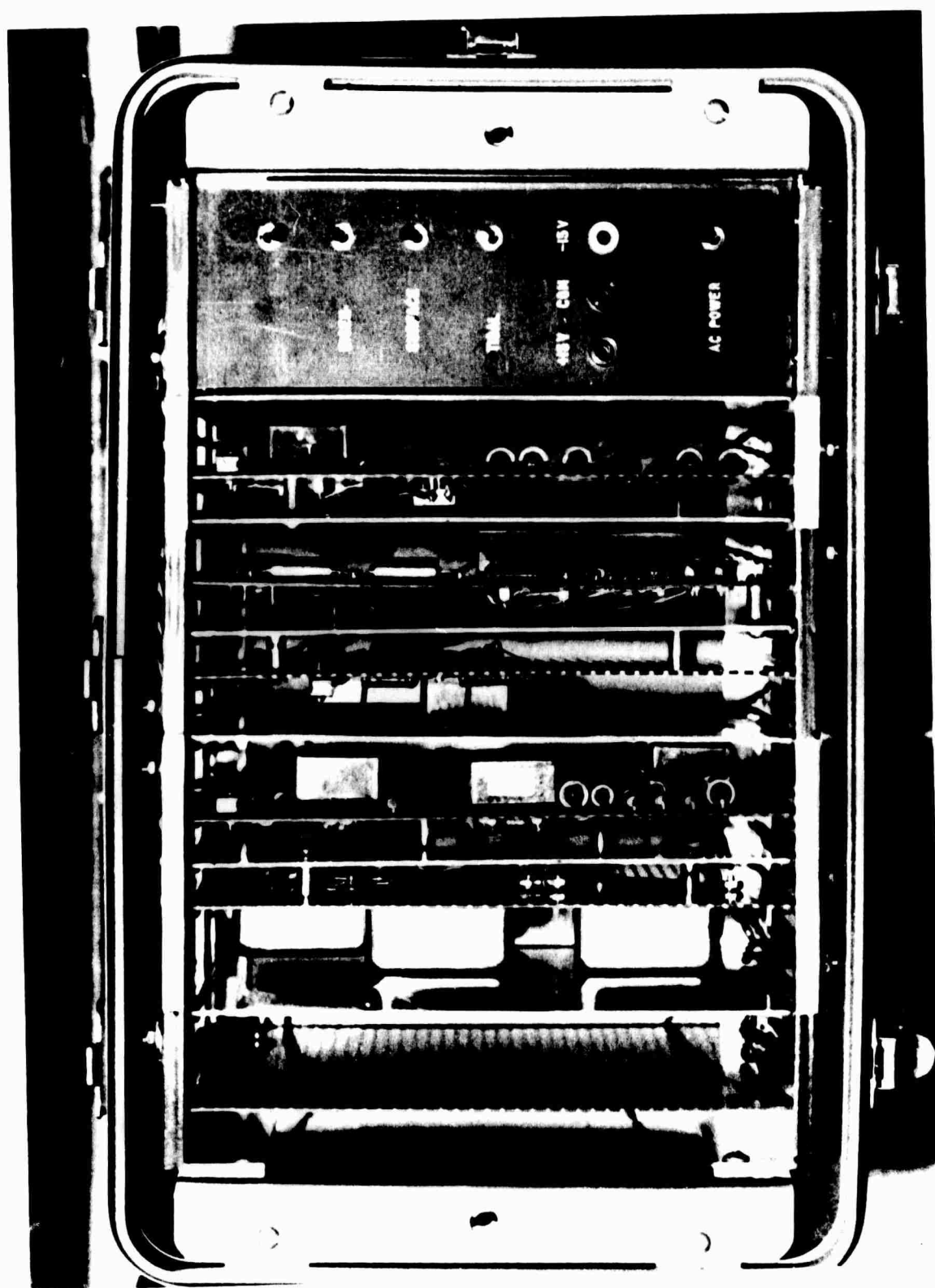


Fig. 4-11 Filter networks—control panel.

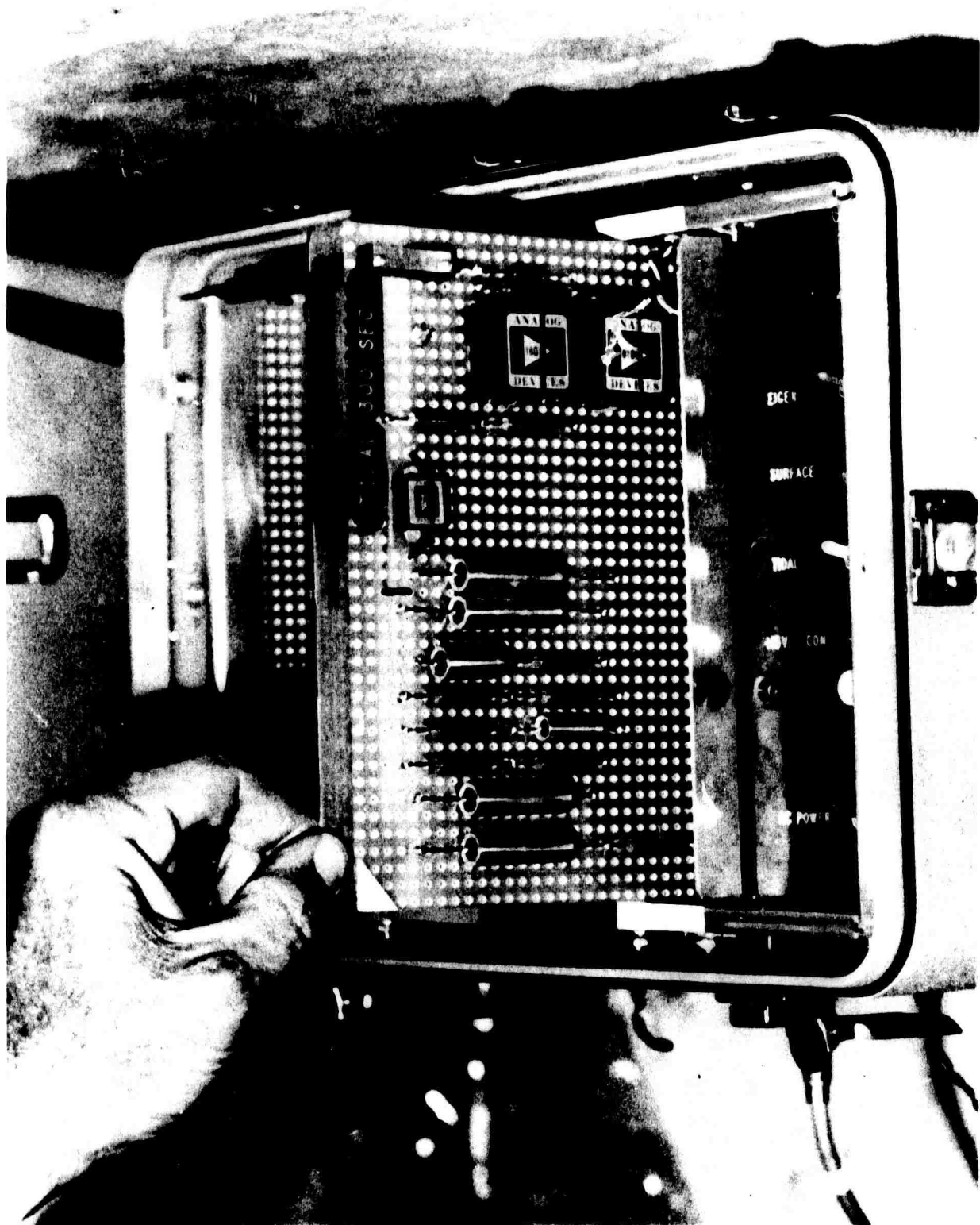


Fig. 4-12 Filter networks—tidal low pass filter.

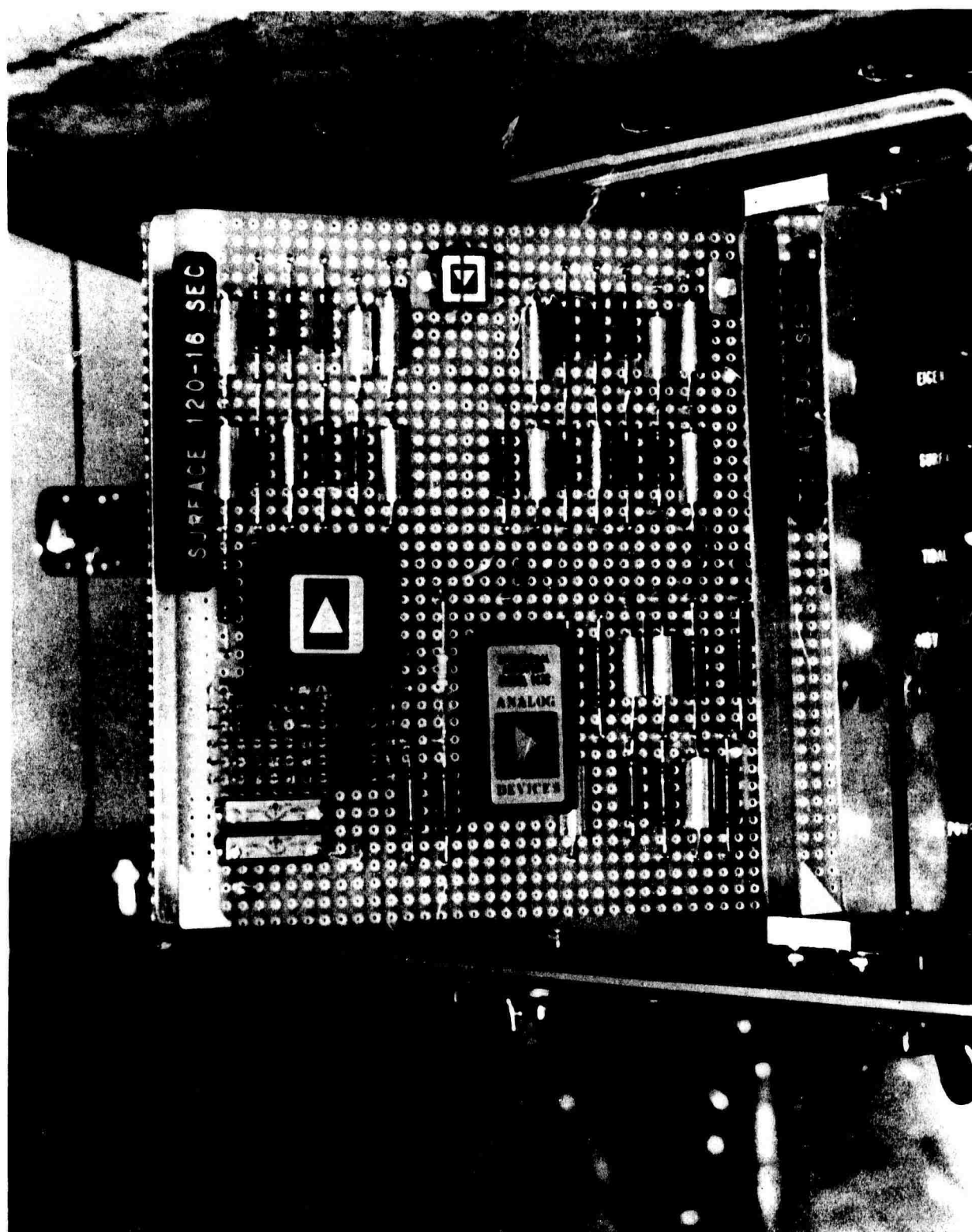


Fig. 4-13 Filter networks—surface band pass filter.

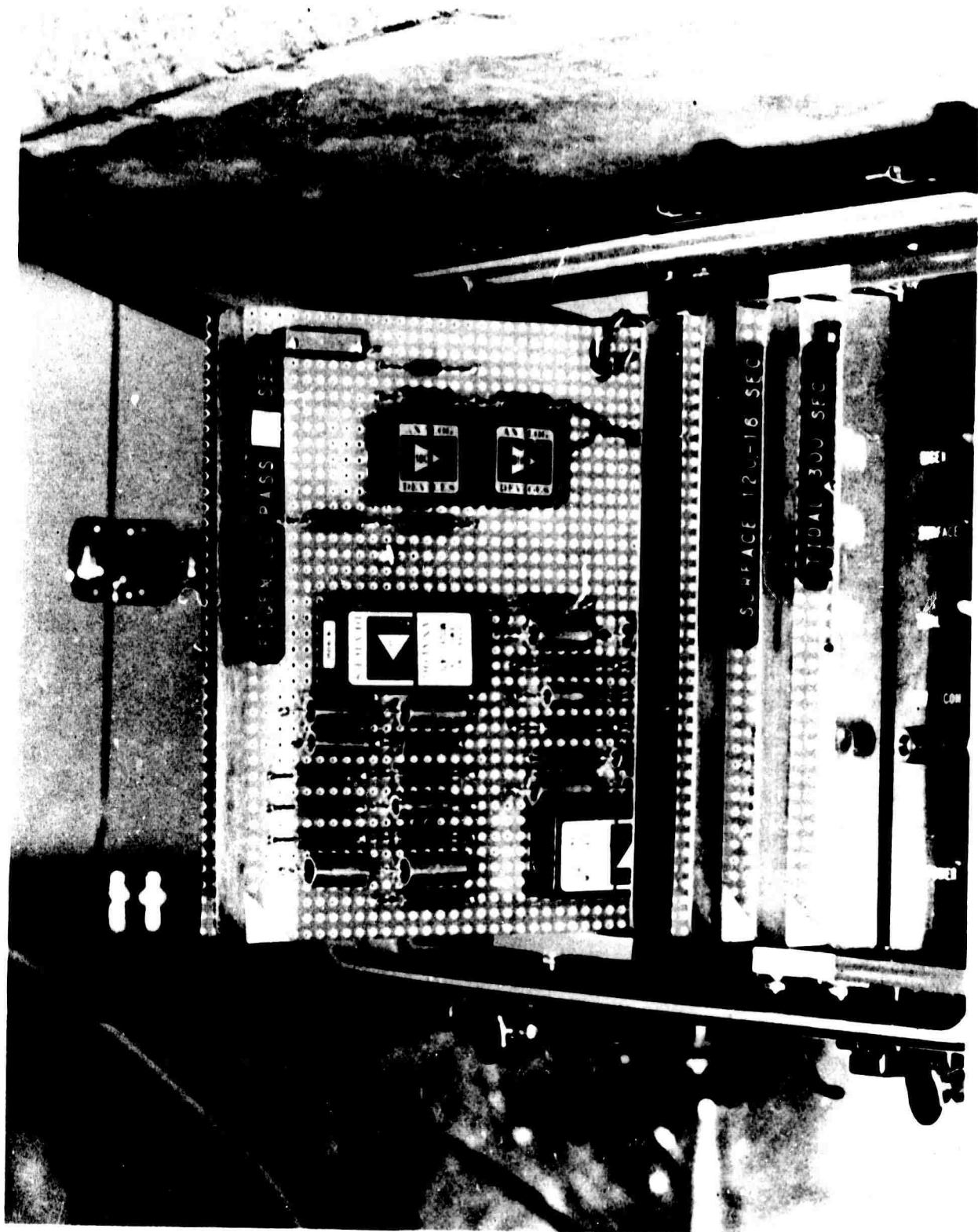


Fig. 4-14 Filter networks—eigen low pass filter.

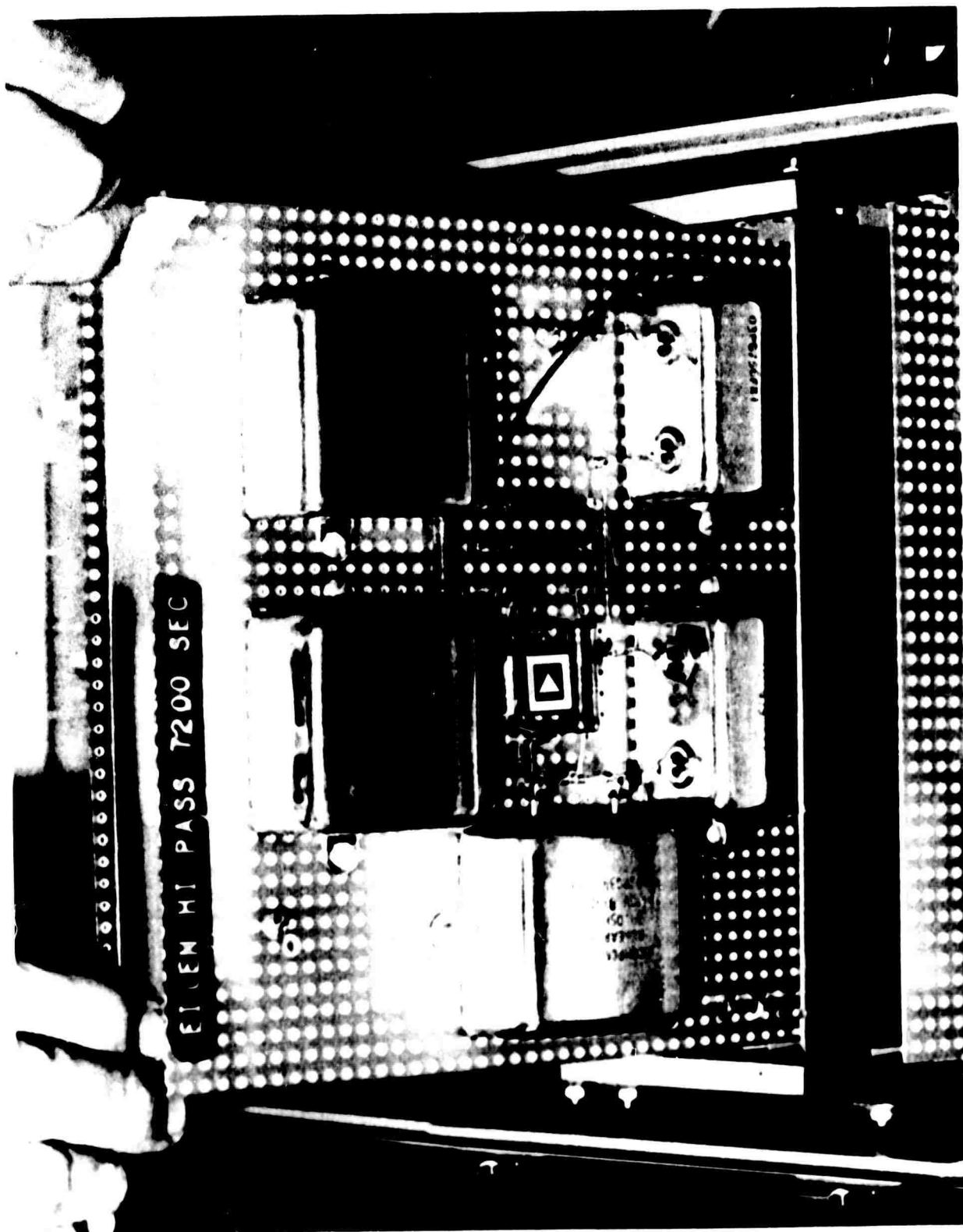


Fig. 4-15 Filter networks—eigen high pass filter.

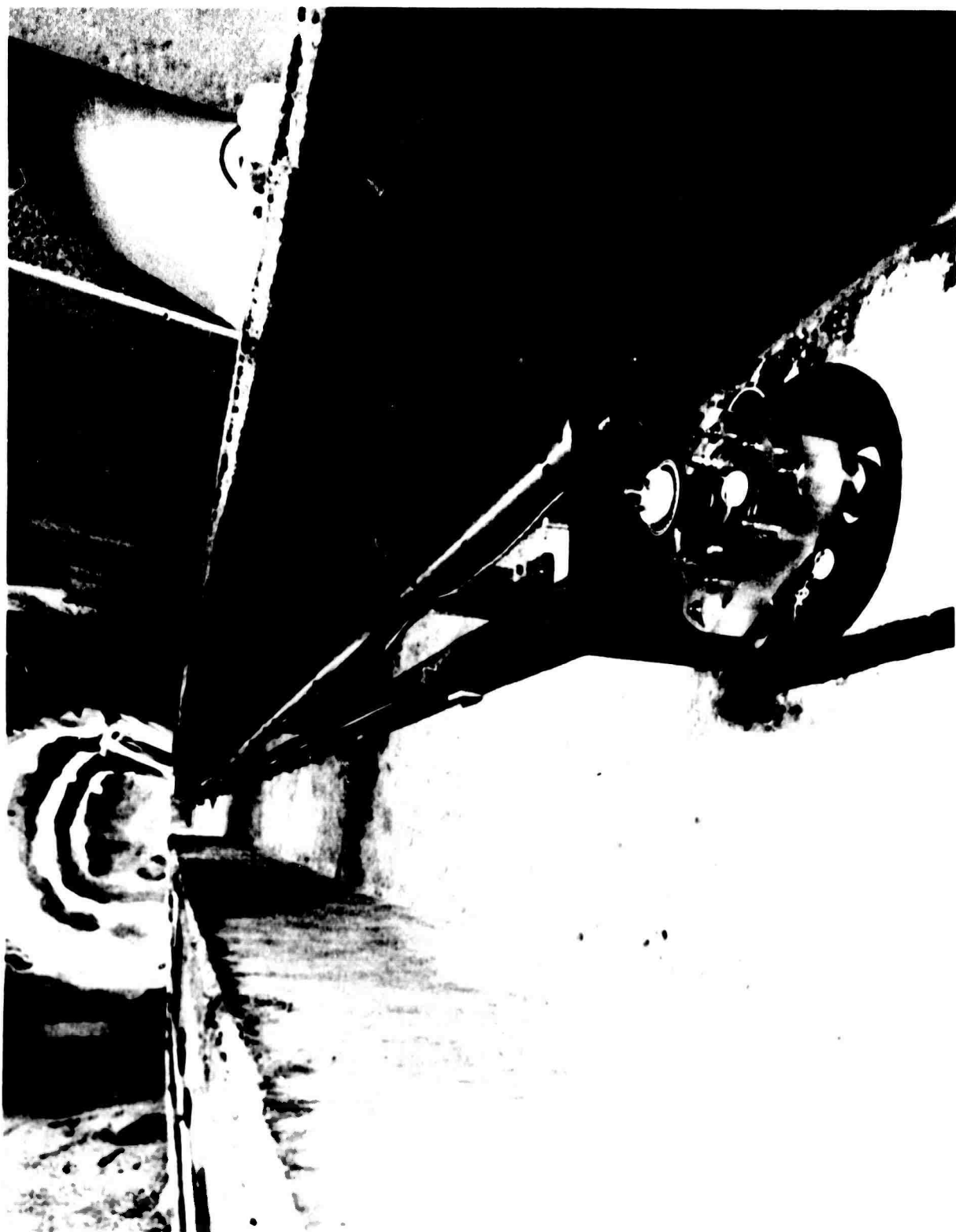


Fig. 4-16 Tiltmeter installation with shields removed.

BLANK PAGE

CHAPTER 5

PRELIMINARY PERFORMANCE

As of this writing, about three months of records are available to assess the performance of the tiltmeters installed in Eilat. This is not yet a sufficient suite of records to achieve the research goals referred to earlier, but it does provide preliminary indications on the performance of the instruments.

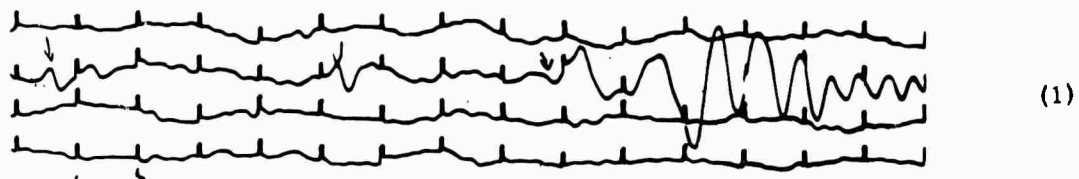
An examination of the records indicates that in the surface-wave band the instruments are operating near the maximum sensitivity permitted by the ground noise characteristic of the winter months. Widening the gap of the transducer capacitance will lead to some improvement in performance in the winter months, and to a marked improvement in the summer and on quiet winter days. The surface wave channel should be markedly improved by this modification.

The records differ from conventional seismographs in showing mantle surface waves from relatively small events. We have not been able to identify most of these events because their magnitudes are too small to be reported through usual channels. In further studies, we will track these tremors down in order to study the efficiency of long wave excitation in the magnitude range less than 5.

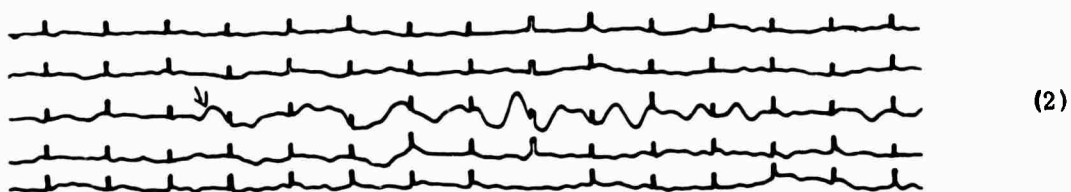
Some sample records are shown in Fig. 5-1. In examining new records, the reader should remember that the response at 20 seconds is down by a factor of about 5 compared to the response at 70 seconds, so that performance of the surface-wave channel should be judged by the detection of waves with periods in the range 50-100 seconds. Other seismographs are better suited for recording surface waves with periods under 30 seconds, and the eigenmode channel will be more useful for waves with periods exceeding 200 seconds.

The records in Fig. 5-1 are typical of a large number of events detected in the three-month operating period showing crustal-mantle surface waves containing energy near 100 seconds from earthquakes with magnitudes near 5. The background noise shown in Fig. 5-1 is typical, indicating that the gain could have been increased by two or more times about 50% of the time. This will be possible with the modification referred to earlier.

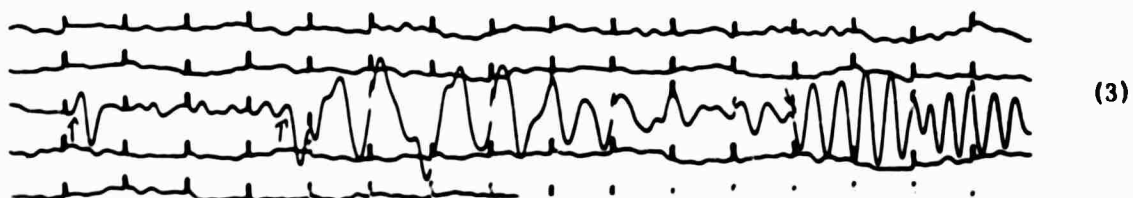
These preliminary results are encouraging. We also look forward to comparing records made by this system with the Lamont-Doherty type of seismograph which has just been installed at the same station.



Record 1. Prince Edward Island, $M = 5.1$, $\Delta = 75^\circ$. Showing excitation
80-second surface waves on E-W component.

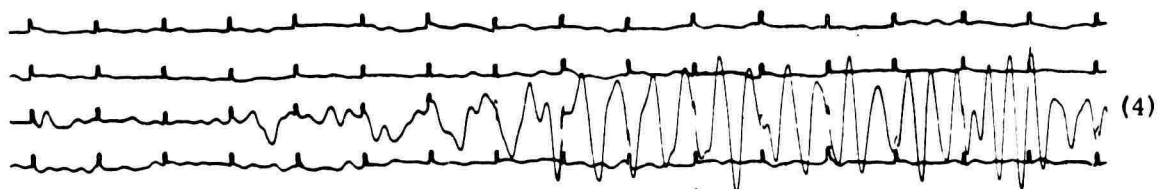


Record 2. California, $M = 5.4$, $\Delta = 110^\circ$. Showing excitation of
100-second surface waves on N-S component.



Record 3. Jun Magen Island, $M = 5.1$, $\Delta = 47^\circ$. Showing excitation
of 80-second surface waves on E-W component.

Fig. 5-1 Surface wave records



Record 4, 5. Large Soviet underground explosion 14 October 1970
on E-W (4) and N-S (5) components, maximum period
about 60 seconds.

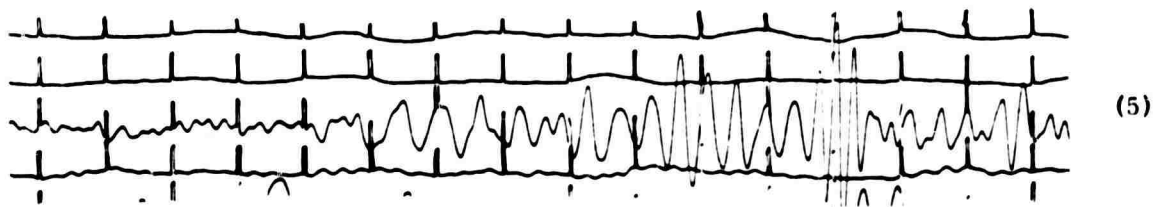


Fig. 5-1 Surface wave records (continued).

BLANK PAGE

APPENDIX A.1

ADJUSTABLE AND FIXED END TANK DESIGN

The two end tank assemblies are very similar except for the manner in which the capacitor plates are positioned. The end tanks of the first pair of tiltmeters were fabricated from Pyrex 10-inch diameter Pyrex lens blank. The end tanks for the second pair of tiltmeters were made entirely from quartz. Pyrex is probably the best material for the end tanks, as it is inexpensive, has consistent quality with uniform properties, is readily available, and grinds or machines well. Quartz, unless it is of select grade and highest quality, has been found to be of variable quantity, with sometimes severe bubble and dirt contamination, and is difficult to machine because of high internal stresses. The problems encountered in using quartz can only be overcome with a higher grade of material, which is much more expensive than Pyrex. Pyrex is sufficient for the application, since the optical properties and extremely low thermal coefficient of expansion of quartz are not needed. Plexiglas and other plastics were not used in end tank construction due to their mechanical instability and thermal hysteresis. Metals such as 316 stainless steel were not used because of the introduction of additional stray capacitance and contamination of the mercury surface from amalgamation. Experience with manometers and other mercury-filled devices has shown that clean, polished glass and mercury have the most uniform wetting action.

The problem of providing a stable support for the end tank, while allowing for relative expansion with respect to the concrete piers, was solved by using a non-redundant, three-point design. (See Fig. A.3-1-4.) Three ball joints with fixed, V-grooved (1 degree of freedom), and flat plate (2 degrees of freedom) provide a self-aligning system free of any stresses save friction between the lapped V-groove and flat plate surfaces. Friction is minimized through hard-lapped surfaces and a special chromium coating (electrolizing). The end tanks are leveled with ground washers and shims between the support feet and the end tanks.

The end tanks are hermetically sealed with silicone-impregnated O-rings and epoxy joints. A sealed system is necessary to prevent mercury oxidation and condensation of water vapor.

The capacitor plate is in the shape of a ring. The center hole minimizes damping, and avoids the mercury entrance fitting at the bottom of the end tank. The capacitor plate is a stainless steel ring, ground for flatness and chromium-coated for corrosion resistance. It is attached on the adjusting shaft by means of a quartz disk which acts as a mechanically-stable insulator. A single-path electrical connection is made between the capacitor plate and a BNC fitting.

In the adjustable end tank (Fig. 4-5), the capacitor plate is moved vertically by a differential screw mechanism. The differential screw is made of two opposing threads: one with 46 threads per inch and the other with 48 threads per inch. Since one screw advances while the second screw retracts, the resulting combined motion provides a vertical adjustment of 0.0009 inches per turn.

The threads are lapped, hardened, relapped, and lubricated to minimize friction (adjustment torque). One of each of the mating threads employs a split collar and tapered collet, with a tapered nut to minimize thread play or backlash. The middle or floating shaft (containing both threads) has a knurled knob which insulates the hand when making a capacitor gap adjustment. The capacitor plate does not rotate with respect to the end tank while moving vertically, making electrical connection and sealing simpler. The differential screw has an adjustment range of 44 turns, equivalent to ± 0.02 inches. A dial indicator provides a reference for partial turns.

APPENDIX A.2

THEORETICAL RESPONSE OF THE TILTMETER

Part I: Simple Tiltmeter Dynamics

An idealized mechanical model of the tiltmeter is shown in Fig. A.2-1. It consists of two mercury reservoirs, each of cross-sectional area A , connected by a tube of cross-sectional area a , and length l . Two independent input coordinates are considered:

$X(t)$ = absolute horizontal displacement of tiltmeter

$\theta(t)$ = absolute angular displacement of tiltmeter

Two response coordinates are:

$\bar{x}(t)$ = the average displacement of the mercury relative to the tube

$y(t)$ = the increase of depth of mercury in the reservoir from equilibrium position

The two response coordinates are dependent by the relation $Ay/a = \bar{x}$, and the model possesses only one (1) degree of freedom.

Energy Approach, No Damping

The simplest approach to the tiltmeter dynamics is through energy considerations. We use here the procedure of Lagrange. The input variables $X(t)$ and $\theta(t)$ are treated as constraint variables, and either $\bar{x}(t)$ or $y(t)$ is the independent coordinate.

We assume that the velocity distribution within the tube is parabolic (Hagen-Poiseuille Flow). The actual velocity $\dot{x}(r)$ at a radius r from the tube centerline is related to the average velocity by:

$$\dot{x}(r) = 2\dot{\bar{x}} \left[1 - \left(\frac{r}{r_0} \right)^2 \right] \quad \text{A 2.1}$$

where r_0 = tube inner radius

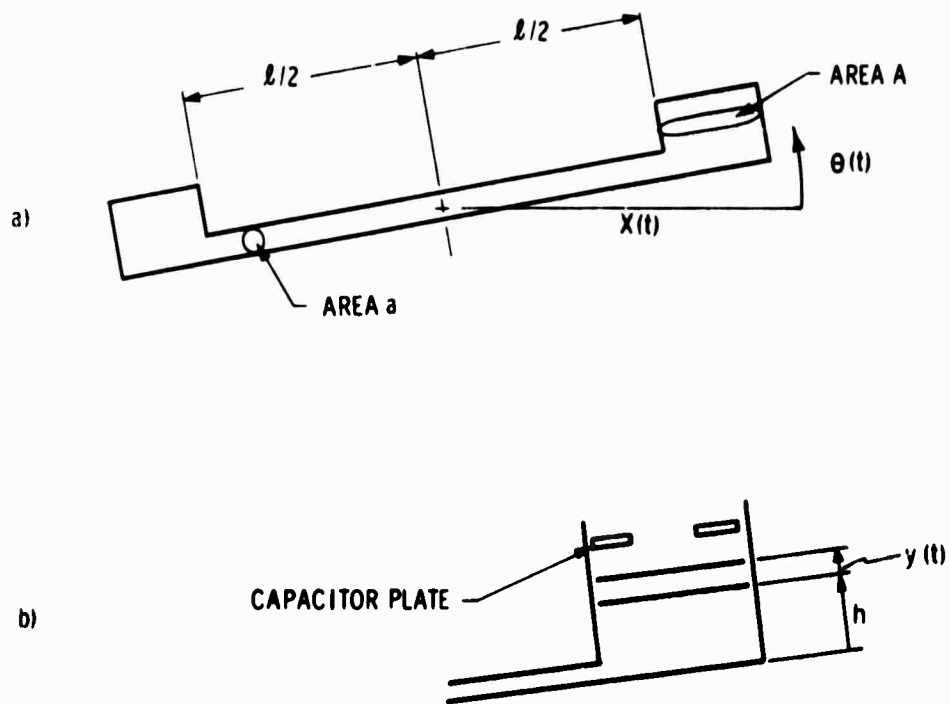


Fig. A.2-1 Tiltmeter mechanical model.

The kinetic energy of the tube mercury is then

$$T_{\text{tube}} = \frac{1}{2} \left[\frac{1}{12} (\rho a l) l^2 \right] \dot{\theta}^2 + \frac{1}{2} \int_0^l (\rho 2\pi r dr l) \left[\dot{X} + \dot{x}(r) \right]^2 \quad A. 2.2$$

Integrating,

$$T_{\text{tube}} = \frac{m}{2} \left[\frac{1}{12} (l \dot{\theta})^2 + \dot{X}^2 + 2 \dot{X} \dot{x} + \frac{4}{3} \dot{x}^2 \right] \quad A. 2.3$$

The kinetic energies of the reservoirs are:

$$T_{\text{left res}} = \frac{1}{2} \left[\rho A (h-y) \right] \left[\left(\frac{l \dot{\theta}}{2} + \dot{y} \right)^2 + \dot{X}^2 \right] \quad A. 2.4$$

$$T_{\text{right res}} = \frac{1}{2} \left[\rho A (h+y) \right] \left[\left(\frac{l \dot{\theta}}{2} + \dot{y} \right)^2 + \dot{X}^2 \right] \quad A. 2.5$$

Since we are considering only the linear approximation for small motions, we consider only terms up to the second order in \dot{X} , \dot{x} , and $\dot{\theta}$. The total kinetic energy relation is therefore:

$$T = \frac{1}{2} \left\{ \left(\frac{m}{12} + \frac{M}{2} \right) (l \dot{\theta})^2 + (m + 2M) \dot{X}^2 + \frac{2m A \dot{X} \dot{y}}{a} + 2M l \dot{\theta} \dot{y} + \frac{4m}{3} \left(\frac{A}{a} \right)^2 \left[1 + \frac{3}{2} \frac{M}{m} \left(\frac{a}{A} \right)^2 \right] \dot{y}^2 \right\} \quad A. 2.6$$

where

$m = \rho a l$, mass of tube mercury

$M = \rho A h$, mass of reservoir mercury

Representative values are $\frac{M}{m} \sim 0 [0.04]$

$$\frac{a}{A} \sim 0 [0.0035]$$

Therefore the term $\frac{3M}{2m} \left(\frac{a}{A} \right)^2$ may be dropped with respect to unity.

We next consider the potential energy. The potential energy changes are:

$$\text{right reservoir; } + \rho A h g \frac{l \theta}{2} + \rho A y g \left(\frac{l \theta}{2} + y \right) \quad A. 2.7$$

$$\text{left reservoir; } - \rho A (h-y) g \frac{l \theta}{2} \quad A. 2.8$$

The net change in potential energy is

$$V(y, \theta) = \rho A g y [\ell \theta + y] \quad \text{A. 2. 9}$$

Kinetic and potential energies are combined to form the Lagrangian $L = T - V$, and the equation of motion follows directly from the Lagrange equation

$$\frac{d}{dt} \left[\frac{\partial L}{\partial \dot{y}} \right] - \frac{\partial L}{\partial y} = 0 \quad \text{A. 2. 10}$$

Since we have not considered damping, all forces are conservative. In standard form the y equation is

$$\frac{4m}{3} \left(\frac{A}{a} \right)^2 \ddot{y} + (2\rho A g) y = -\frac{mA}{a} \ddot{X} - \rho A g \ell \theta - M \ell \ddot{\theta} \quad \text{A. 2. 11}$$

The left-hand side of this equation identifies the tiltmeter as a simple harmonic oscillator with an equivalent mass of $m_1 = \frac{4m}{3} \left(\frac{A}{a} \right)^2$, an equivalent spring constant of $2\rho A g$, and, therefore, a natural frequency

$$\omega_1 = \left[\frac{2\rho A g}{\frac{4m}{3} \left(\frac{A}{a} \right)^2} \right]^{1/2} = \left[\frac{3 a g}{2 A \ell} \right]^{1/2} \quad \text{A. 2. 12}$$

The right-hand side of the equation shows that the tiltmeter oscillator is sensitive to horizontal translational acceleration \ddot{X} , to angular displacement θ , and to angular acceleration $\ddot{\theta}$.

Energy Approach, Including Tube Damping

Assume that significant damping occurs only in the regions of high velocity, i. e., in the tube. Imagine the shear stress acting on the surface of an infinitesimal tubular element of length ℓ , inner radius r , and outer radius $r + dr$. From the Newtonian law of friction,

$$\tau = \mu \, d\dot{x}/dr \quad \text{A. 2. 13}$$

The shear force is then

$$F_{\text{shear}} = \mu \frac{d\dot{x}}{dr} [2\pi r \ell] \quad \text{A. 2. 14}$$

and the power dissipated in the tubular element is

$$d \text{ Power} = \mu \frac{d\dot{x}}{dr} \left[2\pi r l \right] \frac{d\dot{x}}{dr} dr \quad \text{A.2.15}$$

Integrating over all elements,

$$\text{Power} = \int_0^r 2\pi \mu l \left(\frac{d\dot{x}}{dr} \right)^2 r dr \quad \text{A.2.16}$$

The velocity gradient $\frac{d\dot{x}}{dr}$ can be obtained by differentiating Eq A.2.1. Equation A.2.16 can then be integrated to obtain

$$\text{Power} = 8\pi \mu l \left(\frac{A}{a} \right)^2 \dot{y}^2 \quad \text{A.2.17}$$

The power dissipated in an equivalent linear dashpot is

$$\text{Power} = C_{eq} \dot{y}^2 \quad \text{A.2.18}$$

The equivalent dashpot constant is

$$C_1 = 8\pi \mu l \left(\frac{A}{a} \right)^2 \quad \text{A.2.19}$$

The effect of viscous damping in the tube can then be accounted for by adding a damping force $C_1 \dot{y}$ to Eq A.2.11

$$m_1 \ddot{y} + 2\zeta_1 \omega_1 m_1 \dot{y} + m_1 \omega_1^2 y = \frac{-3am}{4A} \ddot{X} - m_1 \omega_1^2 \frac{l\theta}{2} - Ml\ddot{\theta} \quad \text{A.2.20}$$

where the damping ratio

$$\zeta_1 = \frac{C_1}{2\sqrt{k_1 m_1}} = \frac{12\nu}{d^2 \omega_1} \quad \text{A.2.21}$$

and ν = the kinematic viscosity at mercury

ω_1 = the natural frequency of the tiltmeter oscillator.

Frequency Response Function

Dividing Eq A.2.20 through by m_1

$$\ddot{y} + 2\zeta_1\omega_1 \dot{y} + \omega_1^2 y = -\frac{3a}{4A} \ddot{X} - \omega_1^2 \frac{l\theta}{2} - \frac{Ml\ddot{\theta}}{m_1} \quad \text{A.2.22}$$

Assume that $y = y_0 e^{j\omega t}$, $X = X_0 e^{j\omega t}$, $\theta = \theta_0 e^{j\omega t}$, and substitute in Eq A.2.22

$$y_0 = \frac{\frac{3a}{4A} \frac{\omega^2}{\omega_1^2} X_0 + (\frac{2M}{m_1} \frac{\omega^2}{\omega_1^2} - 1) \frac{l\theta_0}{2}}{1 - \frac{\omega^2}{\omega_1^2} + j2\zeta_1 \frac{\omega}{\omega_1}} \quad \text{A.2.23}$$

Since the system is linear, we may consider superposition valid and treat the response to X_0 and $l\theta_0/2$ separately. The frequency responses for X_0 and $l\theta_0/2$ are

$$\frac{y_0}{X_0} = \frac{\frac{3a}{4A} (\frac{\omega}{\omega_1})^2}{1 + j2\zeta_1 \frac{\omega}{\omega_1} - (\frac{\omega}{\omega_1})^2} \quad \text{A.2.24}$$

$$\frac{y_0}{l\theta_0/2} = \frac{-1 + \frac{2M}{m_1} \frac{\omega^2}{\omega_1^2}}{1 + j2\zeta_1 \frac{\omega}{\omega_1} - (\frac{\omega}{\omega_1})^2} \quad \text{A.2.25}$$

Part II: Refined Tiltmeter Dynamics

Summary of Oil/Mercury Subsystem Analysis

In the preceeding analysis we have assumed that the tiltmeter output y is measured by some kind of ideal sensor which does not affect the flow of mercury in the reservoirs. Consider now a particular variable capacitor sensor which utilizes a viscous dielectric oil between the fixed annular electrode and the mercury-free surface. See Fig. A.2-2.

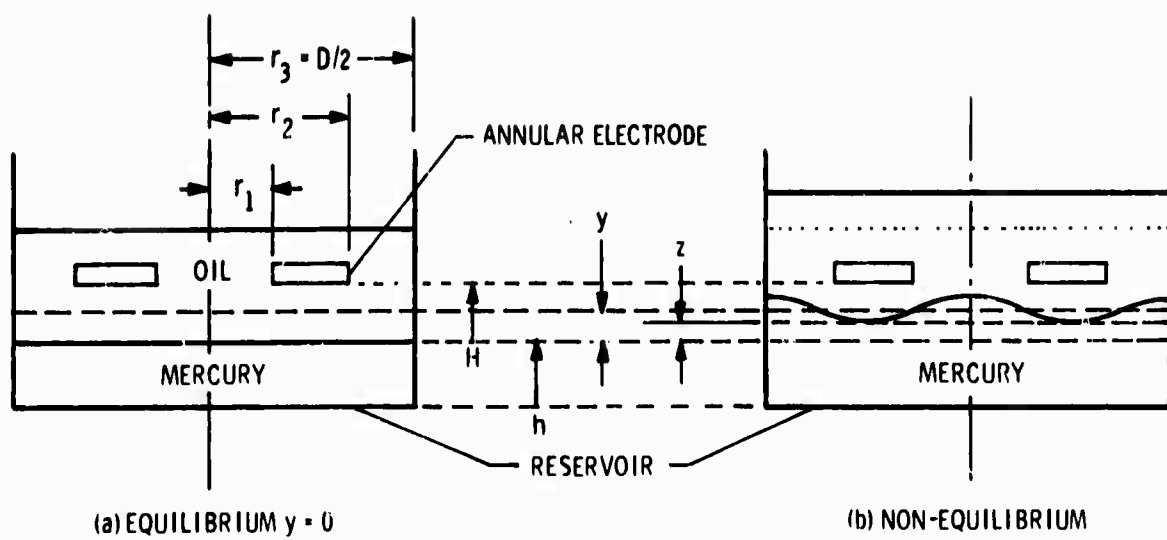


Fig. A. 2-2 Oil-filled capacitor.

The equilibrium configuration of the right-hand reservoir is shown in Fig. A.2-2(a). In the non-equilibrium state, Fig. A.2-2(b), we show that an increase of mercury volume Δy does not necessarily result in a gap decrease of y , since the oil must be squeezed out from between the fixed annular electrode and the deformed mercury surface. The actual gap change is measured by a new variable z , and the relation between y and z is time- and amplitude-dependent. This is a complicated process in which the effects of the viscosity of the oil, and the surface tension and density of the mercury, are significant. An approximate analysis of this phenomenon* shows that, for small inputs $y < H$, the gap change z is governed by the equation

$$\dot{z} + \frac{1}{\tau_c} z = \frac{1}{\tau_c} y \quad \text{A.2.26}$$

where τ_c is a rather complicated function of the oil viscosity μ , mercury weight density γ and surface tension T , and the geometric parameters H and R_i ;

$$R_i = \sqrt{\frac{\gamma}{T}} r_i \quad i = 1, 2, 3$$

$$\tau_c = \frac{3\mu}{2H^3} \frac{T}{\gamma^2} \left[\frac{R_2 - R_1}{R_2 - R_1 + 2} - \frac{R_2^2 - R_1^2}{R_3^2} \right] \left[R_2^2 + R_1^2 - \frac{R_2^2 - R_1^2}{\ln \frac{R_2}{R_1}} \right] \quad \text{A.2.27}$$

Since z and y are related by Eq A.2.26, the oil/mercury subsystem dynamics affect the tiltmeter response described in Part I. Physically, the additional pressure caused by the oil/mercury interactions impedes the flow of mercury into and out of the reservoir. This pressure is the result of the squeeze film bearing action of the oil and the additional hydrostatic pressure of the deformed mercury.

Proceeding now with the refined tiltmeter dynamics, we combine Eq A.2.22 and (A.2.26) to obtain the equation

$$m_1 C_2 \ddot{z} + (C_1 C_2 + k_2 m_1) \dot{z} + (C_1 k_2 + k_1 C_2 + k_2 C_2) z + k_1 k_2 z = -k_1 k_2 \frac{4\theta}{2} - \frac{3a}{4A} k_2 m_1 \ddot{X} \quad \text{A.2.28}$$

where the forcing term $\frac{2M}{m_1} \frac{4\theta}{2}$ has been dropped as insignificant for the parameter values of interest, and the time constant τ_c has been set equal to C_2/k_2 . Applying the Laplace transform to Eq A.2.28 yields two transfer functions in terms of the Laplace variable s and the transformed variables \bar{z} , $\bar{\theta}$, and \bar{X} :

* Dynamic Analysis of a Mercury Tiltmeter, by D. Shepard, to be published as an E note by the Charles Stark Draper Laboratory.

$$\frac{\bar{z}}{i\theta/2} = \frac{-\Omega/2\zeta_2}{S^3 + 2\zeta_1 S^2 + (1 + \Omega^2)S + \frac{\Omega}{2\zeta_2} [S^2 + 2\zeta_1 S + 1]} \quad \text{A.2.29}$$

and

$$\frac{\bar{z}}{X} = \frac{-\frac{3}{4} \frac{a}{A} \frac{\Omega}{2\zeta_2} S^2}{S^3 + 2\zeta_1 S^2 + (1 + \Omega^2)S + \frac{\Omega}{2\zeta_2} [S^2 + 2\zeta_1 S + 1]} \quad \text{A.2.30}$$

where

$$\Omega = \sqrt{\frac{k_1}{k_2}} \quad \zeta_2 = \frac{C_2}{2\sqrt{k_2 m_1}}, \text{ and } S = \frac{s}{\omega_1}$$

For a fixed tiltmeter geometry and working fluid (mercury), all the parameters in the two preceding equations are fixed, with the exception of C_2 , which depends on the ratio μ/H^3 .

By the root locus technique, the roots of the characteristic equation of the system can be studied as a function of $\zeta_2 \sim C_2$. In standard root locus form, the characteristic equation is

$$\frac{S [S^2 + 2\zeta_1 S + 1 + \Omega^2]}{S^2 + 2\zeta_1 S + 1} = \frac{-\Omega}{2\zeta_2} \equiv -K \quad \text{A.2.31}$$

where K is to vary over the range $0 < K < \infty$. By inspection, the pole-zero array is

Poles: $S = 0; S = -\zeta_1 \pm j \sqrt{\Omega^2 + (1 - \zeta_1^2)}$

Zeros: $S = -\zeta_1 \pm j \sqrt{1 - \zeta_1^2}$

These poles and zeros are plotted on the $S = \sigma/\omega_1 + j \omega/\omega_1$ plane in Fig. A.2.3. Representative values of $\zeta_1 = 0.7$, $\Omega \approx 1$ have been assumed. When $K \approx 0$, (large μ , small H), the oil squeeze film effect drastically reduces any changes in the capacitance gap. The mercury can, of course, bulge up around the capacitance plate and continue its oscillatory motion between the two reservoirs. For this case, the characteristic roots are located near the three poles (marked by X's). At the other extreme, when $K \rightarrow \infty$ the oil squeeze film effect disappears, and the system reduces to the simple tiltmeter described in Part I. For this case, the roots of the characteristic equation are located near the two finite zeros (marked as O's), one zero being located at infinity along the negative real axis.

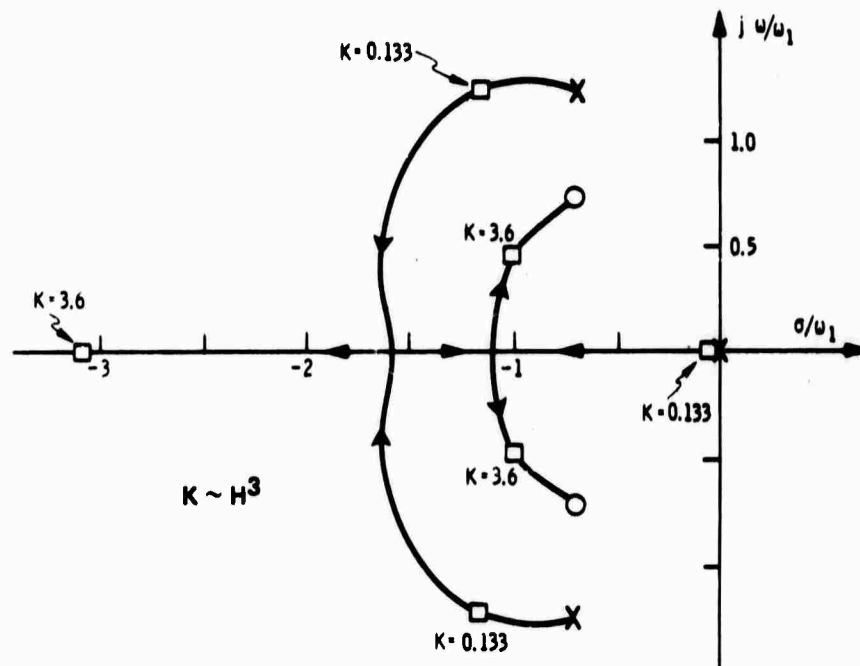


Fig. A.2-3 Root locus plot.

For the representative values

$$\mu \approx 0.13 \frac{\text{dyne} \cdot \text{sec}}{\text{cm}^2} \quad @ 100^\circ \text{F}$$

$$H \approx 10^{-2} \text{ cm.}$$

the value of $K \approx 0.133$, and the three characteristic roots are located near the poles (indicated on Fig. A.2-4 by \square 's, $K = 0.133$). The natural response of the tiltmeter to a disturbance will then be of the form

$$z(t) = C_1 e^{-t/\tau} + C_2 e^{-\zeta \omega_n t} \sin(\omega_n \sqrt{1 - \zeta^2} t + \alpha) \quad \text{A.2.32}$$

where $\tau \approx 348 \text{ s}$, $\zeta \approx 0.68$ and $\omega_n \approx 7.5 \times 10^{-2} \text{ rad/s}$; and the constants C_1 , C_2 and phase α are determined by the initial conditions and the form of the disturbance input. The frequency response corresponding to $K = 0.133$ will be presented in the next section of this chapter.

The question immediately arises as to how the system could be modified to match the more desirable response characteristics of the simple system described in Chapter 1. From a physical point of view, it is clear that the obstructive effect of the viscous oil squeeze film must be significantly reduced. This can be

accomplished by decreasing the ratio μ/H^3 . Since the viscosity of the dielectric oil is relatively difficult to change, the desired effect can be obtained by increasing the gap dimension H.

To study the effect of gap change on the system response, consider an increase in H by a factor of three over its original value of 10^{-2} cm. Then K changes to $K = 3.6$ ($K \sim H^3$), and the corresponding characteristic locations change as indicated in Fig. A.2-3. The natural response will be given by Eq A.2.32, but with new values of τ , ζ , and ω_n .

These values, as well as values corresponding to other gap changes, are tabulated below.

H	K	τ	ζ	ω_1
0 cm	0	∞ s	0.35	6.1×10^{-2} rad/s
10^{-2}	0.133	348	0.68	7.3×10^{-2}
3×10^{-2}	3.6	7.5	0.9	4.8×10^{-2}
10×10^{-2}	133	0.175	≈ 0.7	$\approx 4.3 \times 10^{-2}$
∞	∞	0	0.7	4.3×10^{-2}

For values of $H > 3 \times 10^{-2}$ cm, the time constant τ can be approximated by

$$\tau \approx \frac{1}{K\omega_1} = \frac{1.75 \times 10^{-4}}{H^3} \tag{A.2.33}$$

where H must be given in centimeters and τ in seconds.

Frequency Response Functions

We assume steady-state harmonic inputs $X = X_o e^{j\omega t}$ and $\theta = \theta_o e^{j\omega t}$, and output to $z = z_o e^{j\omega t}$. Then the transfer functions, Eq (A.2.29) and (A.2.30) can be inverted back from the S domain and put in the form of the frequency response functions

$$\frac{z_o}{\frac{l}{2}\theta_o} = \frac{-1}{(j\omega\tau + 1) \left[1 + j2\zeta \frac{\omega}{\omega_1} - \left(\frac{\omega}{\omega_1} \right)^2 \right]} \tag{A.2.34}$$

$$\frac{z_o}{X_o} = \frac{+ \frac{3a}{4A} \left(\frac{\omega}{\omega_1}\right)^2}{(j\omega\tau + 1) \left[1 + j2\zeta \frac{\omega}{\omega_1} - \left(\frac{\omega}{\omega_1}\right)^2 \right]} \quad \text{A. 2. 35}$$

A log magnitude plot for these functions is given in Chapter 2 for various values of gap dimension H taken from the table on page A.2-9. The first-order break frequency occurs at $\omega_b = \frac{1}{\tau}$. For values of $H > 3 \times 10^{-2}$ cm, the approximation for τ given by Eq A.2-33 is valid, and

$$\omega_b \approx \frac{H^3}{1.75 \times 10^{-4}}$$

APPENDIX A.3

MECHANICAL DRAWINGS AND LIST

Mechanical Drawing List

MIT Seismic Tiltmeter Mod II

Installation Outline Assembly	E 175003
Coaxial tube assembly	E 174952
Coaxial tube junction box	E 174959
Mercury chamber--adjustable	E 174990
Mercury chamber--fixed	E 174991
Mercury shielding base plate--short	C 175005-1
Mercury shielding base plate--long	C 175005-2
Mercury shielding tube--short	C 175006-1
Mercury shielding tube--long	C 175006-2
Mercury chamber elec. shield	D 175014
Coaxial tube support	C 175015
Filter electronics package	E 175020
Filter electronics package weldment	E 175021
Filter box	C 175042
Bridge electronics	D 175049
Mercury Chamber--Adjustable	E 174990
Capacitor shaft	C 174988
Capacitor shaft support	C 174958
Capacitor shaft driver	C 174957
Capacitor plate	B 174981
Capacitor mounting disc	C 174945
Upper locking nut	A 174971
Lower locking nut	A 174970
Sliding mount	B 174972
Sliding mount body	B 174973
Floating mount body	A 174974
Mercury chamber	D 174943
Floating mount	A 174975
Fixed mount	A 174976
Shim	A 174955
Air inlet tube sub-assembly	B 174951
Cover plate	C 174944

Mechanical Drawing List (cont)

Handwheel segment	B 174979
Mercury inlet elbow	B 174953
Elbow adapter	B 174977
Elbow adapter washer	A 174978
Air inlet bushing	A 174980
Capacitor mounting disc retainer	A 174982
Oil inlet bushing	A 174983
Index mount	B 174984
Index rod	B 174985
Dial machining	B 174992
Mercury Chamber--Fixed	E 174991
Mercury chamber	D 174943
Cover plate	C 174944
Capacitor shaft--fixed	C 174986
Fixed shaft support	C 174987
Oil inlet bushing	A 174983
Retainer shim	A 174956
Retainer plate	A 174989
Mercury inlet elbow	B 174953
Elbow adapter washer	A 174978
Elbow adapter	B 174977
Capacitor mounting disc	C 174945
Capacitor plate	B 174981
Capacitor mounting disc retainer	A 174982
Air inlet bushing	A 174980
Air inlet tube sub-assembly	B 174951
Fixed mount	A 174976
Shim	A 174955
Sliding mount	B 174972
Sliding mount body	B 174973
Floating mount	A 174975
Floating mount body	A 174974
Capacitor mounting disc sub-assembly	C 174948

Mechanical Drawing List (cont)

Coaxial Tube Assembly	E 174952
Coaxial tube junction box adapter	C 174998
Coaxial tube end plug	C 174999
Wire holder	B 175000
Coaxial tube cable disc	B 175001
Coaxial tube coupling	B 175002
Coaxial tube insulating end cap	C 175004
Inner tube	C 175009-1
Inner tube	C 175009-2
Coaxial tube B	C 175010
Coaxial tube A	C 175011
Inner tube with drain holes	C 175012
Coaxial tube C	C 175013
Coaxial Tube Support	C 175015
Component Board	C 175023
Air Inlet Tube Sub-Assembly	B 174951
Air inlet, block	A 174940
Air inlet, tube	B 174941
Filter Box Modifications and Lettering Plate	C 175042
Bridge Electronics	D 175049
Micrometer Syringe Sub-Assembly	B 174996
Retainer ring	A 174993
Retainer	B 174994
Syringe support	B 174996
Level Assembly	D 175097
Level base assembly	D 175077
Level adapter	C 175078
Hinge	B 175079
Adjustment screw	B 175093
Level fastening bushing	B 175094
Calibration Fixture	
Micrometer adapter	C 175086
Calibration panel	D 175098
Adapter bellows	C 175099

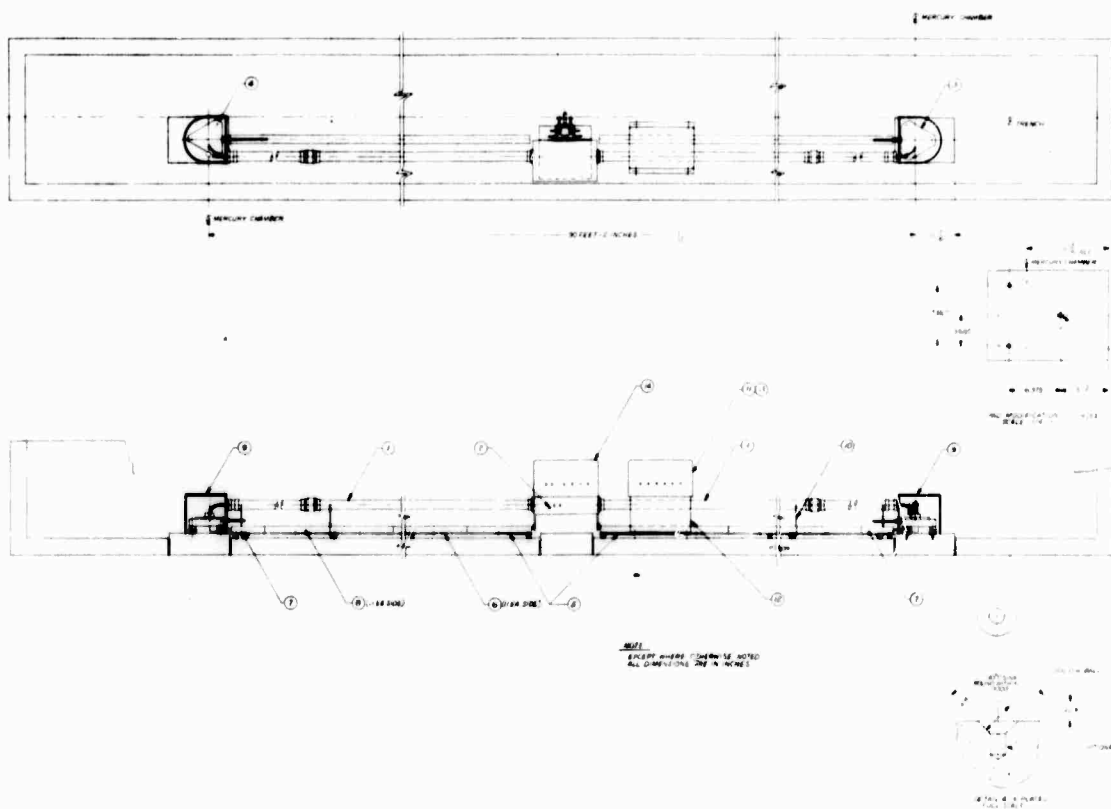


Fig. A. 3-1 Seismic tiltmeter - Mod II - installation.

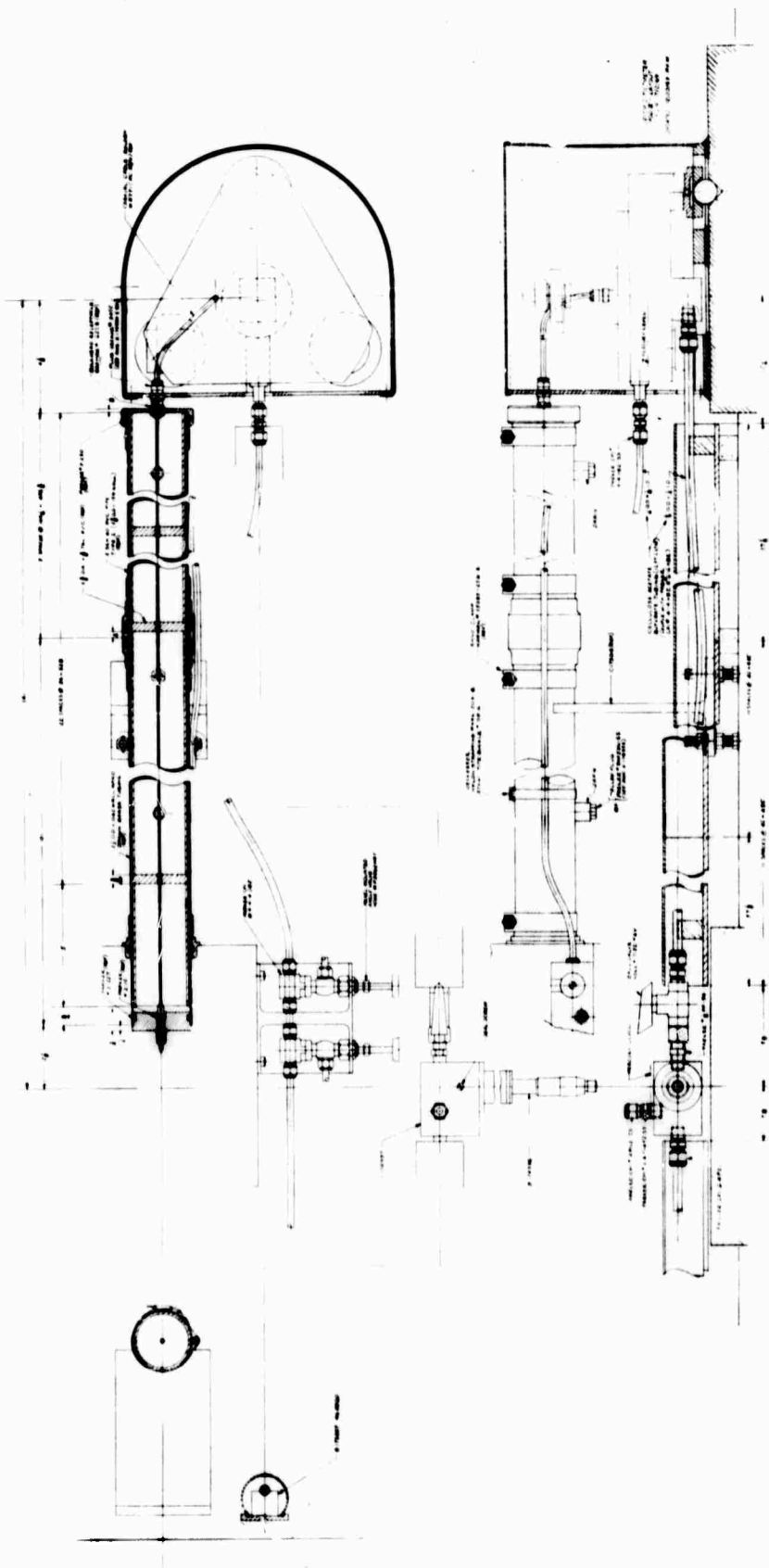


Fig. A. 3-2 Seismic tiltmeter - Mod II - layout.

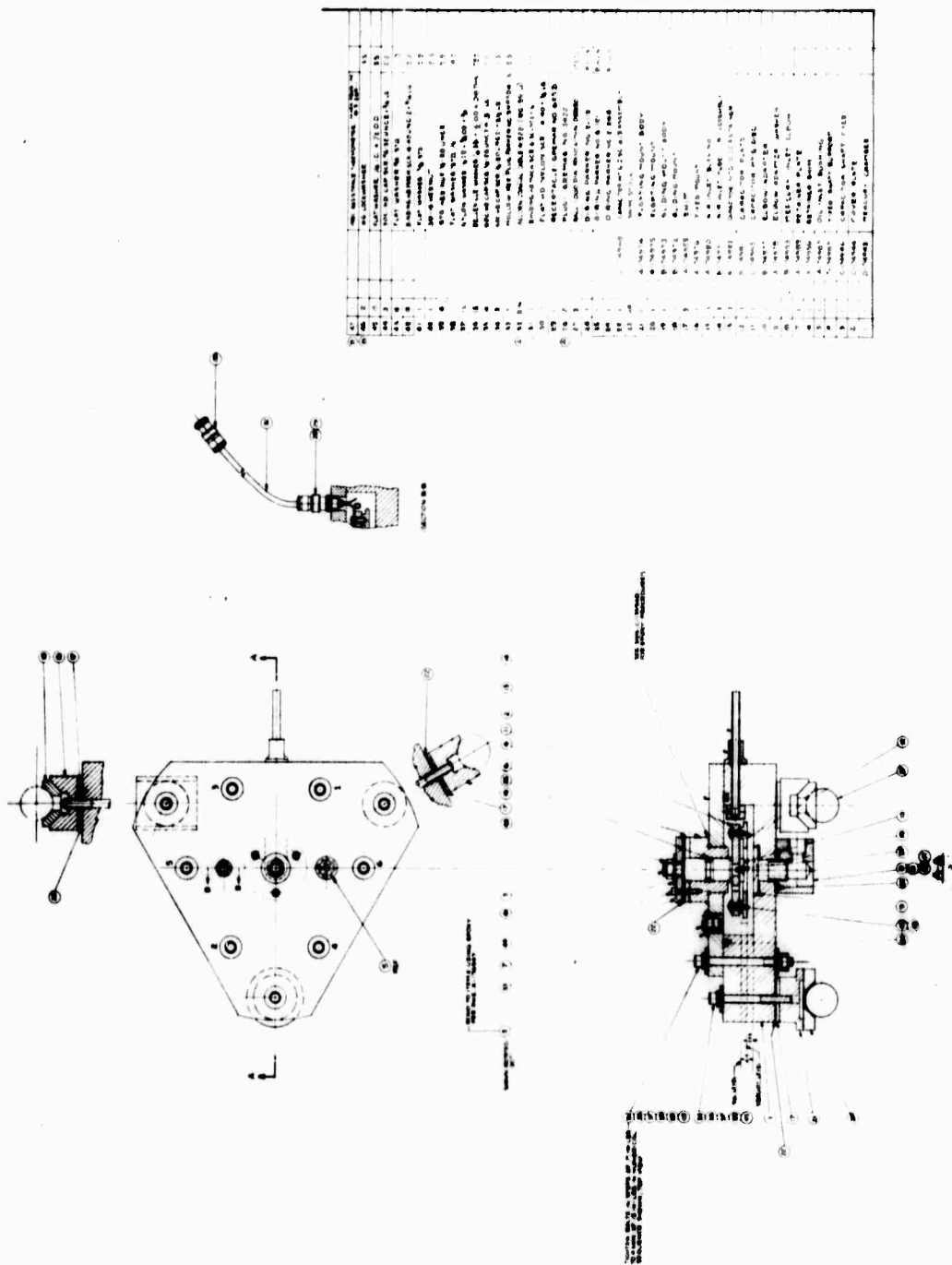


Fig. A. 3-3 Mercury chamber-fixed seismic tiltmeter - Mod II.

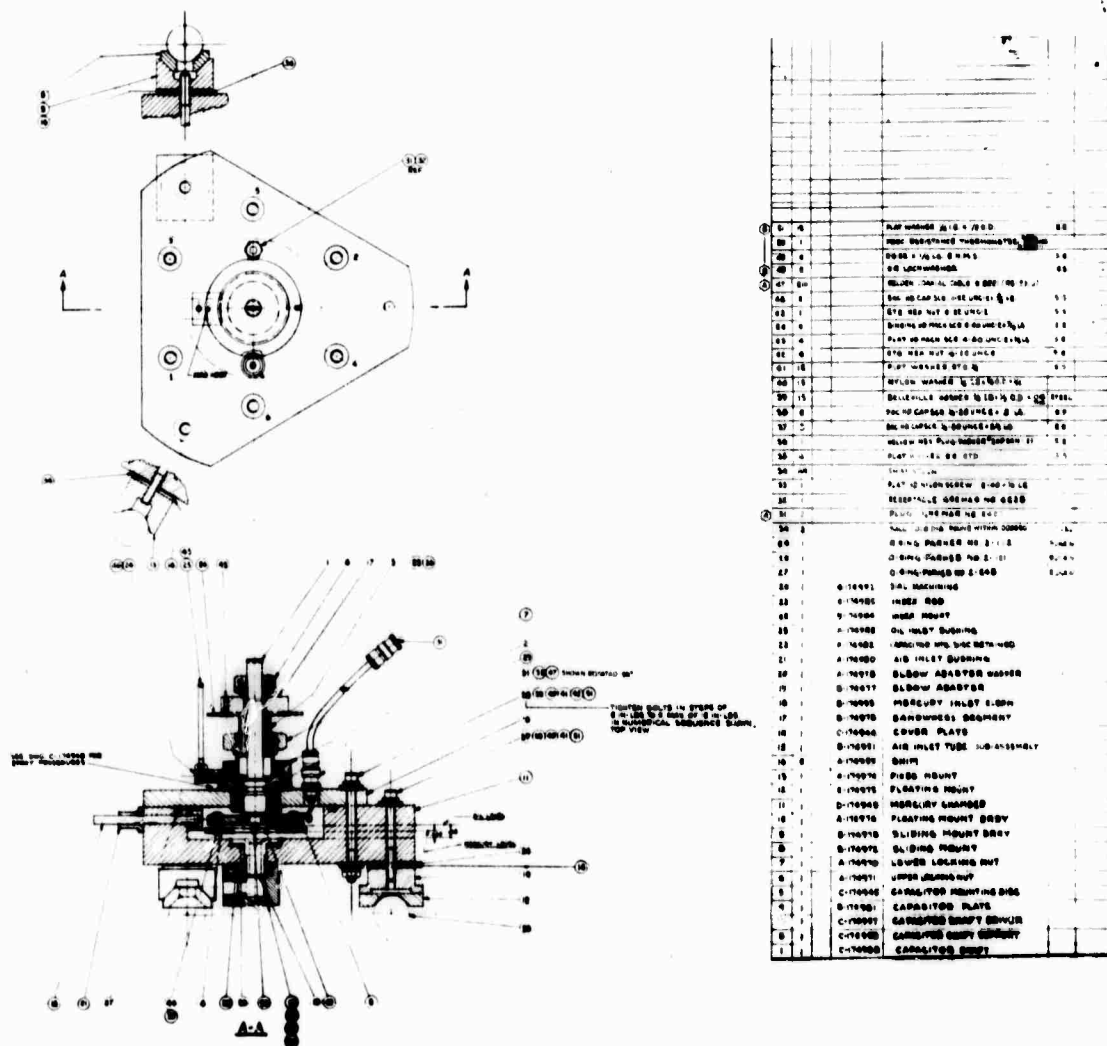


Fig. A.3-4 Mercury chamber-adjustable seismic tiltmeter - Mod II.

APPENDIX B.1

TILTMETER HIGH-FREQUENCY CIRCUITS

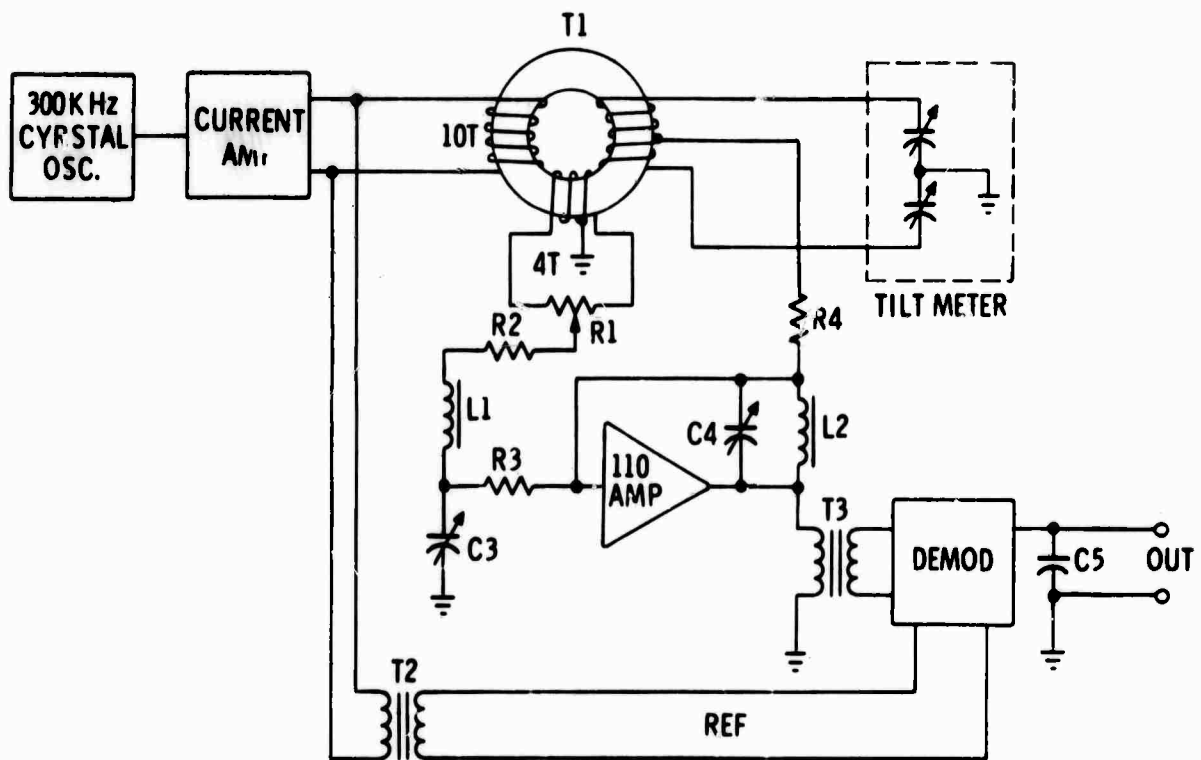


Fig. B.1-1 Tiltmeter high frequency circuits.

Overall Circuit

The high-frequency circuits of the tiltmeter are shown in Fig. B.1-1. The operation of the circuit as a whole will first be described, followed by a more detailed discussion of each component.

The crystal oscillator drives the current amplifier, which delivers its output to bridge transformer T_1 . T_1 steps up the voltage from the current amplifier 10:1, and one of its secondaries constitutes two arms of an ac bridge circuit; the other two arms consist of the differential capacity tiltmeter mercury tanks.*

*See Appendix B.4

An auxiliary winding on T_1 via a potentiometer R_1 and resonant circuit $L_1 C_3$ provides quadrature correction. The output of the bridge is the centre tap of T_1 's main secondary. This signal is fed into a tuned feedback amplifier with a voltage gain of about 10.

The output of the signal amplifier drives a phase-sensitive demodulator which obtains its reference voltage via transformer T_2 whose primary is in parallel with T_1 's primary. The output of the demodulator is a dc signal of about 10 volts max; this is positive for positive tilt angles, and vice versa. The dc signal is filtered by large condenser C_5 since speed of response is unimportant.

Since the tiltmeter is an open-loop system, all components must be precise and stable, and all amplifiers must employ negative feedback both for gain stability and linearity. DC drift has been reduced by making the high-frequency signal as large as possible before it is demodulated. This expedient reduces the drift problem encountered in the dc amplifiers following the demodulator.

Crystal Oscillator

The Greenray Industries oscillator produces a 300 kc output at 10 volts rms. Its frequency is constant to $\pm 0.001\%$ with time and temperature, and its amplitude is constant to 0.1%.

Current Amplifier

The circuit of the current amplifier is shown in Fig. B.1-2.

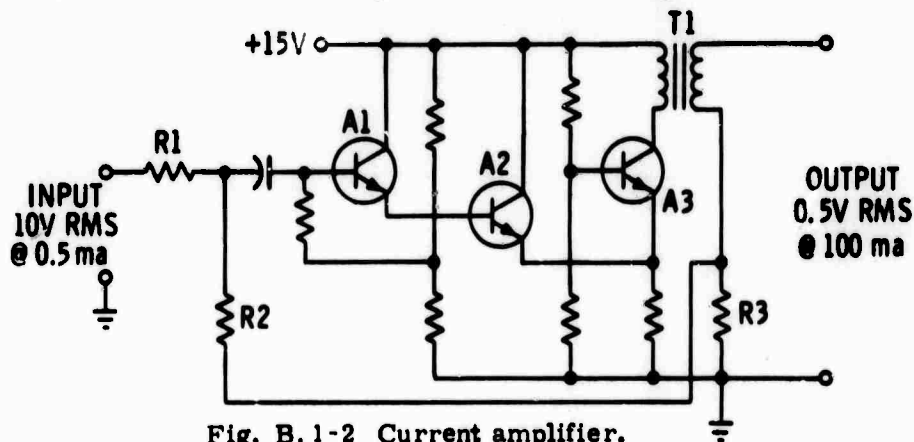


Fig. B.1-2 Current amplifier.

It consists of output stage A_3 , operated in a common base configuration having an inherently high output impedance. A_3 's low input impedance is driven by emitter follower A_2 . A_2 's base is driven by another emitter follower, A_1 . To augment further the output impedance, negative current feedback is employed via R_1 , R_2 , R_3 . This feedback also increases gain stability and linearity. The output impedance of this amplifier is about 300 ohms, which is large compared with the 5-ohm impedance reflected into the T_1 primary by the tiltmeter. A change of 10% in tiltmeter impedance will produce only 0.15% change in T_1 primary current.

Bridge Transformer, T_1

Transformer T_1 may be considered one of the most important parts of the system because it is a part of the tiltmeter bridge. This transformer consists of a ferrite toroid, considerably larger than necessary, so that all windings are in single layers, minimizing interwinding capacity. Also, large wire is used to minimize copper drops. Sufficient primary and secondary turns are used to produce a small magnetic flux in the core (about 200 gauss), resulting in very low core loss. Furthermore, the toroid configuration has no air gaps to vary with time, temperature, clamping pressure, etc. Bifilar winding of the center-tapped secondary results in identical resistances and close coupling of the two halves. The secondary is electrostatically shielded with copper foil on both top and bottom. Inductance of the windings is small so that the transformer primary looks almost purely capacitive (the capacity reflected by the tiltmeter), i.e., transformer and load are operated above their resonant frequency. A small auxiliary winding of four turns is provided for quadrature correction. With 0.5 volt rms @ 100 mA in the primary, 5.0 volts @ 10 mA appears at the main secondary and 0.2 volt @ 0.8 mA at the auxiliary secondary.

Use of transformer secondary for two of the bridge arms isolates the circuitry so that the mercury in the tiltmeter may be grounded.

Quadrature Correction

Provided the losses in the tiltmeter are small and nearly identical, a bridge signal of 0.5 volt exactly in phase with the primary should be produced with a perfect null at zero tilt angle. Moreover, since the demodulator is phase-sensitive, it rejects quadrature. However, some quadrature is always present and is compensated by means of the four-turn winding on T_1 , a potentiometer R_1 , and the series resonant circuit L_1C_3 . R_1 is a 250-ohm wire-wound potentiometer. When C_3 is adjusted for resonance, a voltage in quadrature with the main signal is produced. It can be made of either polarity because the centre tap of the four-turn secondary is grounded. The quadrature correction is fed into the signal amplifier via R_3 . It represents only a few percent of the maximum bridge output.

Signal Amplifier

The signal amplifier is an Analog Devices model 110. This amplifier is completely solid-state and has an open-loop voltage gain of about 200. The closed-loop gain is about 10, giving a negative voltage feedback factor of 20, which is sufficient for stability and linearity. Parallel resonant circuit L_2C_4 appears as 150,000 ohms at resonance. The other arm of the feedback is R_4 . A tuned amplifier reduces noise at the amplifier output. The maximum output is about 5 volts rms.

Demodulator

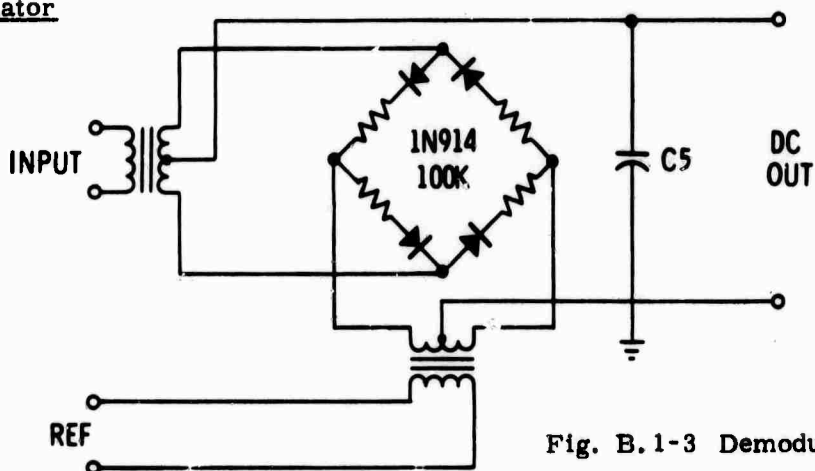


Fig. B.1-3 Demodulator.

The circuit of the demodulator is shown in Fig. B. 1-3. It is a standard diode ring consisting of four diodes, four resistors and two transformers with center-tapped secondaries. The diodes are switched by the reference voltage; the dc output voltage is approximately equal to the peak voltage across half the T_3 secondary, provided this voltage is smaller than half of the voltage across the T_2 secondary. When the signal voltage becomes large enough to be nearly equal to the reference voltage, no increase in dc output is produced for a further increase in signal voltage, i. e. the demodulator limits. To insure linearity, the reference voltage is twice the expected maximum signal voltage.

The demodulator obtains its reference from the T_1 primary. The phase angle between signal and reference voltages must be maintained at zero, however much the phase angle with respect to some absolute reference may change (as a result of change in tiltmeter impedance). It can be seen that, however much the impedance of the tiltmeter may change, the phase relations between bridge output, quadrature correction and reference do not change at all (provided T_1 is a perfect transformer). The demodulator output versus signal input varies little with the phase angle between signal and reference voltage when this angle is near zero, since the demodulator output is a cosine function of the angle. The quadrature rejection ratio is a sine function of this angle, however, so for good quadrature rejection it is important to keep the phase angle small. It has been found possible to make this ratio as high as 50:1 in practice. When adjusting the circuits, this phase angle is adjusted by detuning C_4 slightly from resonance to compensate for small phase shifts in T_1 , T_2 , and T_3 . This results in a loss of gain in the signal amplifier of about 10%.

For good linearity in this type of demodulator, both signal and reference voltages should be large with respect to the voltage breaks of the diodes. The overall circuit linearity was checked by substituting accurately-calibrated variable

air condensers for C_1 and C_2 in the tiltmeter, varying C_1 and C_2 and measuring the dc output from the demodulator. Since the nonlinearity of the system is less than 3% the linearity of the demodulator is even better.

Impedance Considerations

Common mode rejection approaching the ideal can be attained, provided the source driving the bridge (referred to T_1 secondary) is at least 5000 ohms. The effect of all of the shunt paths on T_1 primary (referred to the secondary) will be considered here.

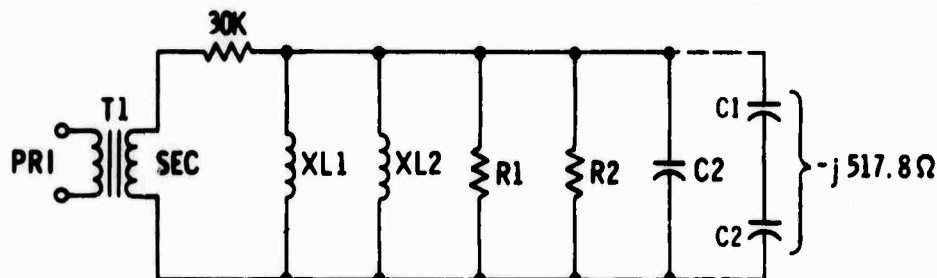


Fig. B. 1-4 Capacitance bridge.

All of these components are shown in the equivalent circuit in Fig. B. 1-4. An itemized list with values is shown below:

X_{L1} , T_1	shunt inductance	$j\ 56,500$ ohms
X_{L2} , T_2	shunt inductance	$j\ 43,300$ ohms
R_1 ,	reflected resistance from demod.	25,000 ohms
R_2 ,	reflected from quad. correction secon	156,250 ohms
C_L ,	fixed shunting capacity (line and strays)	$-j\ 13,200$ ohms

When all of these components are added vectorially the result is:

21,550 ohms in parallel with $-j\ 28,600$ ohms

The absolute value is 17,000 ohms shunting the 30,000-ohm Z down to 10,300 ohms, still a sufficiently high input impedance for nearly-ideal linearity and common mode rejection. The most important component is seen to be R_1 , the resistance reflected by the demodulator. This could be eliminated by interposing a buffer amplifier between T_1 and T_2 primaries, but the extra components seem to be unwarranted.

The effects of X_{L1} and X_{L2} are actually beneficial since they partially tune out C_L . By placing a small adjustable inductance of the right value in parallel with C_L , it would be possible to eliminate C_L entirely and make the bridge behave as if there were no constant capacitive component. The correct value of inductance to use in this case would be about 15 millihenrys.

APPENDIX B. 2

SPECIAL ELECTRONICS FOR 4 MIL TILTMETER

The high-frequency circuits of the 4-mil tiltmeter are shown in semi-block form in Fig. B. 2-1.

Much of the circuitry has been discussed previously in Appendix B. 1, but has been modified considerably. At the risk of some repetition, it will be described again in more detail.

Overall Circuit

The crystal oscillator drives the current amplifier; the latter's output drives bridge transformer T_1 . T_1 steps up the voltage from the current amplifier 10:1. One of its secondaries constitutes two arms of an ac bridge circuit. The other two arms consist of the differential capacity tiltmeter mercury tanks. An auxiliary winding on T_1 via a potentiometer R_1 and resonant circuit $L_1C_1C_2$ provides quadrature correction. The output of the bridge is the centre tap of T_1 's main secondary. This signal is fed into a feedback amplifier with a voltage gain of about 28.

The output of the signal amplifier drives a phase-sensitive demodulator which obtains its reference voltage by amplifying the voltage across T_1 primary with an amplifier identical to the signal amplifier. The reference voltage is applied to the demodulator via T_3 . The output of the demodulator is a dc signal of about 15 volts maximum which is positive for positive tilt angles, and vice versa. The dc signal is filtered by large condenser C_3 since speed of response is unimportant.

Since the tiltmeter is an open-loop system, all components must have high precision and stability, and all amplifiers must employ negative feedback for both gain stability and linearity. DC drift has been reduced by making the high-frequency signal as large as possible before it is demodulated. This reduces the drift problems which may be encountered with dc amplifiers following the demodulator.

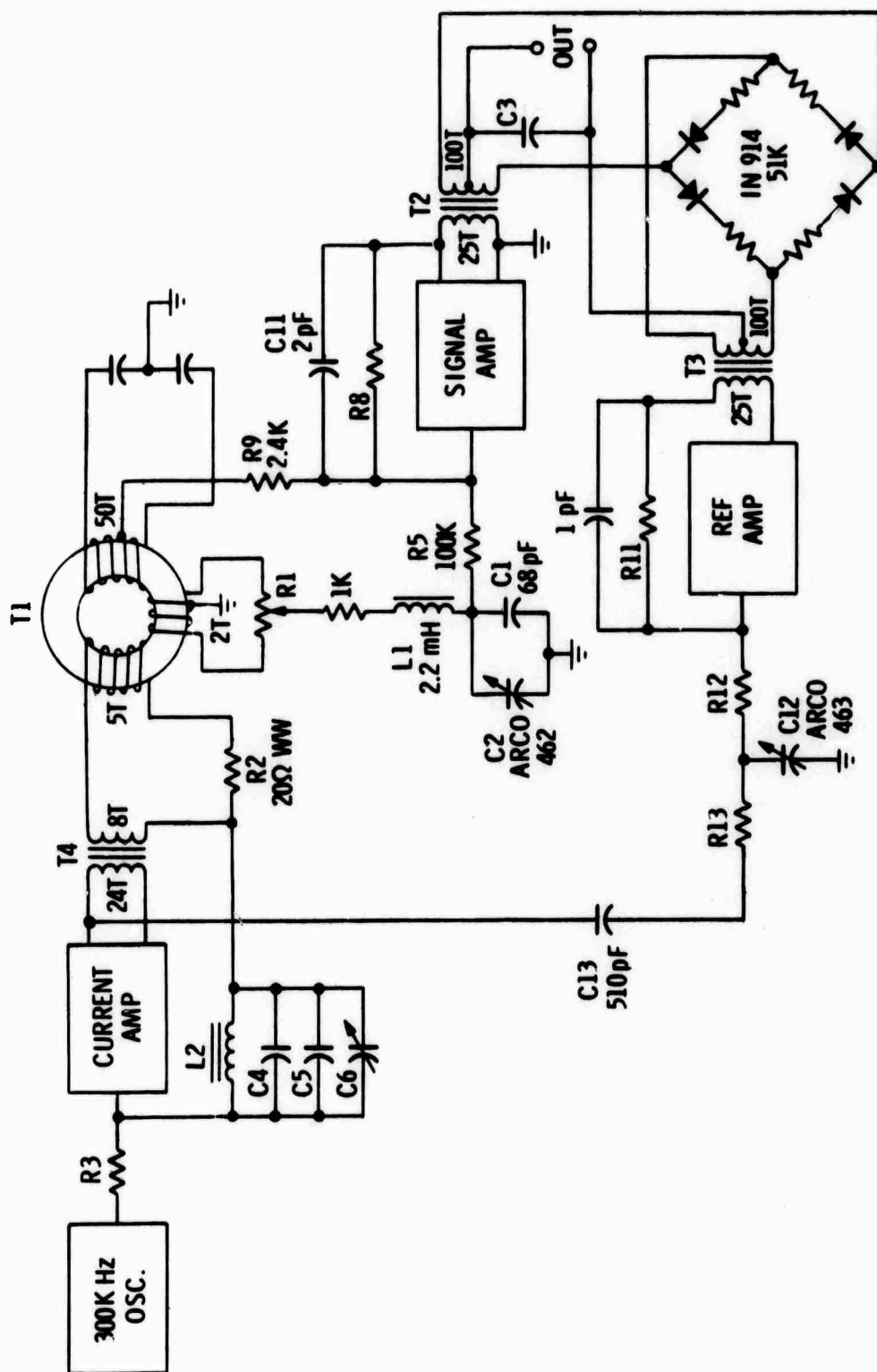


Fig. B.2-1 Differential capacitance bridge.

Current Amplifier

The circuit of the current amplifier is shown in Fig. B.2-2. It consists of output stage A_3 operated in a common base configuration having inherently high output impedance. A_3 's low input impedance is driven by emitter follower A_2 . A_2 's base is driven by another emitter follower A_1 which makes the input impedance high (100,000 ohms). Zener diode D_1 holds the base of A_3 at zero RF potential.

The output impedance at A_3 's collector is about 5000 ohms. This impedance is stepped down 9:1 by T_4 . This is undesirable but necessary because of the low load impedance (4 ohms looking into the bridge transformer primary) which must be driven. The overall output impedance is augmented by negative current feedback via R_2 , R_3 , L_2 , C_4 , C_5 , C_6 . The feedback factor of this network is about 2500. Feedback also increases gain stability and linearity. The parallel resonant circuit L_2 , C_4 , C_5 , C_6 filters the somewhat-distorted output of the crystal oscillator. The parallel resonant resistance is 2500 ohms, which together with R_2 and R_3 , determines the gain. R_4 C_7 suppresses oscillations at extremely high frequencies. High-frequency suppression is used in several of the circuits described herein. It should be further noted that RF decoupling filters (e.g. L_3 C_8) are provided in the supply leads of all circuits. The overall output impedance of the current amplifier is at least 1000 ohms. A 10% change in load resistance will produce a change in output current of 0.05%. A source impedance of ten times the load impedance has been found to be sufficient in practice. The current amplifier's source impedance is at least 200 times this value, and therefore more than sufficient.

When subjected to a temperature change from 30°C to 65°C, the only observable effect on the circuit was an increase in DC current drain of 1%.

Bridge Transformer

This component may be considered one of the most important parts of the system because it is a part of the tiltmeter bridge. The ferrite toroid is considerably larger than necessary so that all windings are in single layers minimizing inter-winding capacity. Large wire is used to reduce copper drops. Also a sufficient number of primary and secondary turns are used to produce a small magnetic flux in the core (about 400 gauss), resulting in very low core loss. Furthermore, a toroid configuration has no air gap to vary with time, temperature, clamping pressure, etc. The centre-tapped secondary forms two arms of the bridge. It is, therefore, bifilar wound so that the resistances of each half are identical and the coupling between halves is very close. The main secondary is electrostatically shielded with copper foil on both top and bottom. Inductive reactance of the windings is so much higher (about 100 times) than the capacitive

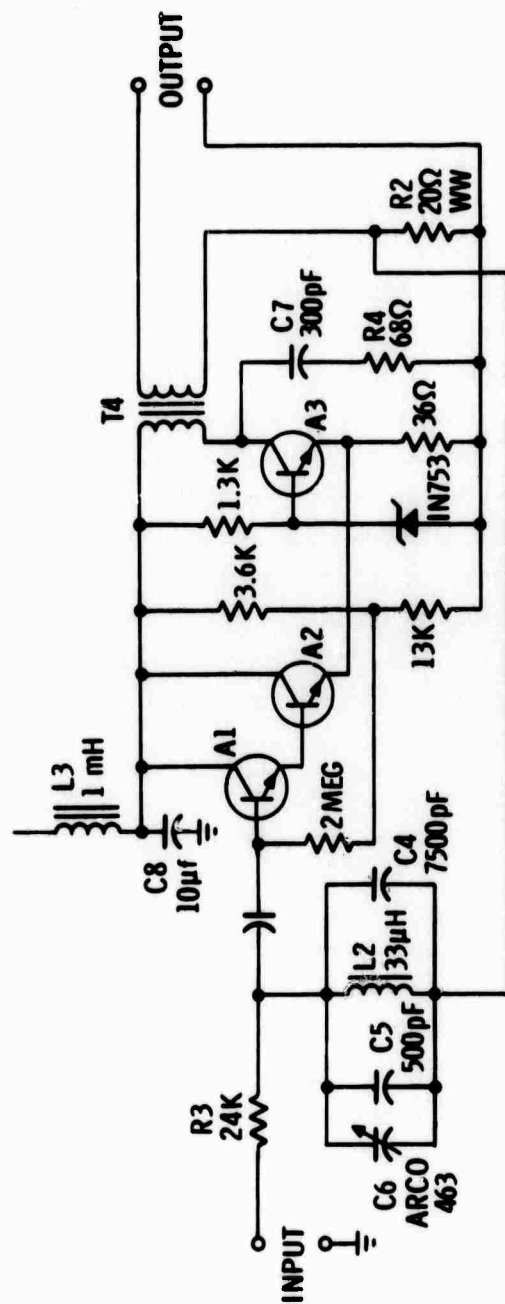


Fig. B.2-2 Current amplifier.

reactance reflected by the tiltmeter that the transformer primary looks almost purely capacitive; i.e., transformer and load are operated well above their resonant frequency. A small auxiliary winding of two turns is provided for quadrature correction. With 0.28 volt rms @ 70 mA in the primary, 2.8 volts @ 7.0 mA appears at the main secondary and 0.11 volt @ 0.44 mA at the auxiliary secondary.

A transformer is used for two of the bridge arms so that the mercury in the tiltmeter may be grounded.

Quadrature Correction

If the losses in the tiltmeter capacities are either identical or small and nearly equal, a bridge output signal of 0.314 volt rms (1 mil tilt) max exactly in phase with the primary will be produced, with a perfect null at zero tilt angle. Moreover, since the demodulator is phase-sensitive, it rejects quadrature. However, some quadrature is always present, and it is bucked out by means of the two-turn winding on T_1 , a potentiometer R_1 , and a series resonant circuit L_1, C_1, C_2 . R_1 is a 250-ohm wire-wound potentiometer. When C_2 is adjusted for resonance, a voltage in quadrature with the bridge signal is produced. It can be made either \pm quadrature because the centre tap of the two-turn secondary is grounded. The quadrature is fed into the signal amplifier via R_5 . It represents only a few percent of the maximum bridge output.

Signal and Reference Amplifiers

These amplifiers are identical except for input and feedback resistors. They were designed specifically for this application because no standard amplifier could be found which had a high-enough output voltage or a large-enough open-loop gain at this frequency. It is also desirable for an amplifier of this type to recover from gross overload without "latchup", a form of hysteresis. The amplifiers require transformer-coupled outputs to drive the demodulator.

One major consideration in the design of these amplifiers was maximum output voltage (for reasons previously mentioned). It was found difficult to design output transformers with turns-ratio step-up of more than 1:4 because of interwinding capacity. However, it was possible to design amplifiers which would produce a maximum voltage of 18 volts rms at the output transformer primary (72 volts across the secondary). A second important design consideration was the maximum feedback factor. At high frequency, it is necessary to minimize the number of stages because the accumulation of phase shifts due to the input capacity of each stage leads to instability. Two stages were the most usable in this application. With only two stages, dc feedback for stabilization of the operating points became difficult. Voltage feedback was desired for low output impedance, but two

stages produced the wrong sense of feedback. Therefore, it was necessary to use negative current feedback. This type of feedback is desirable from all points of view except for its effect on output impedance. An examination of the circuit in Fig. B.2-3 will show how these conflicting factors were handled.

DC negative current feedback via R_6 R_7 stabilizes the operating points of A_4 and A_5 . C_9 is large ($0.1 \mu f$) and prevents current feedback from operating at 300 kc. It is estimated that the dc feedback factor is about 1000. AC negative voltage feedback is provided in an outer loop via a feedback winding on T_2 , R_8 and R_9 . The shortcomings of this arrangement were minimized with bifilar and feedback windings, insuring tight coupling, and taking advantage of the fact that the loading on the output winding was a constant, high impedance. In this connection, all measurements of the amplifier output must be made either at A_5 collector or at the high end of the feedback winding since loading due to oscilloscope capacity will completely alter impedance relations when making measurements at the secondary terminals.

Calculation of the open-loop gain of this amplifier at low frequency yields a figure of about 200,000. Due to the input capacitance of each stage, the realized gain is about 10,000. Even this value can be obtained only by making R_8 and R_9 as small as possible (limited by source impedance at the input). In spite of these limitations a feedback factor as high as 500 can be obtained, more than sufficient for the requirements.

As previously mentioned, oscillation suppression was necessary as shown in Fig. B.2-3 by C_{10} , R_{10} and C_{11} . The time constant of R_8 C_{11} should be about 0.1 microsecond, depending upon the value of R_8 for the closed-loop gain required. If C_{11} is too small, oscillations at > 1 MHz will occur, while if it is too large it will cause phase shift at the operating frequency. In any case, C_{11} is very small (< 10 pF).

The reference amplifier (B.2 4) is operated at a voltage gain two-three times higher than the signal amplifier. Consequently, its feedback factor and performance are correspondingly lower. However, the requirements of the reference amplifier are lower. The only difference between these amplifiers is in input circuitry. The signal amplifier contains provision for two inputs: bridge and quadrature correction, while the reference amplifier has provision for a precise adjustment of the phase angle between signal and reference voltages. A summary of signal amplifier performance is given below:

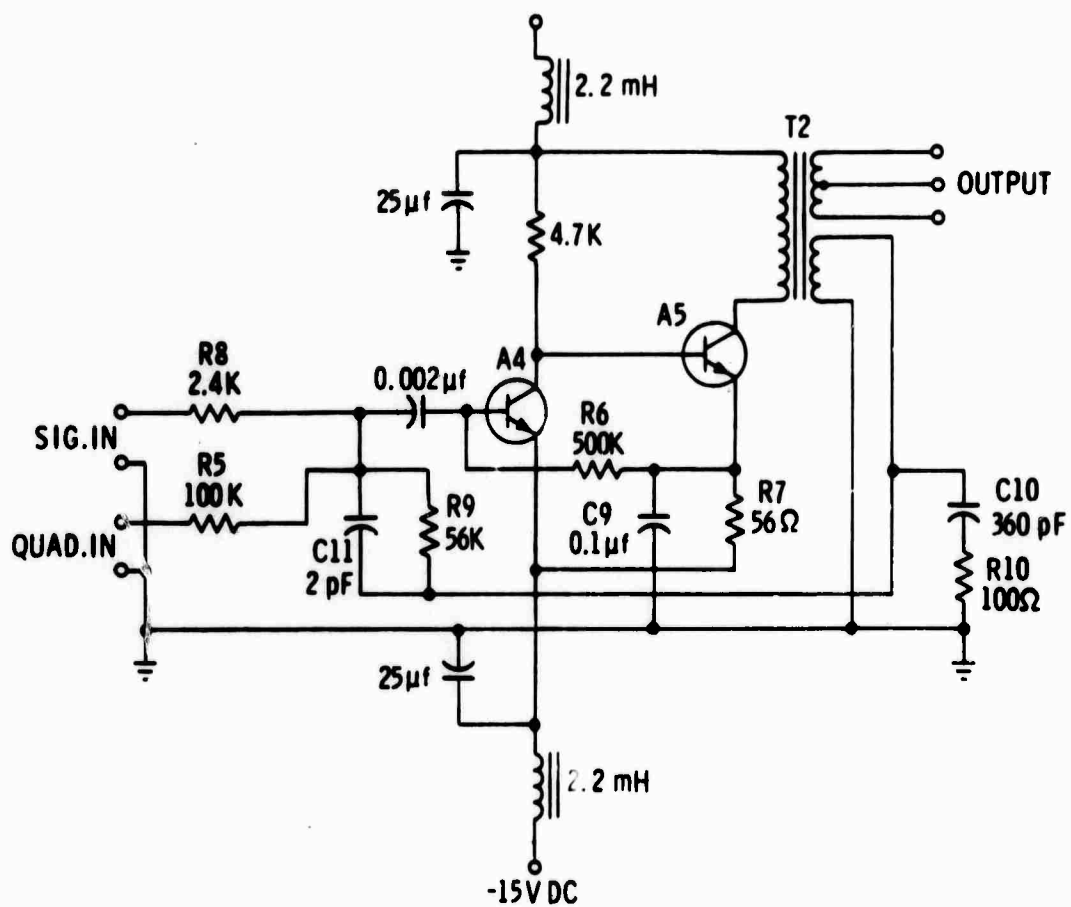


Fig. B.2-3 Signal amplifier.

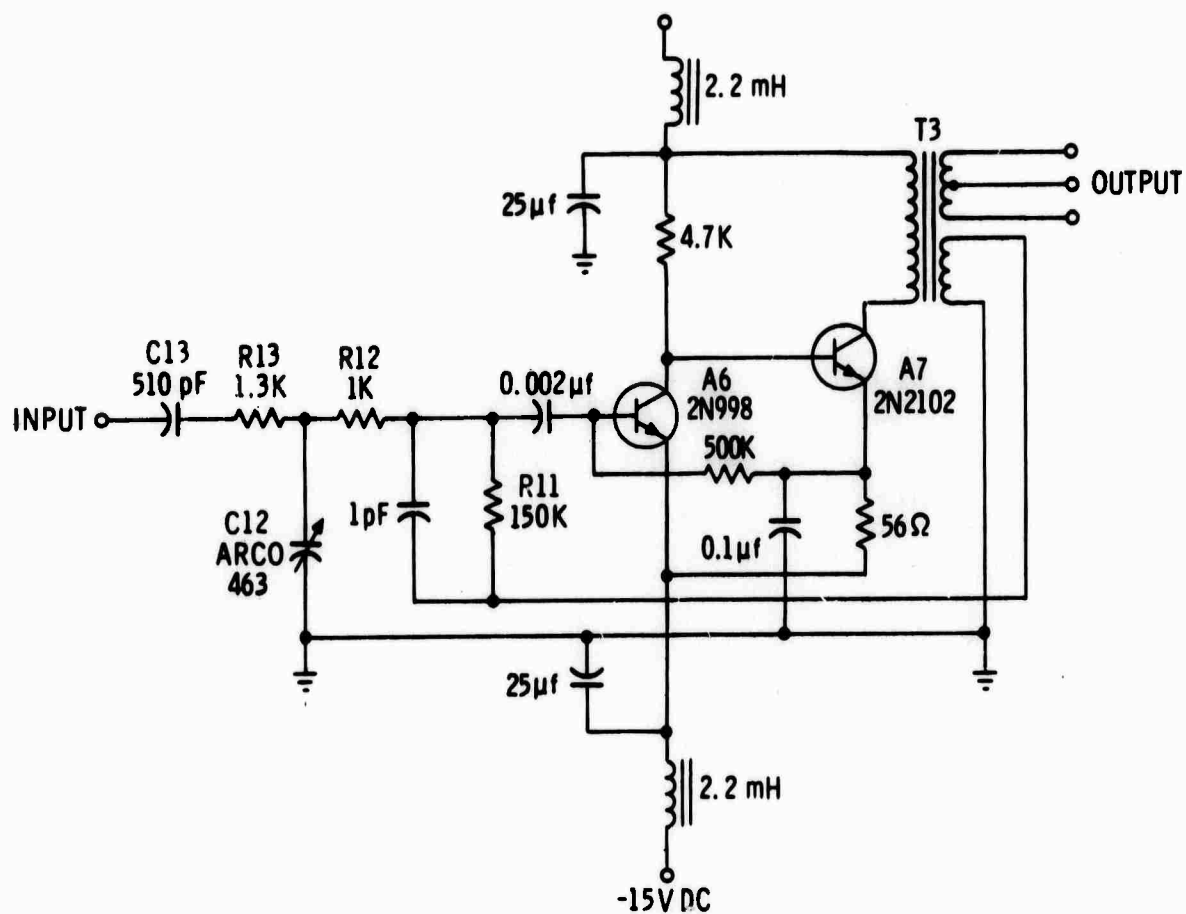


Fig. B.2-4 AC reference amplifier.

Feedback factor:	500
Output impedance:	15 ohms
Harmonic distortion:	0.15%
Overload point:	14.7 volts rms
Input impedance:	2.4K
Noise:	0.7 mv rms

Tests for Putting System into Operation

Equipment required

Oscilloscope with zero phase shift in X and Y inputs at 300 kc and capable of detecting 0.5 mV at Y input at dc and 300 kc. If the tiltmeter itself is not available, it may be simulated by fixed condensers and trimmers. To simulate null, each condenser should have about 2250 pF capacity. To simulate maximum tilt, one should have 1850, the other 2917 pF.

Step 1

Scope X at output of crystal oscillator; scope Y at high end of R_2 (20-ohm resistor in current amplifier); adjust C_6 until voltage across R_2 peaks. It should peak at 1.4 volts rms approximately in phase with the input. If this voltage is not this value, change R_3 . Transfer scope Y to high end of T_1 primary. The voltage there should be 0.28 volts in quadrature with the input.

Step 2

Scope X at high end of T_1 primary; scope Y at high end of signal amplifier (T_2) feedback winding; make simulated tiltmeter condensers 2250 pF each (adjust for null). Set R_1 at one end of its travel and adjust C_2 for open ellipse or circle. Y should have maximum amplitude for this setting of C_2 .

Step 3

Make one simulated tiltmeter condenser 1850 pF; the other 2917 pF (maximum tilt); the voltage at the signal amplifier feedback winding should be between 8 and 9 volts rms. It may be adjusted by changing the value of R_9 .

Step 4

Scope Y at high end T_1 primary; scope X at high end of feedback winding of the reference amplifier; the voltage at this point should be between 12 and 14 volts rms. It may be adjusted by changing the value of R_{11} .

Step 5

Scope X at high end of T_1 primary; scope Y at demod output; scope set for dc; simulated tiltmeter capacity as in Step 3; demodulator dc output should be about 15 volts; reversing the positions of 1850 pF and 2917 pF condensers should produce the same demodulator output with reversed polarity (the two polarities will differ somewhat if there is appreciable demodulator unbalance at bridge null).

Step 6

Scope as in Step 5; simulated tiltmeter capacity as in Step 2. Turn R_1 through its full travel and adjust C_{12} so that changing R_1 does not change demodulator output (this puts signal and reference voltages exactly in phase for best quadrature rejection). C_{13} should be selected by trial so that C_{12} is near the middle of its range when quadrature rejection is obtained. If C_{12} must be made larger for quadrature rejection, C_{13} should be made larger, and vice versa. After these adjustments have been made, check the reference voltage again as in Step 4.

Step 7

Scope X at high end of T_1 primary; scope Y at high end of signal amplifier feedback winding; simulated tiltmeter condensers 2250 pF each; adjust these and R_1 for null (a few millivolts).

APPENDIX B.3

OPERATION OF DIODE RING DEMODULATOR

The circuit of the diode ring demodulator is shown in Fig. B.3-1 (a). The reference voltage must be larger than the signal voltage. Suppose that, at some instant, point A is positive with respect to point B; diodes D_1 and D_2 conduct and the circuit can be redrawn as in Fig. B.3-1 (b). Since D_3 and D_4 are reverse-biased by the reference voltage at this instant, they can be considered open circuit. The whole reference secondary is charged to $1/2$ the signal secondary potential through R_1 and R_2 , as is C.

On the next half-cycle, the conditions are shown in Fig. B.3-1 (c). D_3 and D_4 conduct, while D_1 and D_2 are open circuits. The circuit behaves exactly as on the first half-cycle, except C is charged through R_3 and R_4 instead of R_1 and R_2 . C is still charged positively, since the upper half of the signal secondary is positive on this half-cycle.

Thus it is seen that the rectification is full wave and that C is charged to $1/2$ the peak voltage of the reference secondary, provided R_1 and R_2 (and R_3 and R_4) in parallel constitute with C a short time-constant compared with half an ac period, and RC is long. This implies that the resistors should be made as small as possible (provided the reference and signal sources can supply the current), and that the diodes' forward impedance should be low. Also, C should be loaded as lightly as possible (R large). Therefore, the diode ring demodulator has a low-input impedance and a high-output impedance.

There is amplitude comparison between the instantaneous potential on C and the signal potential, since the diodes are held switched on by the reference voltage, and signal current can flow through them in either direction. Therefore the output of the demodulator is updated with respect to the signal on each half-cycle. This property is important when speed of response must be considered.

If the signal secondary terminals were reversed with respect to the reference secondaries (or vice versa), the charge on C would be reversed also. Therefore, the rectification is phase-sensitive.

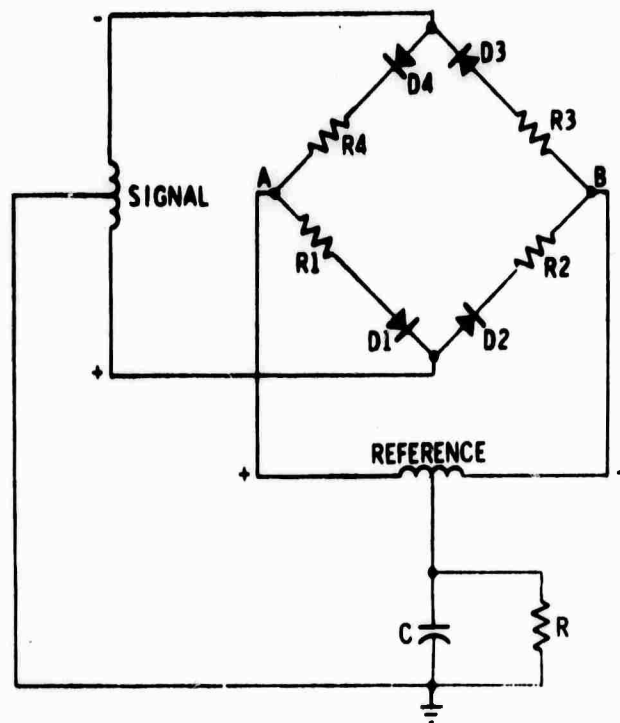


Fig. B. 3-1 (a) Demodulator.

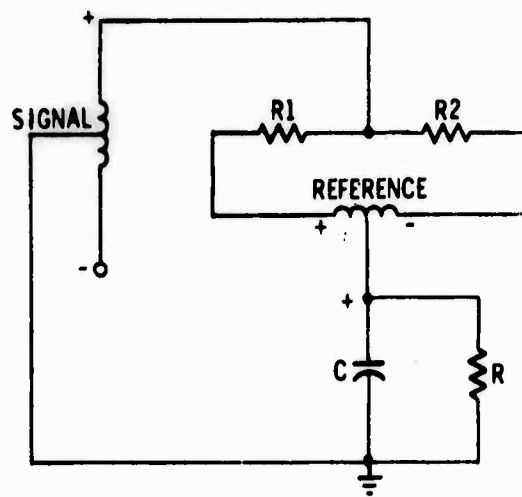


Fig. B. 3-1 (b) Demodulator.

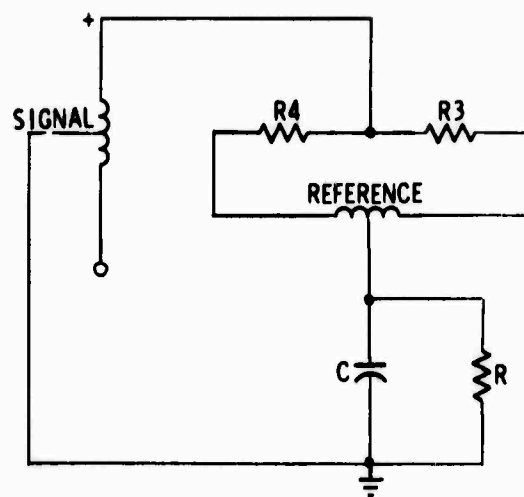


Fig. B.3-1 (c) Demodulator.

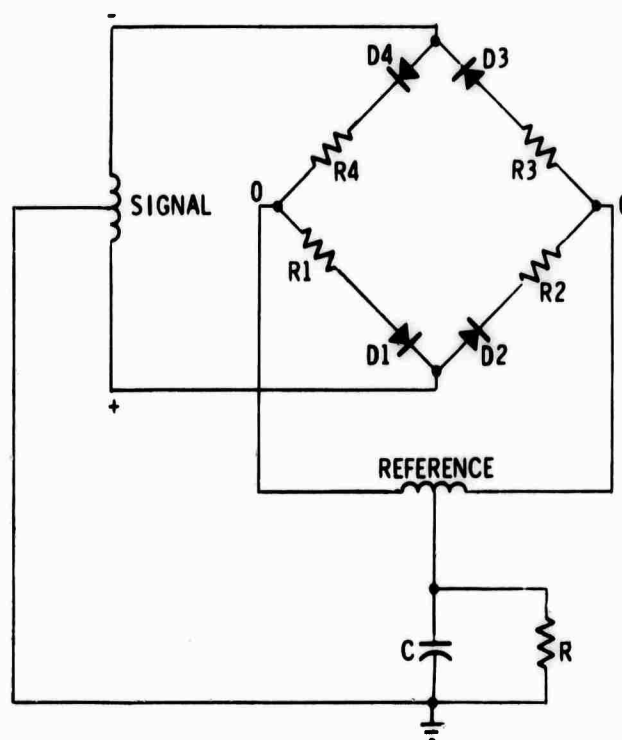


Fig. B.3-1 (d) Demodulator.

If the signal voltage is in quadrature with the reference (or contains a quadrature component), a signal voltage will be present while the reference voltage is passing through zero. Under these conditions, the diodes will be switched by the signal voltage only, as in Fig. B.3-4. Diodes D_2 and D_3 will conduct, while D_1 and D_4 will be open. The voltage at the junction of R_2 and R_3 will be the same as at the signal secondary center tap, and there will be no potential difference to charge C. On the opposite half-cycle the action is the same, except that D_1 and D_4 conduct while D_2 and D_3 are open. Thus, the quadrature component gives zero output, i.e., the diode ring demodulator rejects quadrature.

If there is no reference voltage present, there will be no demodulator output provided the circuit is perfectly balanced. This action will also take place if the reference voltage is smaller than the signal voltage. In fact, the demodulator output will be approximately equal to one-half the signal secondary peak voltage until the latter approaches the reference value. If the signal voltage is made larger than the reference voltage, there will be no further increase in demodulator output, i.e., the demodulator limits.

APPENDIX B.4

CERTAIN NONLINEARITIES AND ERRORS IN A CAPACITIVE BRIDGE TILTMETER

The electrical arrangement for the capacitive bridge tiltmeter is shown in Fig. B.4-1.

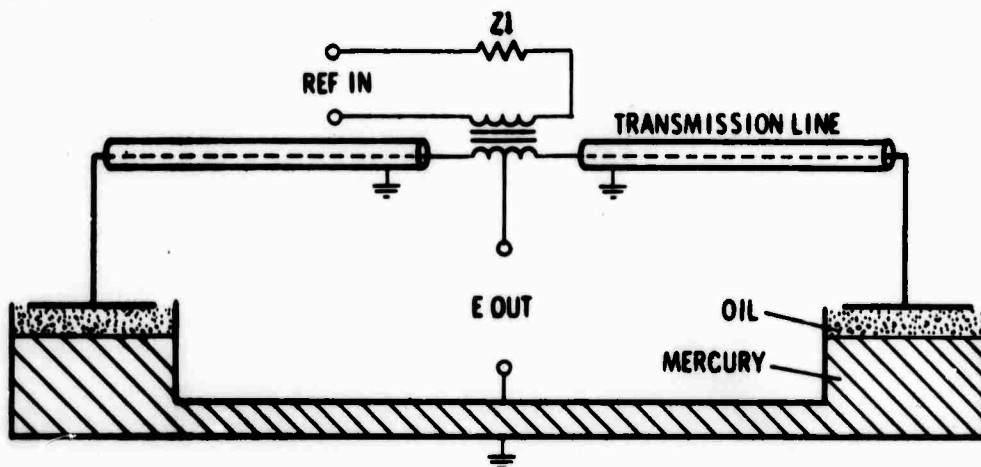


Fig. B.4-1 Capacitance bridge tiltmeter.

Linearity and Scale Factor

If each gap were 40 mils at zero tilt and $K = 5$ for the oil in the gap, $C_1 = (8000/t_1) + 50$ pF and $C_2 = (8000/t_2) + 50$ pF where t_1 is the thickness of gap 1 and t_2 is the thickness of gap 2. The extra 50 pF in each equation is the capacity of each transmission line and strays.

If we redraw Fig. B.4-1 schematically we have:

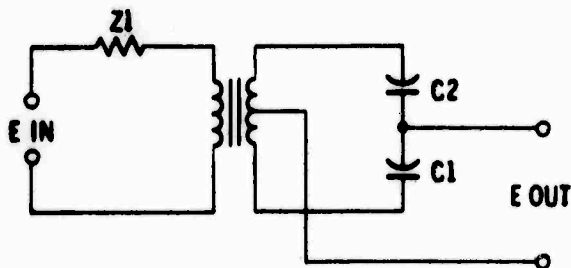


Fig. B.4-2 Bridge transformer.

For a 1:1 ratio center-tapped transformer,

$$\frac{E_{out}}{E_{in}} = \frac{1}{2} - \frac{Xc_1}{Xc_1 + Xc_2} \quad B.4.1$$

$$\frac{E_{out}}{E_{in}} = \frac{1}{2} - \frac{\frac{1}{\omega c_1}}{\frac{1}{\omega c_1} + \frac{1}{\omega c_2}} \quad B.4.2$$

or

$$\frac{E_{out}}{E_{in}} = \frac{1}{2} - \frac{C_2}{C_1 + C_2} \quad B.4.3$$

If we assume that all of the capacity is variable (i.e., neglect the transmission lines and strays)

$$C_1 = \frac{8000}{t_1} \quad B.4.4$$

and

$$C_2 = \frac{8000}{t_2} \quad B.4.5$$

Substituting (4) and (5) in (3)

$$\frac{E_{out}}{E_{in}} = \frac{1}{2} - \frac{\frac{8000}{t_2}}{\frac{8000}{t_2} + \frac{8000}{t_1}} = \frac{1}{2} - \frac{t_1}{t_1 + t_2} \quad B.4.6$$

for gaps of 40 mil varying ± 1 mil

$$\frac{E_{out}}{E_{in}} = \frac{1}{2} - \frac{41}{39+41} = 0.0125 \text{ volt/mil tilt/volt bridge excitation,}$$

Since 10 mil tilt gives exactly 10 times the output as 1 mil, the linearity is perfect.

If we make the gaps 4 mil ± 1 mil max, we obtain exactly the same result.

Since the constant part of the capacity cannot be neglected in practice, we substitute Eq (B.4.1) and (B.4.2) into (B.4.3) to take this component into account:

since $t_1 + t_2 = 80$ mils, $t_2 = 80 - t_1$ and

$$\frac{E_{out}}{E_{in}} = \frac{\frac{8000}{80-t_1} + 50}{\frac{8000}{80-t_1} + 50 + \frac{8000}{t} + 50}$$

or

$$\frac{E_{out}}{E_{in}} = \frac{1}{2} - \frac{240t - t^2}{12,800 + 160t - 2t^2} \quad B.4.7$$

It can be seen from Eq (B.4.7) that the fixed component of capacity introduces higher-order terms which affect the linearity.

To determine the magnitude of this effect, let $t_1 = 41$ mil; from Eq (B.4.7)

$$\frac{E_{out}}{E_{in}} = \frac{1}{2} - \frac{9840 - 1681}{12,800 + 6660 - 3362} = 0.01000 \text{ volt/mil tilt/volt bridge excitation}$$

The first result of adding the line capacity is seen to be a reduction in bridge sensitivity of 25%

if we let $t_1 = 50$ (10 mil of tilt)

$$\frac{E_{out}}{E_{in}} = \frac{1}{2} - \frac{12,000 - 2,500}{12,800 + 8000 - 5000} = 0.101266$$

The second result of adding the line capacity is the introduction of a 1.266% nonlinearity at maximum tilt. It can be shown that this nonlinearity is a smaller percentage for smaller tilt angle.

If we make the gaps $4 \text{ mil} \pm 1 \text{ mil}$, Eq (B.4.7) becomes

$$\frac{E_{out}}{E_{in}} = \frac{1}{2} - \frac{168t - t^2}{1280 + 16t - 2t^2} \quad B.4.8$$

Let $t_1 = 4.1 \text{ mil}$

$$\frac{E_{out}}{E_{in}} = \frac{1}{2} - \frac{688.8 - 16.8}{1280 + 65.6 - 33.6} = 0.012195 \text{ volts/0.1 mil/volt}$$

Let $t_1 = 5 \text{ mil}$

$$\frac{E_{out}}{E_{in}} = \frac{1}{2} - \frac{840 - 25}{1280 + 80 - 50} = 0.012214 \text{ volt/0.1 mil/volt}$$

if we divide the second result by the first to non-dimensionalize

$$\frac{E_{out}}{E_{in}} \text{ for 5 mil is } 1.0016 \text{ or } 0.16\% \text{ nonlinearity}$$

The two results of making the variational part of the capacity 10 times larger than in the first case is to increase the bridge sensitivity about 22%, approaching the 25% value for zero fixed capacity, and to reduce the nonlinearity from 1.266% to 0.16%.

Common-Mode Error

For a 40-mil gap, 1 mil of tilt and $Z = 0$ in Fig. B.4-1.

$$\frac{E_{out}}{E_{in}} = 0.01000 \text{ volt/mil tilt/volt bridge excitation as shown above.}$$

If we now introduce a common-mode error by increasing both gaps by 1 mil, i.e. $t_1' = 40$ mil and $t_2' = 42$ mil from Eq (B.4.1, B.4.2, B.4.3), we have

$$\frac{E_{out}}{E_{in}} = \frac{1}{2} - \frac{\frac{8000}{t_2} + 50}{\frac{8000}{t_2} + 50 + \frac{8000}{t_1} + 50} = 0.009662 \text{ a common-mode error of } 3.38\%$$

Increasing both gaps reduces the loading on the source, making the bridge excitation larger. It follows that increasing Z should make $\frac{E_{out}}{E_{in}}$ larger, thus reducing common-mode error, provided we increase the source voltage to compensate for the loss of voltage caused by inserting Z . This can be done by inserting a physical resistance and correspondingly increasing the source voltage or, preferably, by making the source a negative current feedback amplifier. We examine the way in which the common-mode error varies with source impedance, both for 4-mil and 40-mil gaps.

For the 40-mil case,

$$\frac{E_{out}}{E_{in}} = \left(\frac{\sqrt{Z^2 + X_c}}{X_c} \right) \left(\frac{X_c'}{\sqrt{Z^2 + X_c'^2}} \right) \left(\frac{C_2'}{C_1' + C_2'} \right) \quad \text{B.4.9}$$

The first term on the right side of Eq (B.4.9) represents the amount by which the source voltage must be increased to compensate for the loss in Z , X_c being the capacity looking into the bridge, i.e., the reactance of the two bridge capacities in series. The second term in Eq (B.4.9) is the common-mode correction, and the third term is the bridge sensitivity factor.

X_c and X_c' are found by $X_c = \frac{1}{2\pi fc}$

$$C_1' = 250.0\text{pF}$$

$$C_2' = 240.5\text{pF}$$

for $f = 300\text{kc}$

$$C_1 = 255.1\text{pF}$$

$X_c = 4246\text{ ohms}$ and $X_c' = 4329\text{ ohms}$

$$C_2 = 245.1\text{pF}$$

Substituting these values in Eq (B.4.9) we obtain

$$\frac{E_{out}}{E_{in}} = \left(\frac{\sqrt{Z^2 + 4246^2}}{4246} \right) \left(\frac{4329}{\sqrt{Z^2 + 4329^2}} \right) \quad (0.009662)$$

$\frac{E_{out}}{E_{in}}$ is the bridge output with common mode error. We wish to vary Z to see what effect it has on that error. If first we make Z very large, we see that the CM error approaches a limit $\frac{4329}{4246} \times 1.0338 = 0.009851$, a common-mode error of 1.49%. This shows that, with a perfect current source (infinite Z), the CM error is still nearly half of the uncorrected value. This is because the line capacity shunts and therefore limits the source impedance Z . If we make $Z = 10^4$, the common mode error is 1.55%, or near enough to the limit for all practical purposes. In this case, a source impedance of 2 to 3 times the bridge impedance is the maximum useful value.

For the 4-mil gap we substitute values in Eq (B.4.9) as before and obtain

$$\frac{E_{out}}{E_{in}} = \left(\frac{\sqrt{Z^2 + 571.8^2}}{517.8} \right) \left(\frac{528.3}{\sqrt{Z^2 + 530.5^2}} \right) \quad (0.01188)$$

For $Z = 0$ (uncompensated for CM),

$$\frac{E_{out}}{E_{in}} = 0.01188 \text{ volts/0.1 mil/volt bridge excitation}$$

This represents a CM error of 2.58%. For large Z , the CM error approaches a limit of

$$\frac{528.3}{517.8} \times 0.01188 = 0.012121 = 0.61\%$$

For a Z for 5000 ohms the CM error is 0.66%, near enough to the limit for all practical purposes. In this case a source impedance of about ten times the bridge

impedance is the maximum useful value. It is higher than in the former case because of the reduced shunting by the fixed capacity.

Conclusion

A large fixed value shunting the variable capacitive component is detrimental in three ways:

1. It reduces bridge sensitivity.
2. It increases bridge nonlinearity.
3. It makes it impossible to improve common-mode rejection appreciably by increasing the source impedance above a certain value.

One minor factor which has not been considered is the variation of bridge impedance with tilt angle. In this respect, a fixed capacitive component is helpful, but this factor is too small to be of significance.

It has been demonstrated that increasing the bridge capacity (decreasing the gap) is beneficial in three ways. It has been found possible to increase the bridge excitation 50% and drive impedance to 5000 ohms with a drive amplifier of reliable design. A 4-mil gap increases the sensitivity by 1220%.

APPENDIX B. 5

STUDY OF LINEARITY VERSUS CAPACTOR GAP

TILTMETER SENSITIVITY

$$S = \frac{E_o}{E_i} = \frac{1}{2} - \frac{56t - t^2}{768 + 48t - 2t^2}$$

Gap (mil)	S
9	+ 0.092
9.5	0.077
10	0.061
10.5	0.046
11.0	0.030
11.5	0.015
12.0	0
12.5	-0.015
13.0	-0.030
13.5	-0.046
14.0	-0.061
14.5	-0.077
15	-0.092

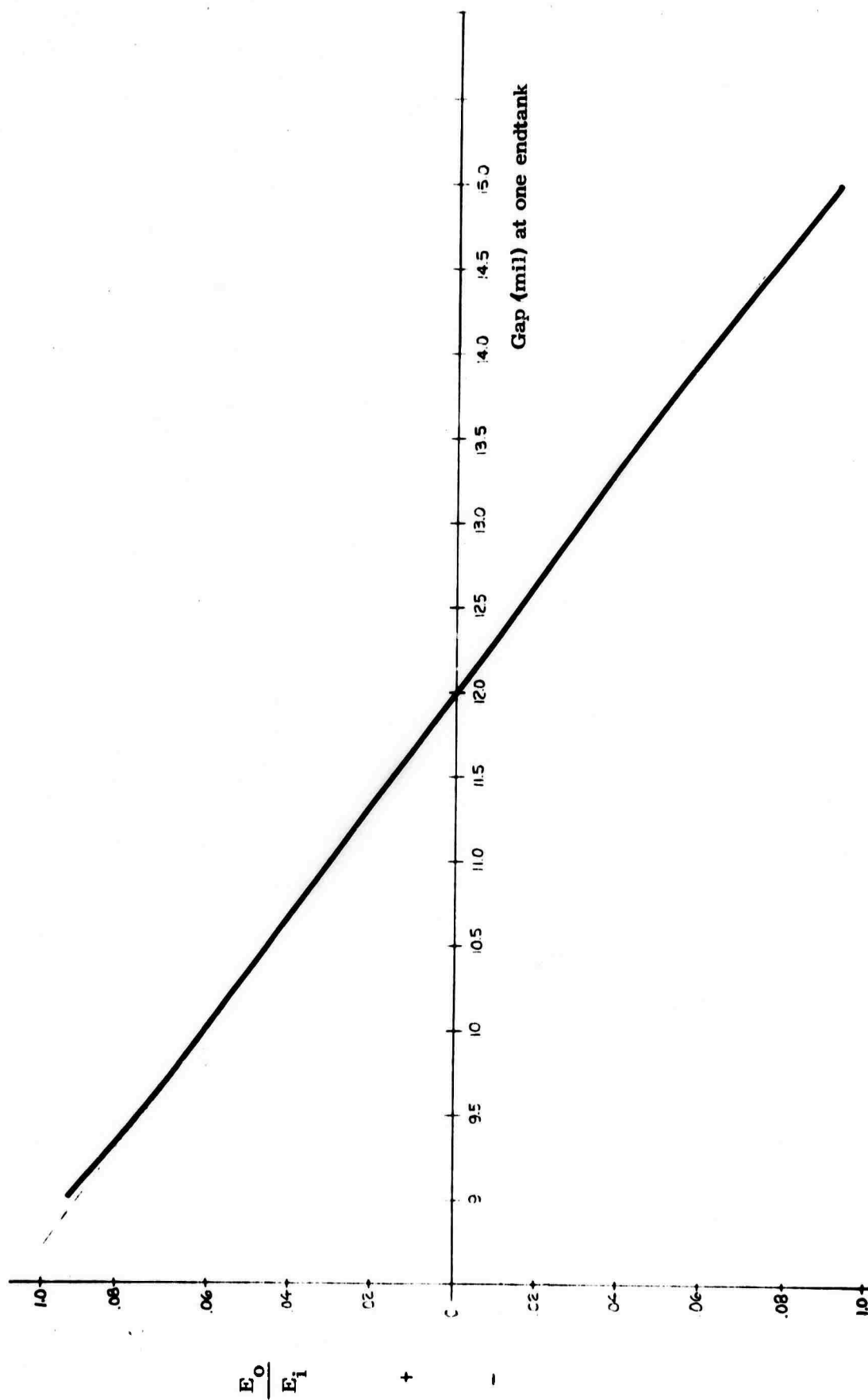


Fig. B. 5-1 Bridge output versus gap (at a 12 mil nominal gap).

BLANK PAGE

APPENDIX B.6

LINEARITY TESTS ON 4-MIL TILTMETER ELECTRONICS

Sources of nonlinearity in the capacitive bridge tiltmeter have been discussed in Appendix B.4, but some question remains as to just what part the amplifiers and demodulator—especially the latter—play in the overall system linearity. It is obvious that the signal and reference voltages should be sine waves as free from distortion as possible; that the amplifiers handling these voltages should introduce as little distortion as possible; that both signal and reference voltages should be large compared with diode breakpoints; that the reference voltage should be twice as large as the signal voltage to avoid limiting. A close examination of the null of the signal amplifier will usually disclose residual harmonic distortion. The question arises, what does the demodulator do with these harmonics? What contribution do they make to the dc output? Hence the possibility exists for nonlinear distortion at both large and small signal levels.

To answer some of these questions, the test procedure shown in Fig. B.6-1 was chosen.

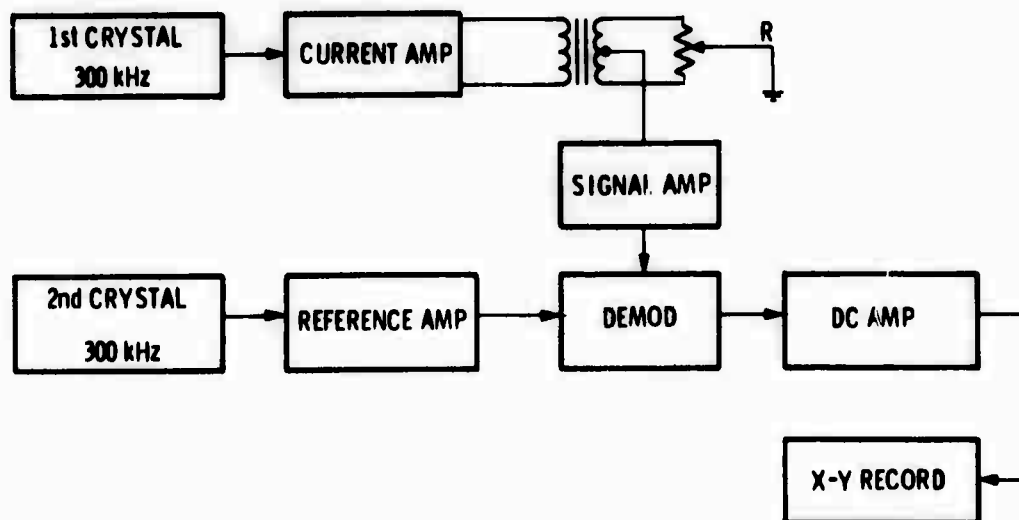


Fig. B.6-1 Test block diagram.

The idea behind this scheme was that when a phase-sensitive demodulator is driven from two independent ac sources, the output of the demodulator, instead of being dc, is a low frequency ac beat corresponding to the frequency difference between the two sources. For this beat to be purely sinusoidal, every component in the system must be linear.

Exactly the same components used in the tiltmeter were used in this test, the only differences being that the reference amplifier was driven from a second crystal oscillator, and the capacitive bridge was replaced by the potentiometer R for greater convenience in setting the signal amplifier input. The linearity was tested over four decades of signal amplifier input (simulated tilt angle). The chosen amplitudes and gains are shown in the table below:

<u>Tilt angle</u>	<u>Input to sig amp</u>	<u>Demod output</u>	<u>DC amp gain</u>	<u>DC amp out</u>
± 1.0 mil	314.00 mv rms	30.000 Vpp	1/30	1 Vpp
± 0.1 mil	31.40 mv rms	3.000 Vpp	1/3	1 Vpp
$\pm 10\mu$ inch	3.14 mv rms	0.300 Vpp	10/3	1 Vpp
$\pm 1\mu$ inch	314.00 μ V rms	0.030 Vpp	100/3	1 Vpp
$\pm 0.1 \mu$ inch	31.40 μ V rms	0.003 Vpp	1000/3	1 Vpp

The dc amplifier used was a high-precision, very low drift type with an open-loop voltage gain of 10^6 . Thus, in its maximum gain position it still had a feedback factor of over 3000. It was always operated at the same output, and the amplitude was always 1 volt peak-to-peak (5% of its maximum dynamic range). It was therefore unlikely that this amplifier contributed significant distortion to the data.

It was convenient to display the data on paper as a permanent record. For this purpose, an X-Y recorder was used, having a 10-inch vertical scale and a 15-inch horizontal scale. The data could be "blown up" to a rather large value for close examination.

Since the X-Y recorder slewing speed was limited, the beat frequency had to be very low, i.e., only a fraction of one Hz. The oscillators were provided with frequency verniers, a great convenience in adjusting the beat frequency.

The beat frequency was fed into the Y axis of the recorder, while the X signal was provided by a linear sweep built into the recorder. When a record was made, the beat frequency and the X sweep speed were so adjusted that three zero

crossings were displayed so that any change in either beat frequency or sweep speed could be seen by measuring the intervals between zero crossings. No difficulty was experienced from this source.

The linearity was checked by comparing ordinates drawn by the recorder with ordinates taken from a trigonometric table. These points were taken every 20° and are shown by dots. Over the first three decades (Fig. B.6-2a, b, c, and d) the linearity was as close as one could measure (1% or better). In the fourth (Fig. B.6-2e) decade the data were largely masked by noise. This difficulty was not unexpected because of the unnecessarily large system bandwidth (200 Hz) and the extremely small signal amplitude.* With a filter placed between the dc amplifier and recorder to reduce the bandwidth to a few Hz, meaningful data could be obtained, and it could be seen that considerable distortion did indeed exist (as much as 10%). It could also be seen that the quadrature bucking circuit had an appreciable effect on the distortion and that reducing the beat frequency increased the distortion. In this type of test the presence of any quadrature at all would contribute to distortion because, with a continuously rotating phase angle between signal and reference, the quadrature would add to the demodulator output for one phase angle, subtract from it for another phase angle, and contribute nothing at other phase angles. Introducing the low-pass filter made the distortion seem less, except at low beat frequencies, because it suppressed the distortion as well as the noise. In other words this test fails where appreciable quadrature exists. Such distortion is probably not present under working conditions. However, the quadrature component is so small that the test was valid down to a simulated displacement of less than 1 microinch and inconclusive for smaller displacements. With very careful quadrature adjustment an undistorted curve for this decade was obtained.

A test more representative of working conditions would be to feed into the signal amplifier a suppressed 300 kHz carrier modulated by a low-frequency oscillator, and record the demodulator output as before. The problem with this arrangement is the difficulty of generating a suppressed carrier with sufficient linearity; in other words, the instrument under test is so good that it is difficult to find a sufficient test method.

*See Fig. B.6-2 (f).

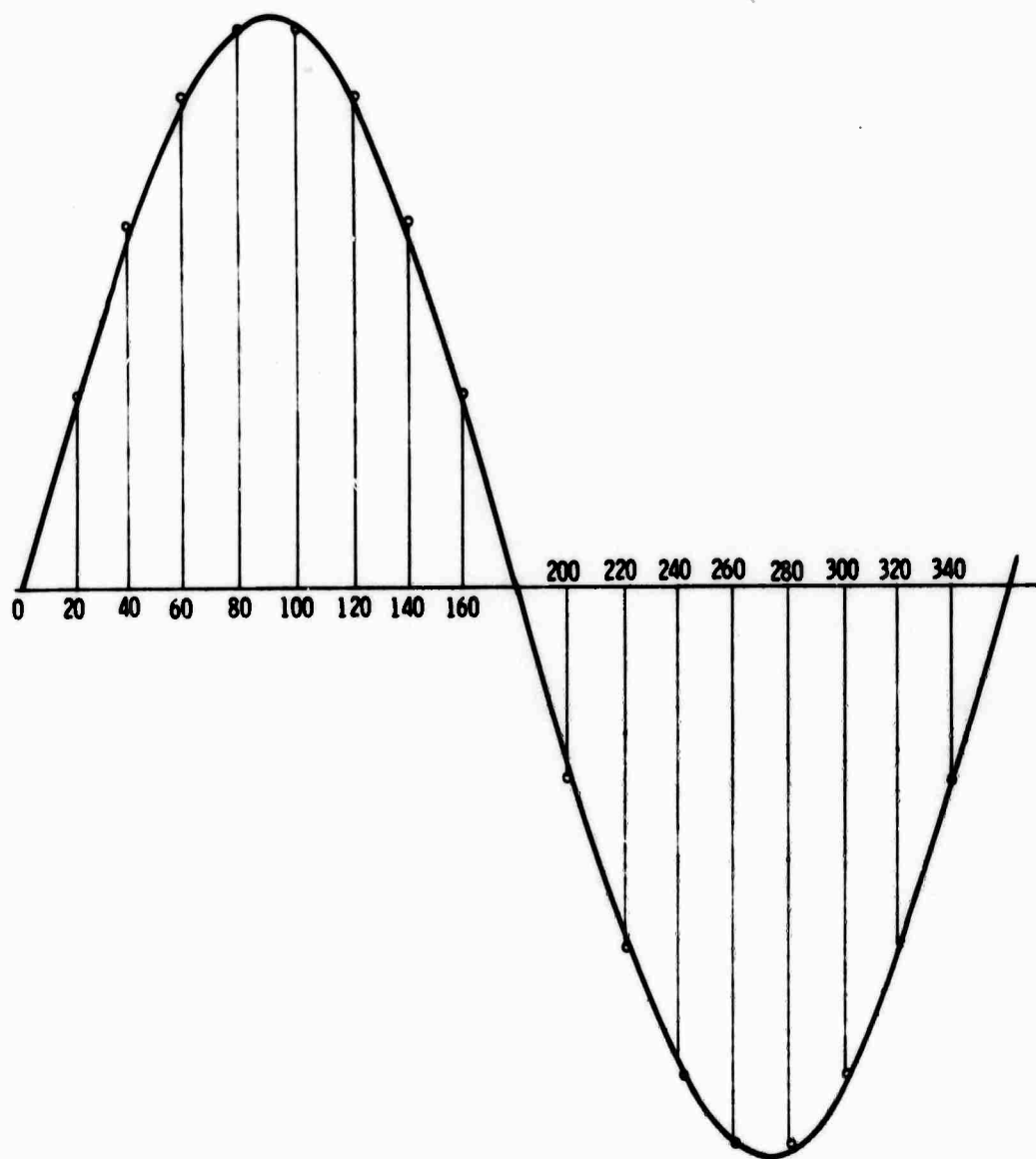


Fig. B. 6-2 (a) Bridge output.

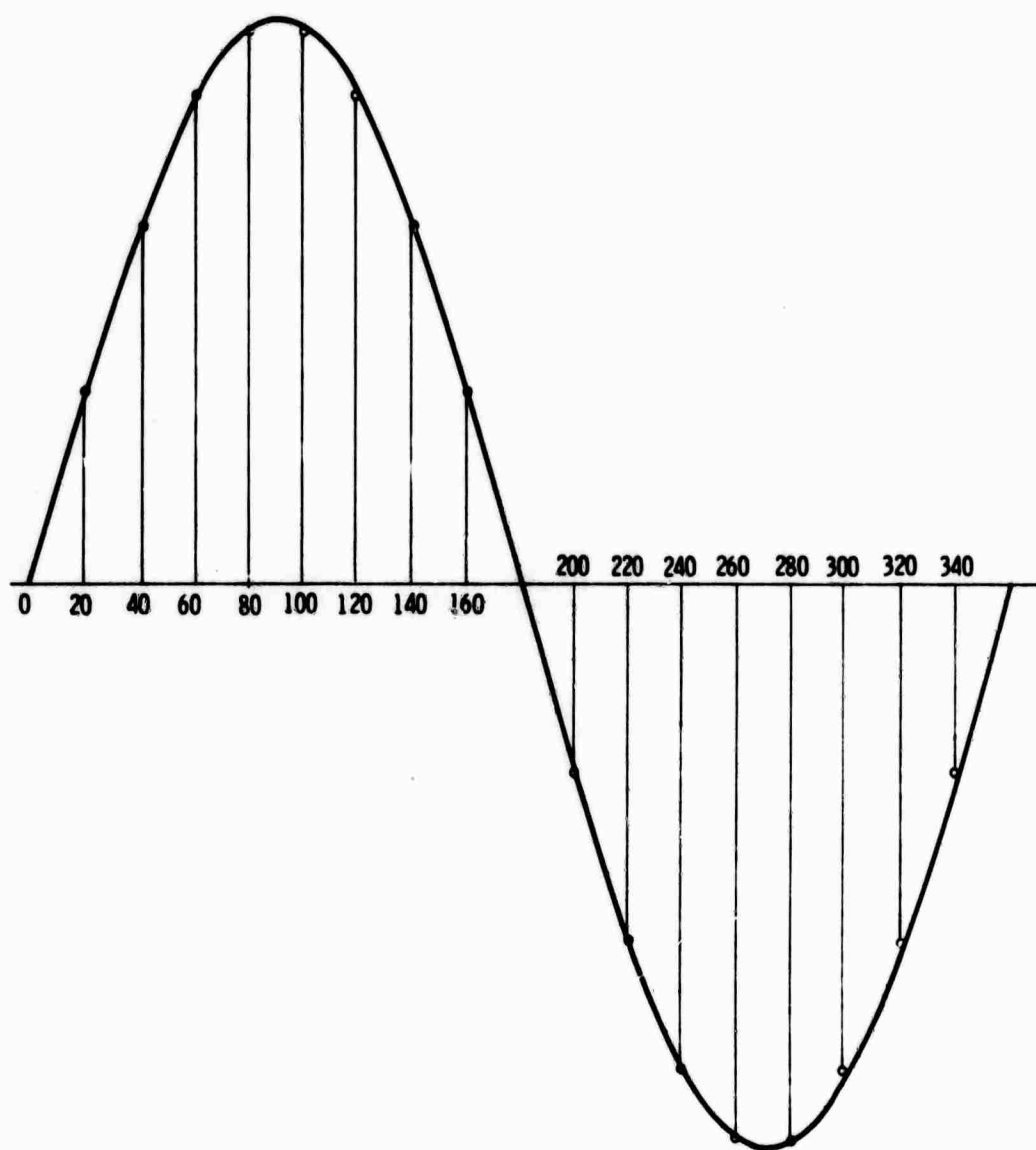


Fig. B.6-2 (b) Bridge output.

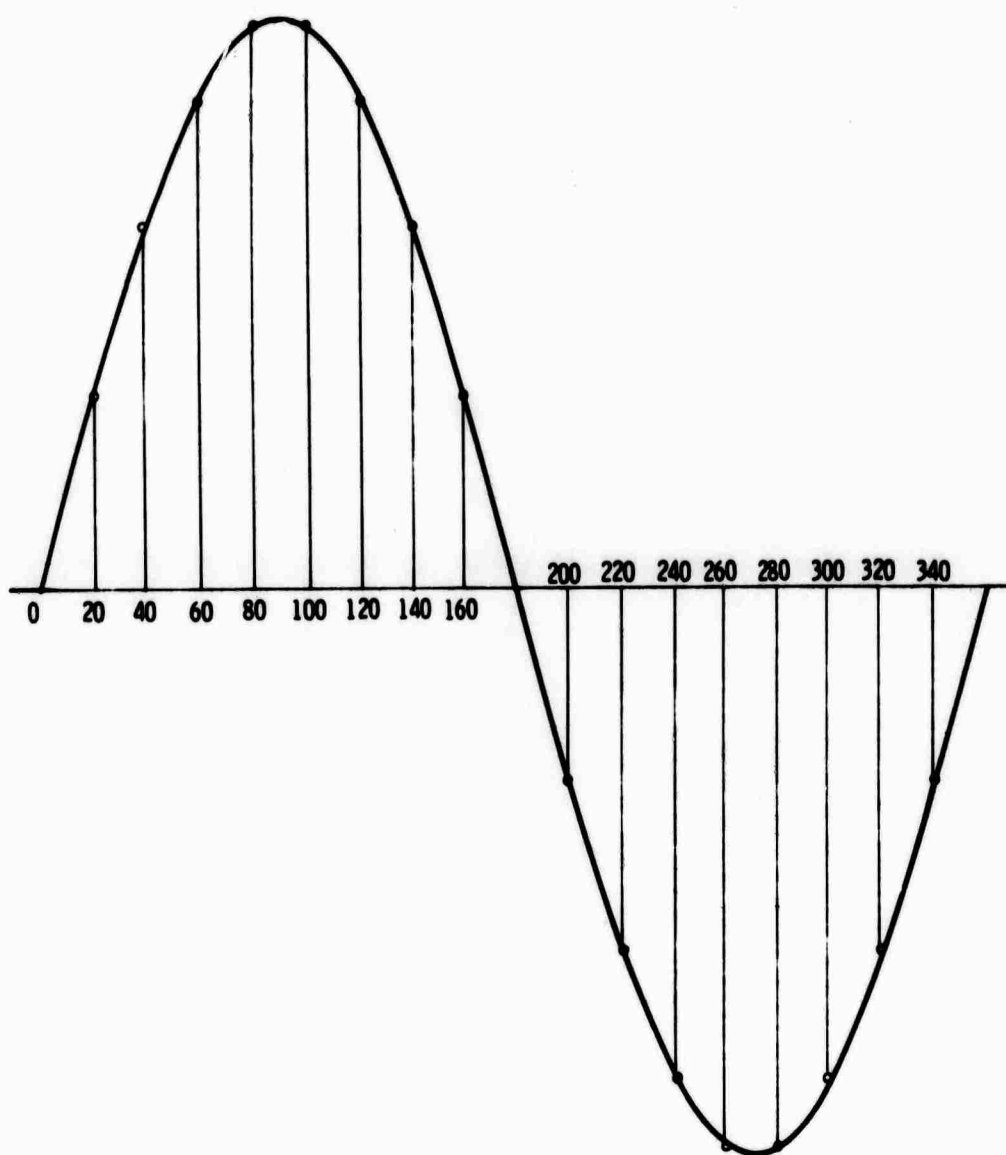


Fig. B.6-2 (c) Bridge output.

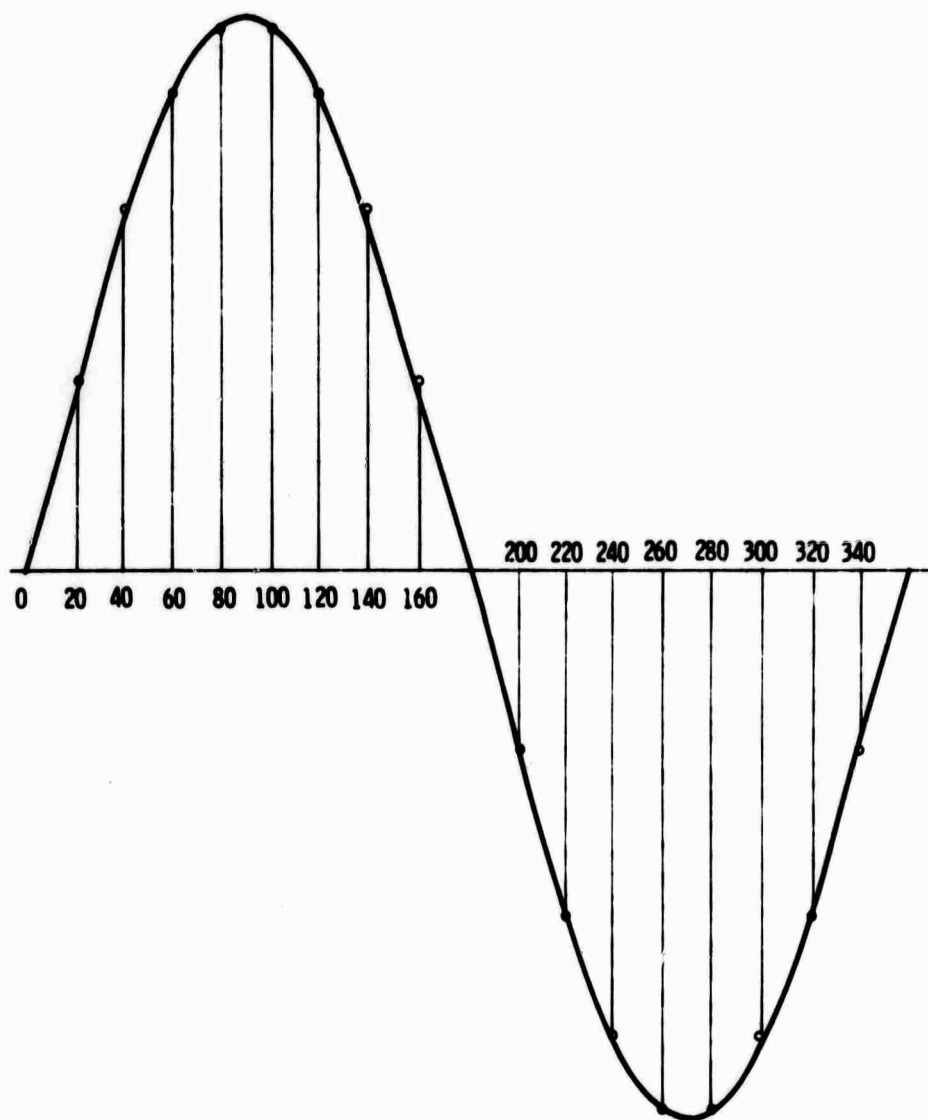


Fig. B. 6-2 (d) Bridge output.

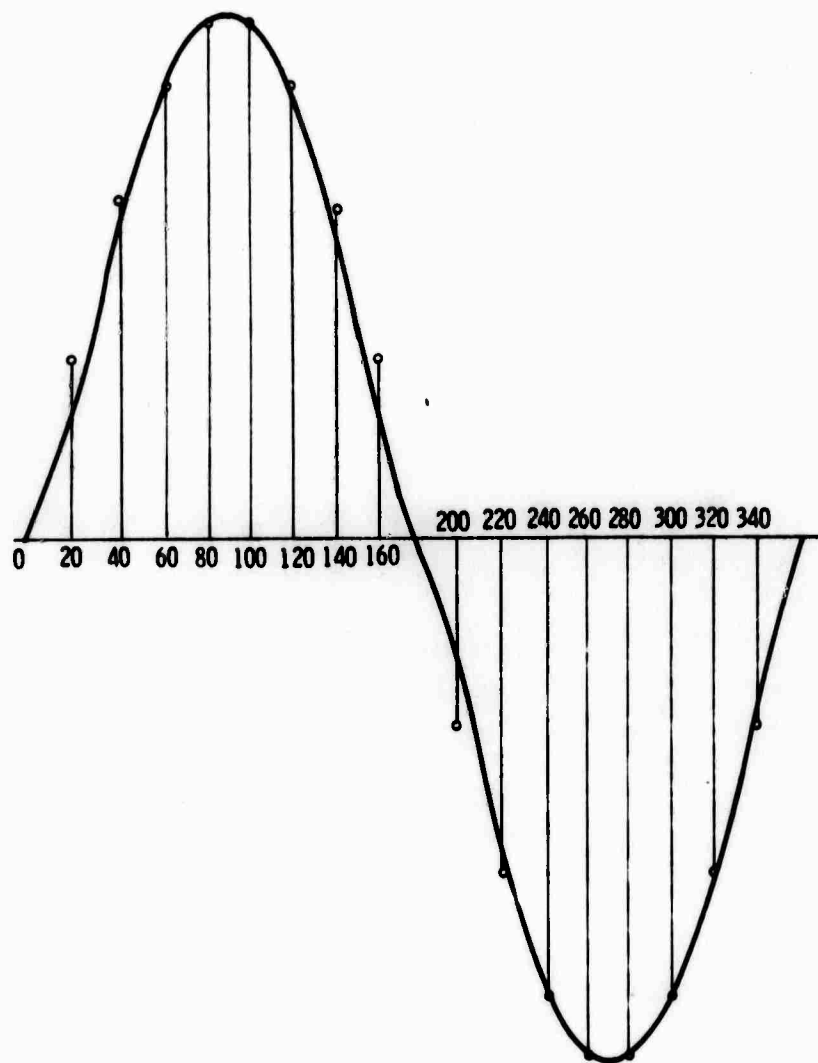


Fig. B.6-2 (e) Bridge output.

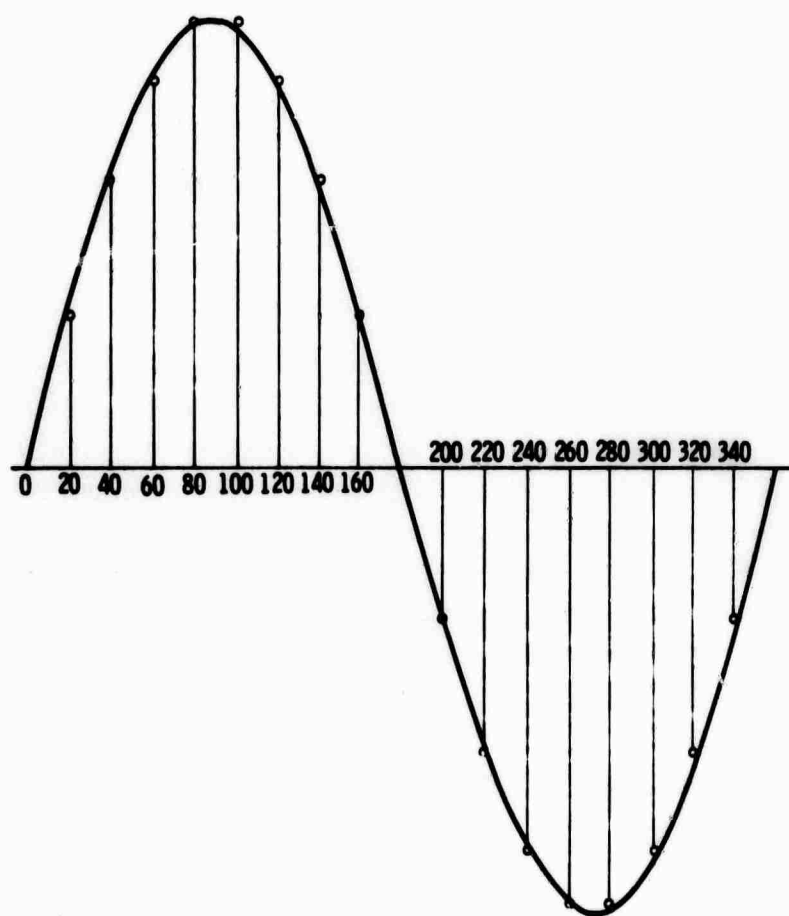


Fig. B. 6-2 (f) Bridge output.

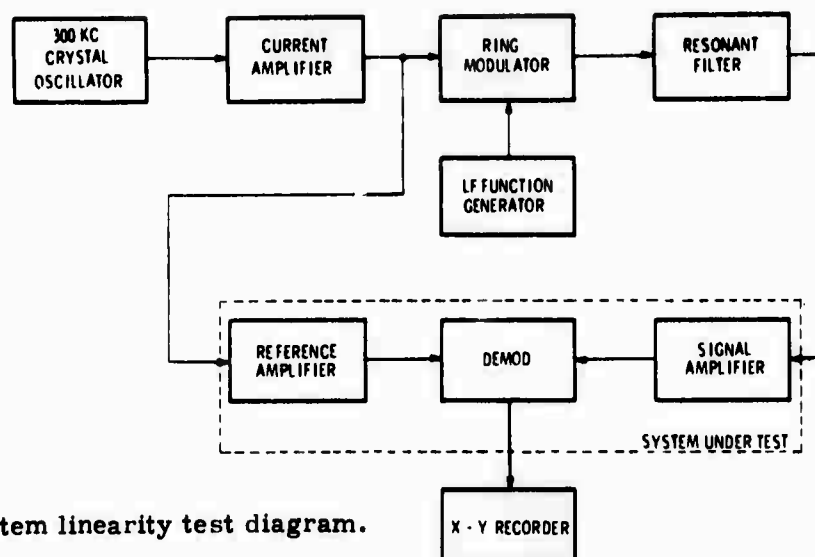


Fig. B. 6-3 System linearity test diagram.

Since the first test described above indicated that the linearity of the ring demodulator was very good, it was thought probable that the identical circuit used as a modulator would have good enough linearity to test the system. Therefore, the second procedure as shown in Fig. B. 6-3 was chosen.

The diode ring modulator generates a 300 KC suppressed carrier, while a function generator provides the envelope. Since the modulator carrier output waveform is a square wave, it was filtered by a resonant LC circuit, tuned to 300 KC. Filtering was necessary because the limited system bandwidth might distort the square wave and contribute to errors. The wave shape of the function generator was a symmetrical ramp. The linearity of this ramp waveform was 0.1% or better. The advantage of using a ramp instead of a sine wave is that the linearity can be inspected directly so that use of trigonometry tables is unnecessary.

The results of the second test are shown in Fig. B. 6-4a, b, c, d and e. It can be seen in Fig. B. 6-4 that there is some demod limiting present, amounting to symmetrical distortion of about 3%. In this case the signal amplitude is about half that of the reference. If the signal were made larger without increasing the reference amplitude, this distortion would increase rapidly. This distortion is so small in Fig. B. 6-4b, c and d that it cannot be measured (probably less than 0.5%). In Fig. B. 6-4e the signal is so small that the noise is the limiting factor but the distortion is still less than 1%. Visual inspection of this smallest amplitude on the cathode ray oscilloscope shows lower distortion than the X-Y recorder displays. It is difficult to obtain a very good plot on the X-Y recorder at such low amplitudes because of system drifts during the recording time.

The purpose of the system under test is to provide a voltage proportional to tilt angle at very low seismic frequencies (> 1 Hz). For applications where greater speeds are required the bandwidth capability of the electronics is 350 Hz for a resolution of 4 nanoinches. This bandwidth is obtained when sufficient filtering is used to reduce the demod ripple to white noise level.

The chance of demod distortion compensating modulator distortion is remote because the amplitude of the modulator output was varied in two ways: (1) adjustment of LF function generator amplitude and (2) insertion of an attenuator between the resonant filter and the signal amplifier. Thus the modulator was operated with so many different percentages and amplitudes that compensation of nonlinearities for all combinations is extremely unlikely.

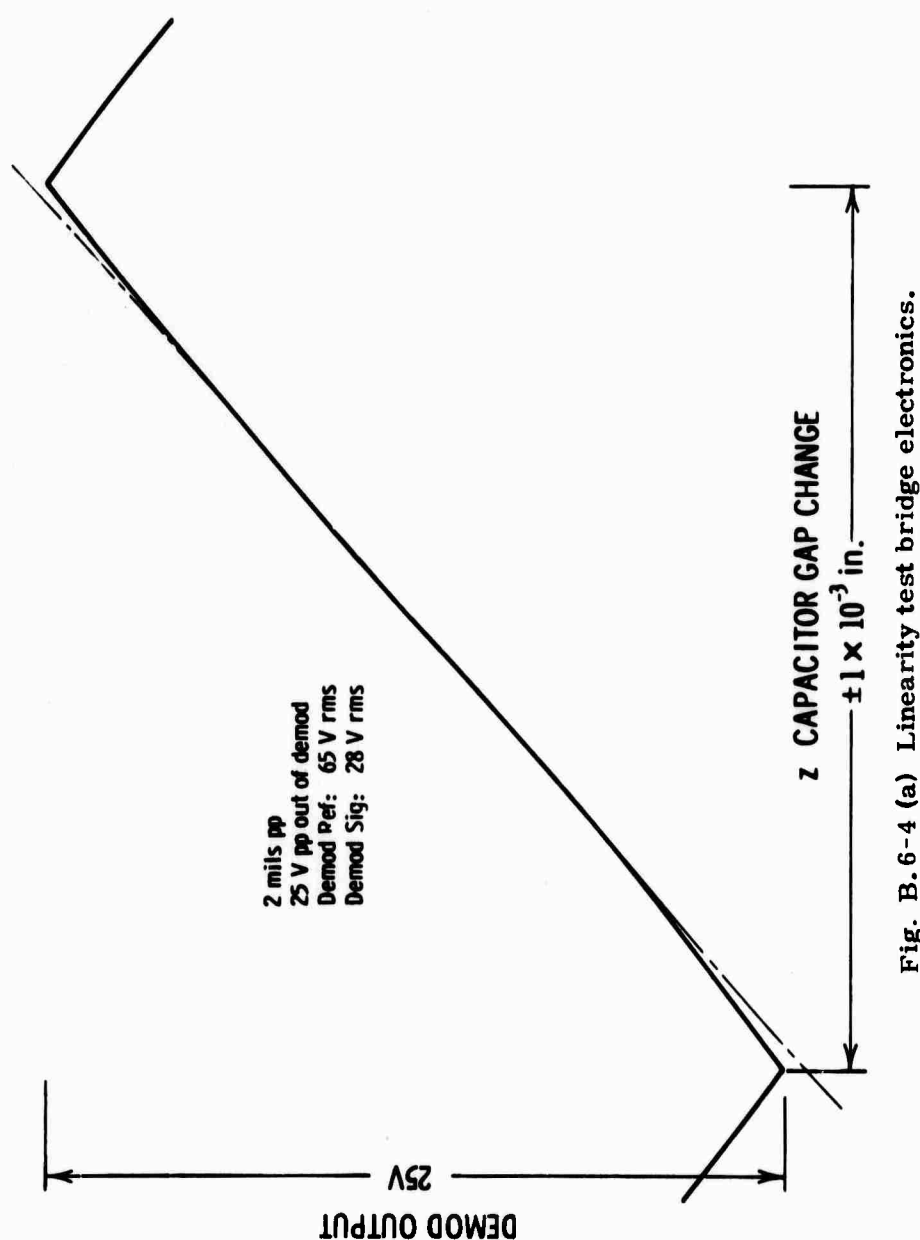


Fig. B.6-4 (a) Linearity test bridge electronics.

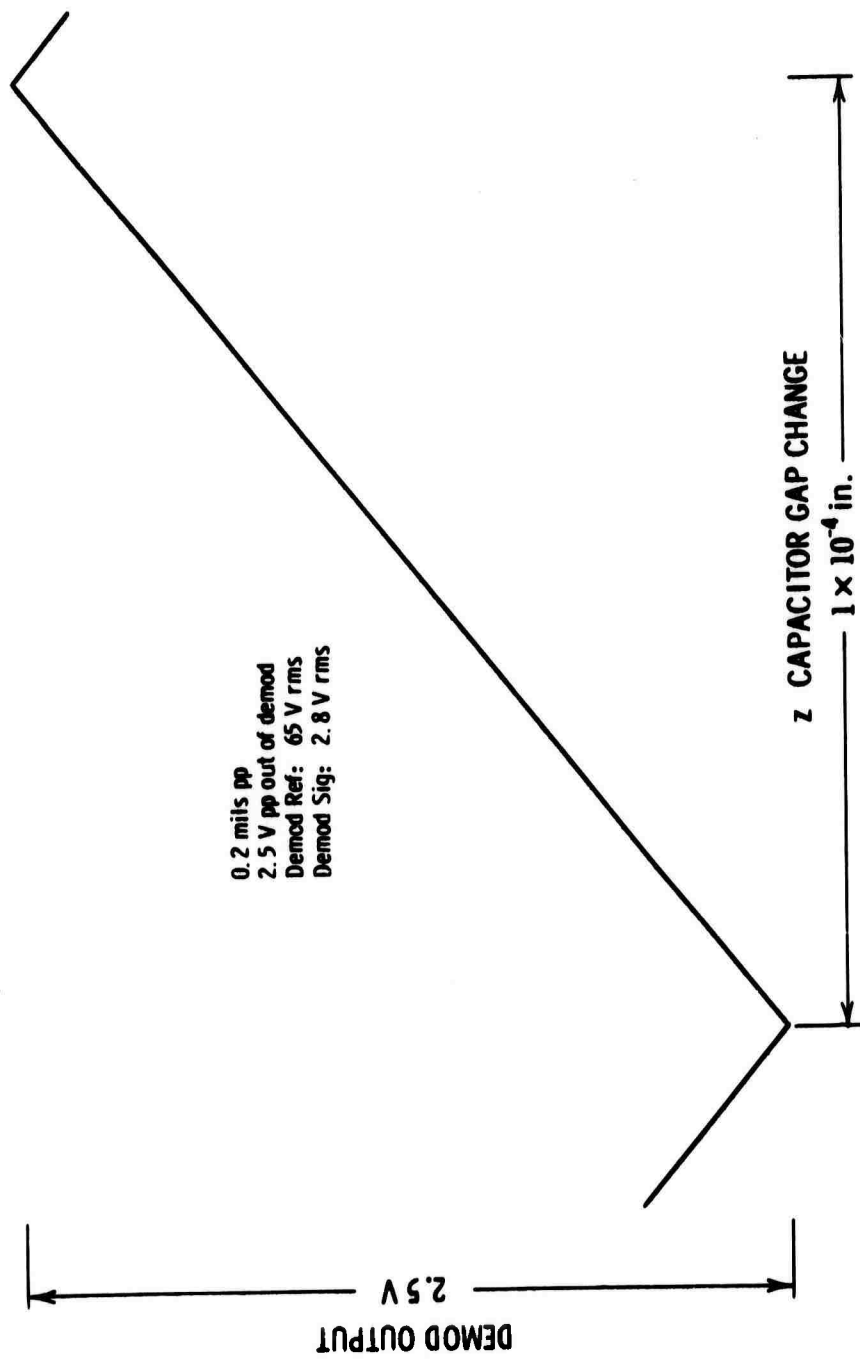


Fig. B.6-4 (b) Linearity test bridge electronics.

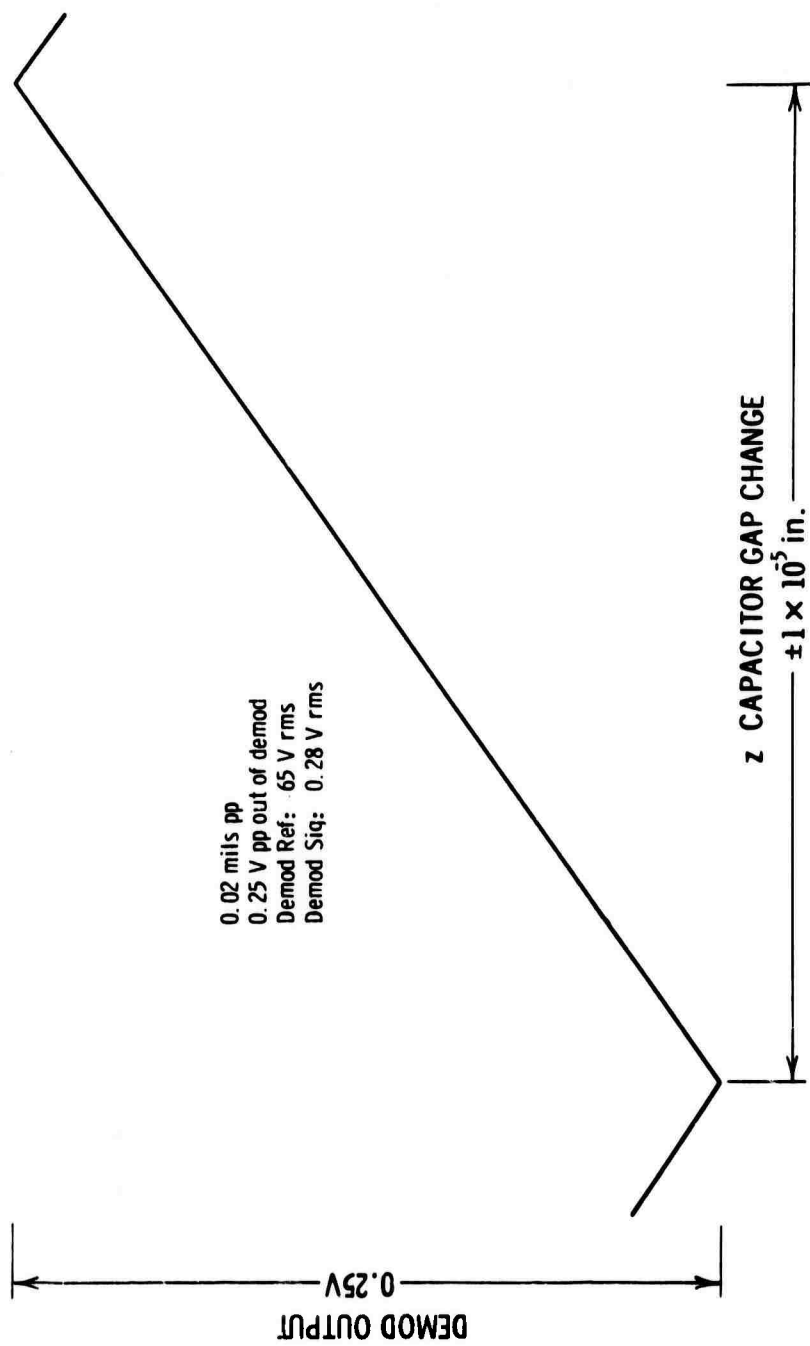


Fig. B. 6-4 (c) Linearity test bridge electronics.

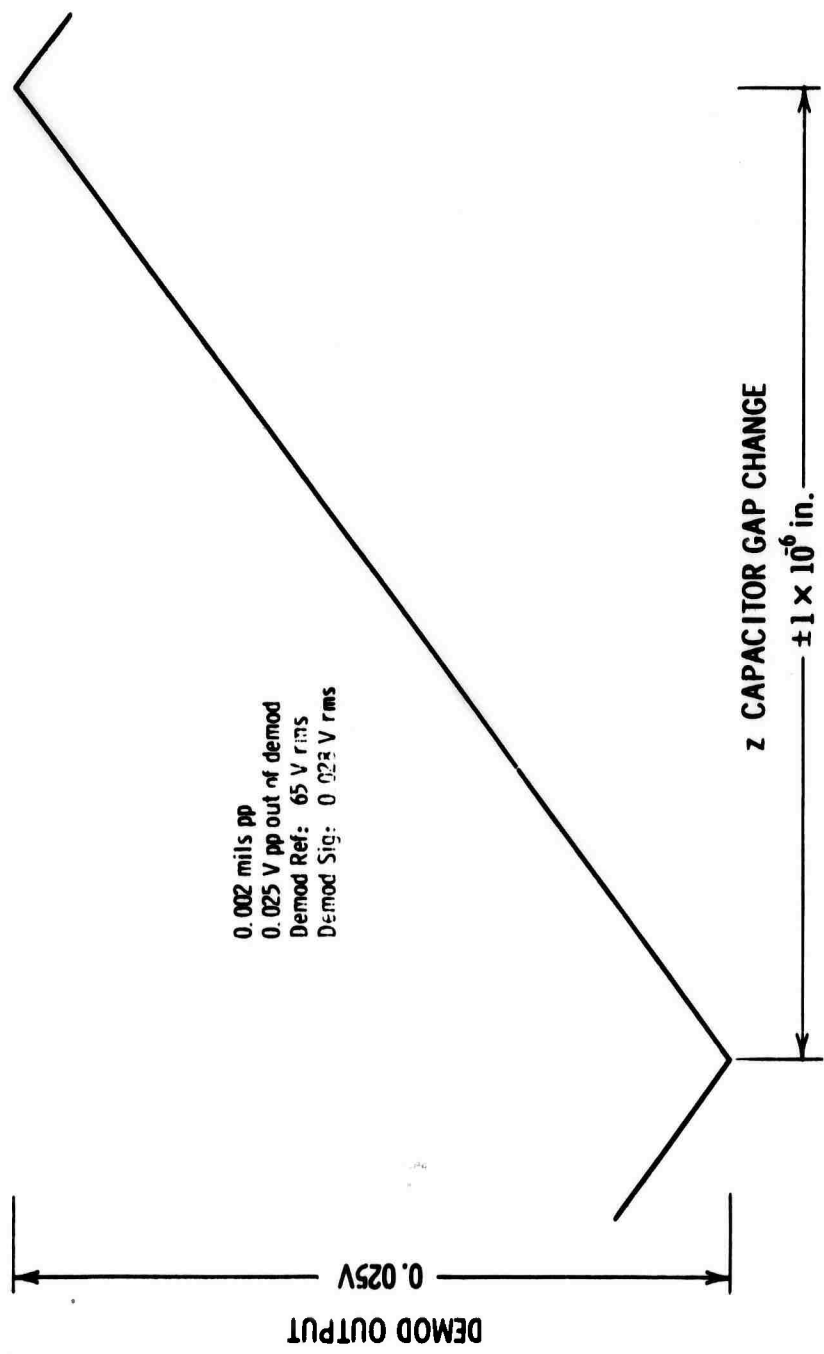


Fig. B.6-4 (d) Linearity test bridge electronics.

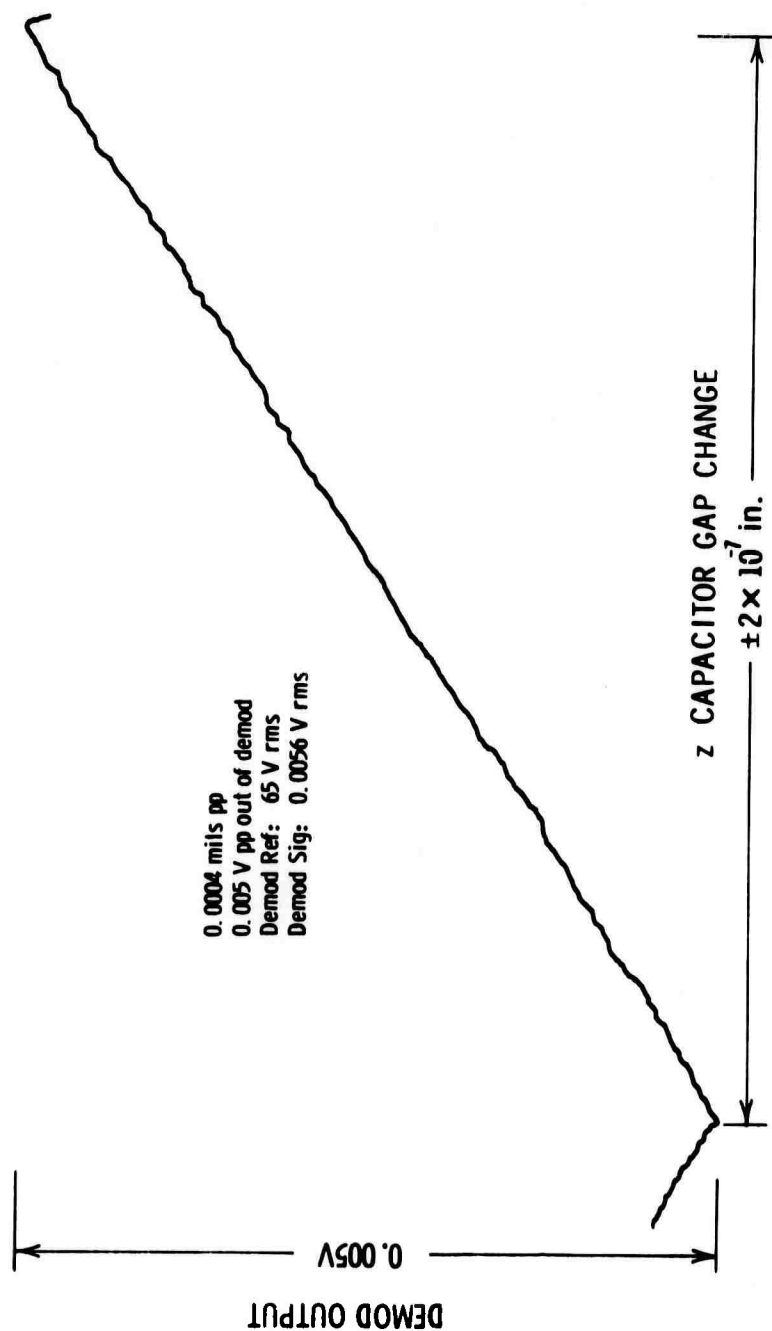


Fig. B. 6-4 (e) Linearity test bridge electronics.

BLANK PAGE

APPENDIX B.7
CIRCUIT DIAGRAMS

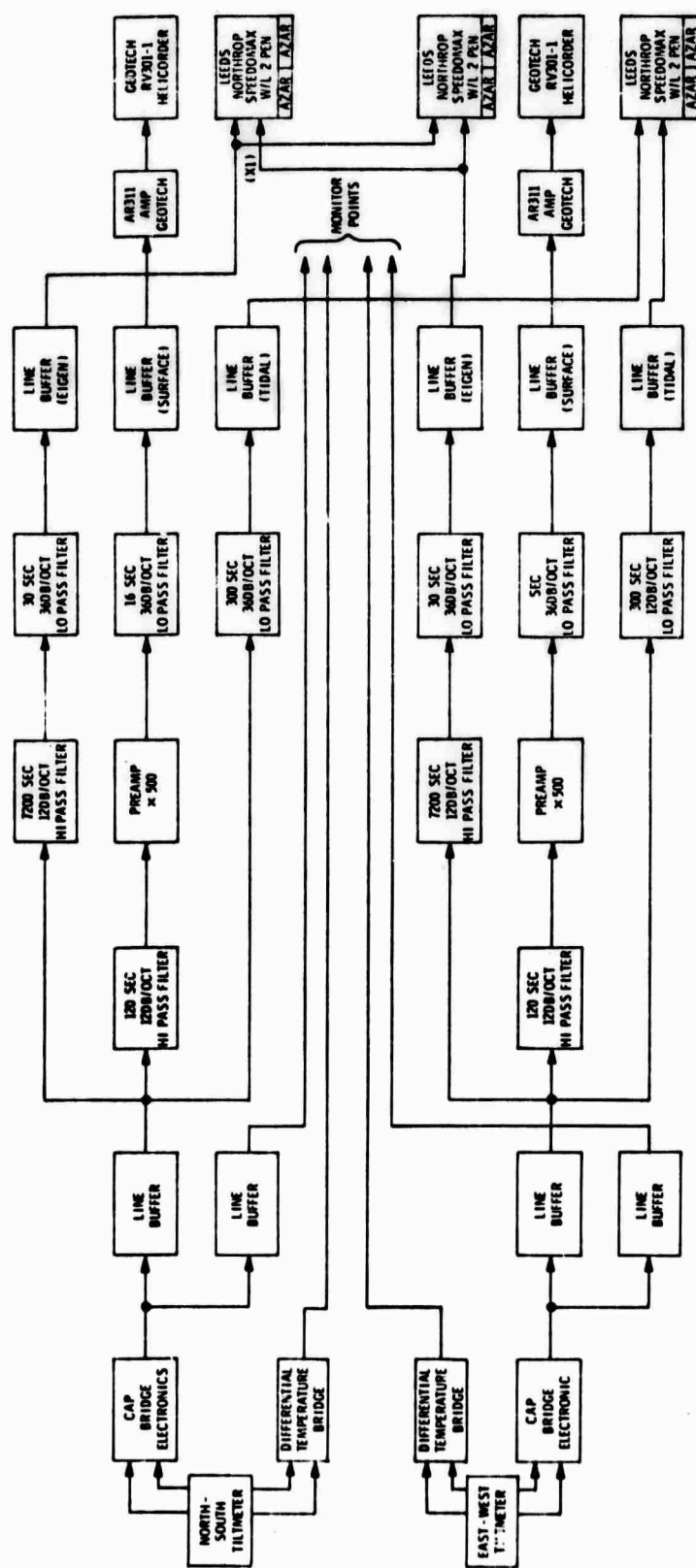


Fig. B.7-1 MIT seismic station.

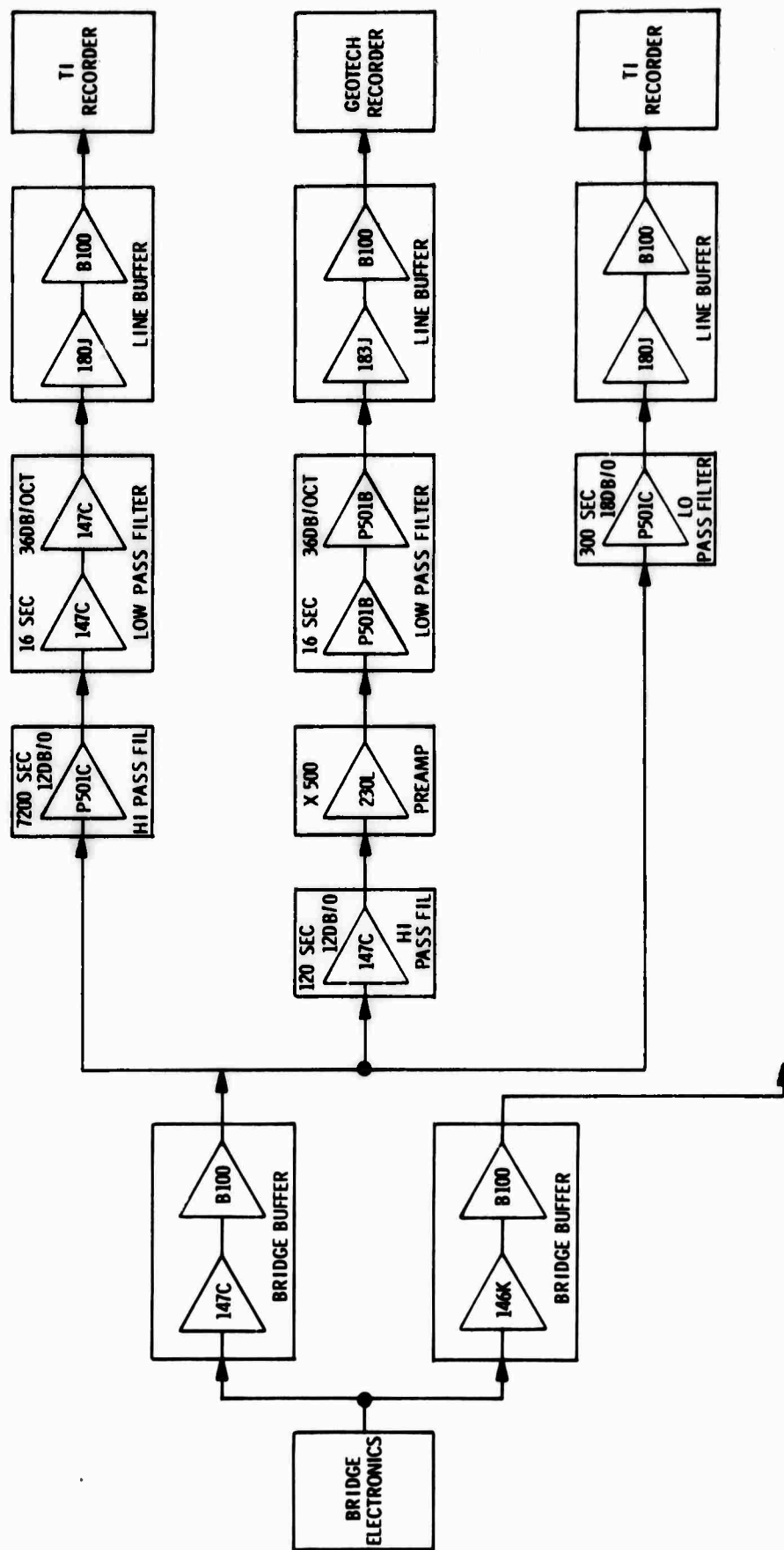


Fig. B. 7-2 System op-amps.

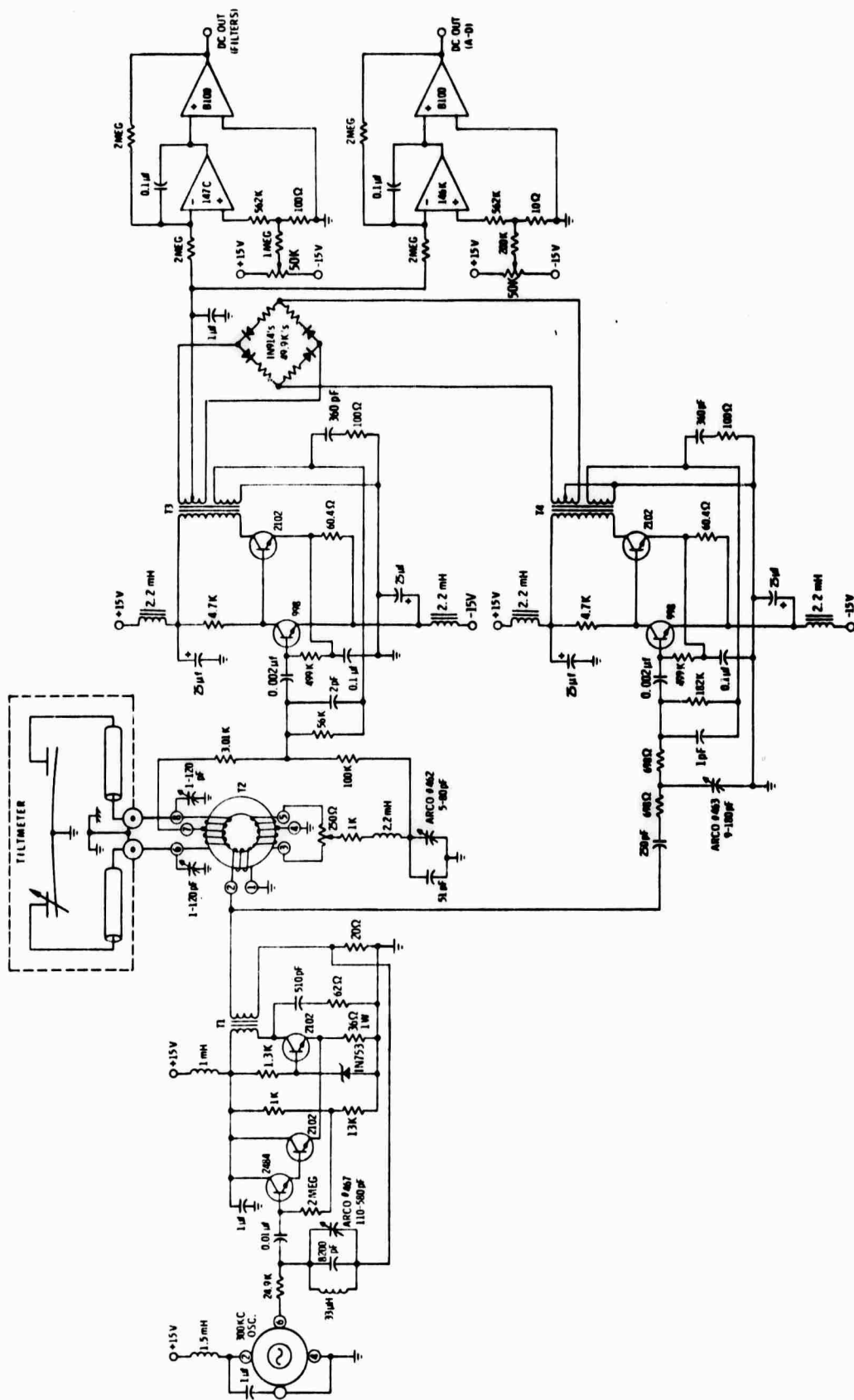


Fig. B. 7-3 Mercury tiltmeter bridge electronics.

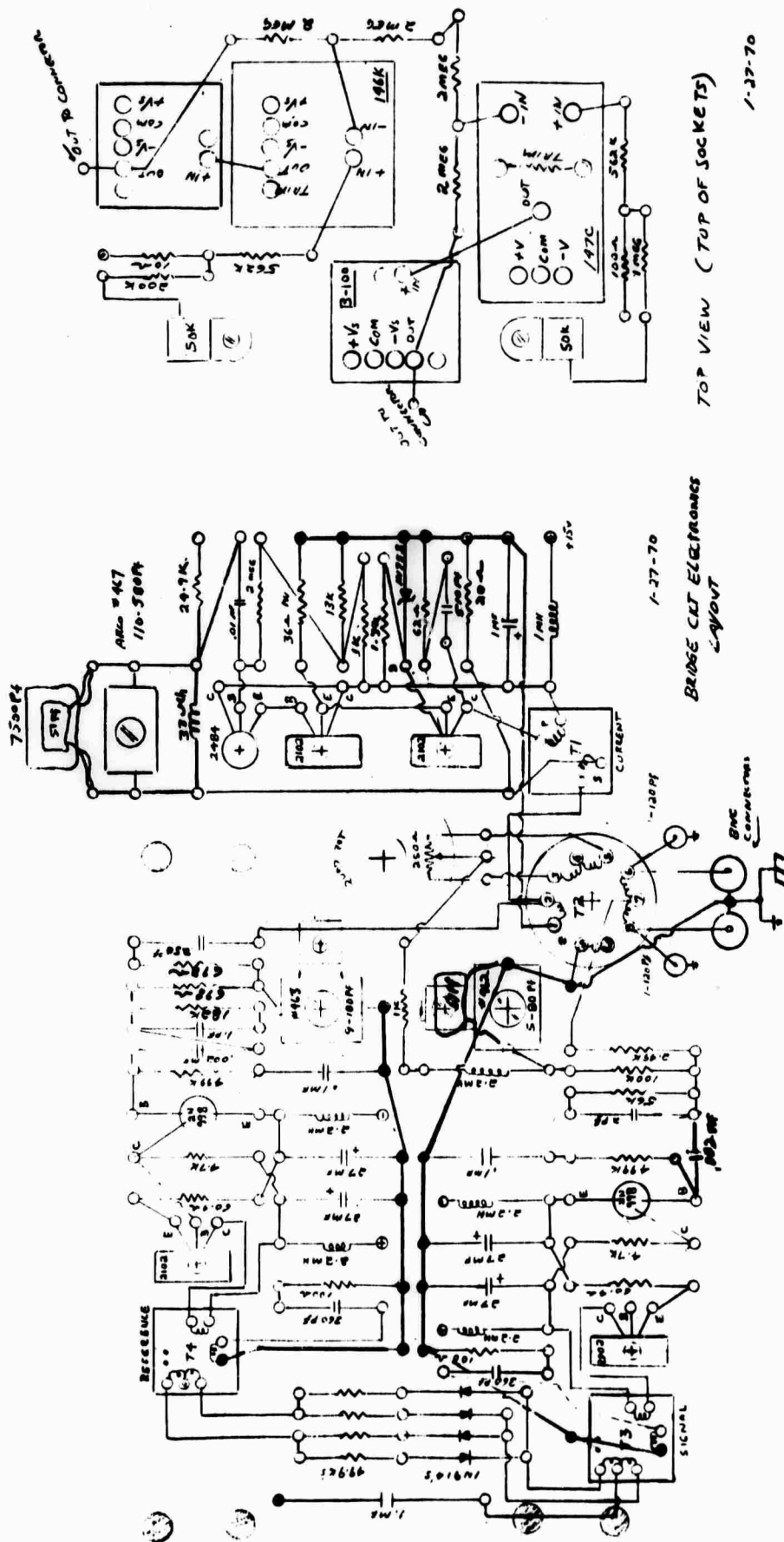


Fig. B.7-4 Bridge electronics - layout.

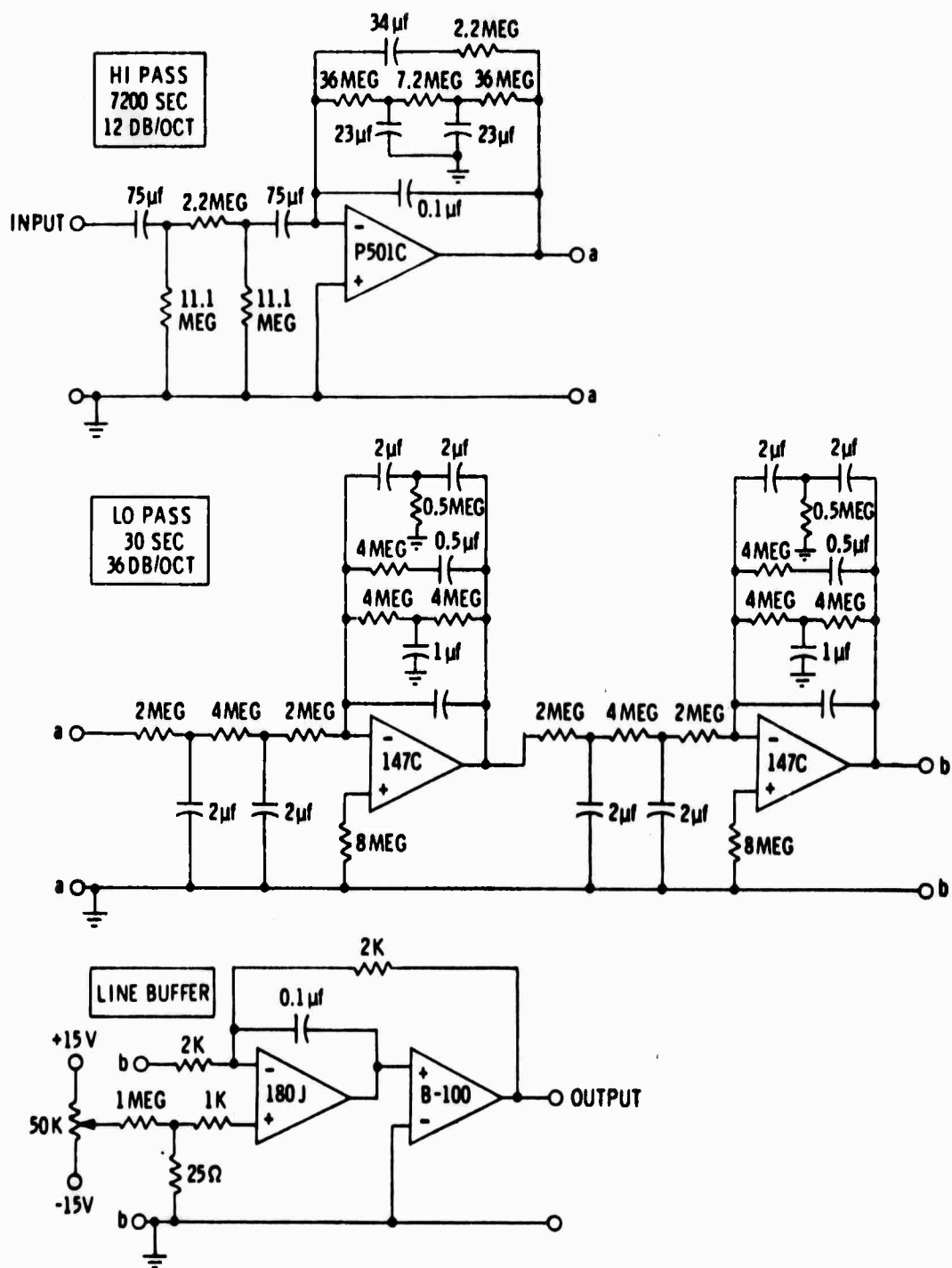


Fig. B. 7-5 Eigen filter.

1 - P501C AMP
2 - 75 MFD
1 - 39 MFD
2 - 23 MFD
1 - .1 MFD (.5" x .25")

2 - 36 MEG \sim
2 - 11.1 MEG \sim
1 - 7.2 MEG \sim
2 - 2.2 MEG \sim

Eigen
720032000
1A DR/OCT
High Pass Filter

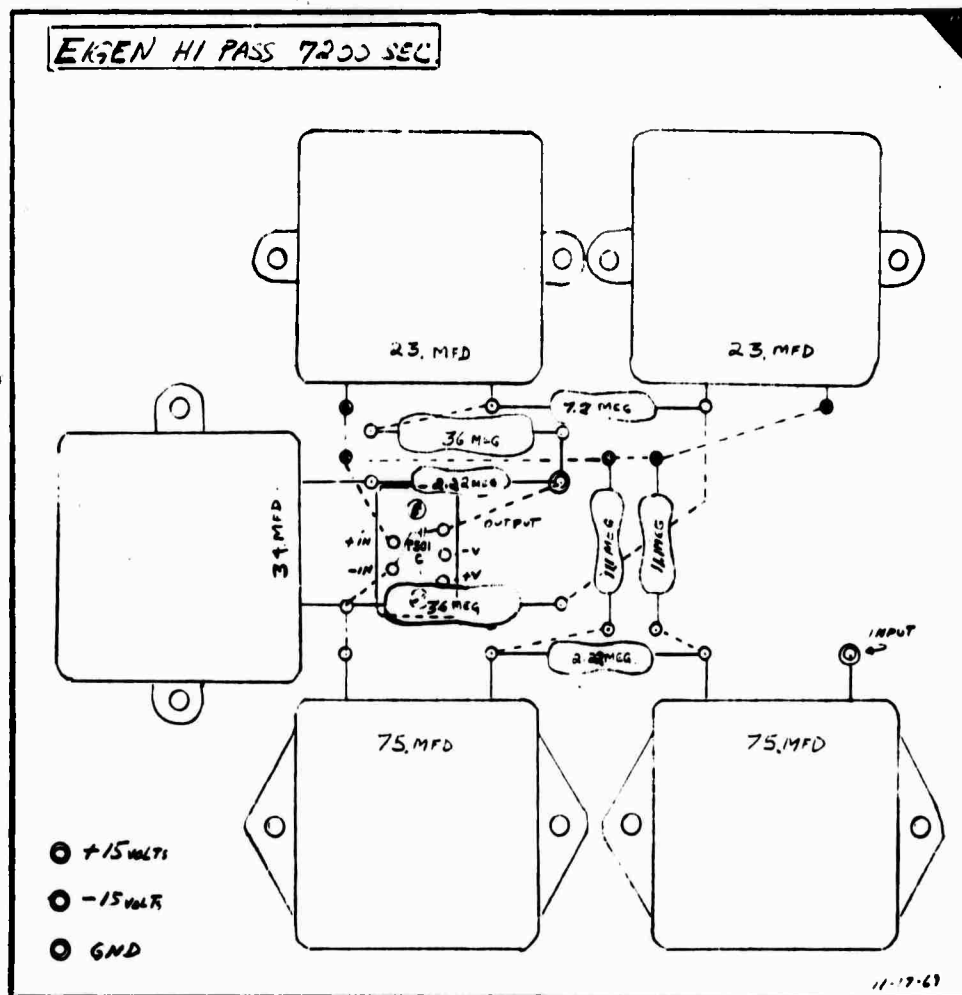


Fig. B.7-6 Eigen high pass - layout.

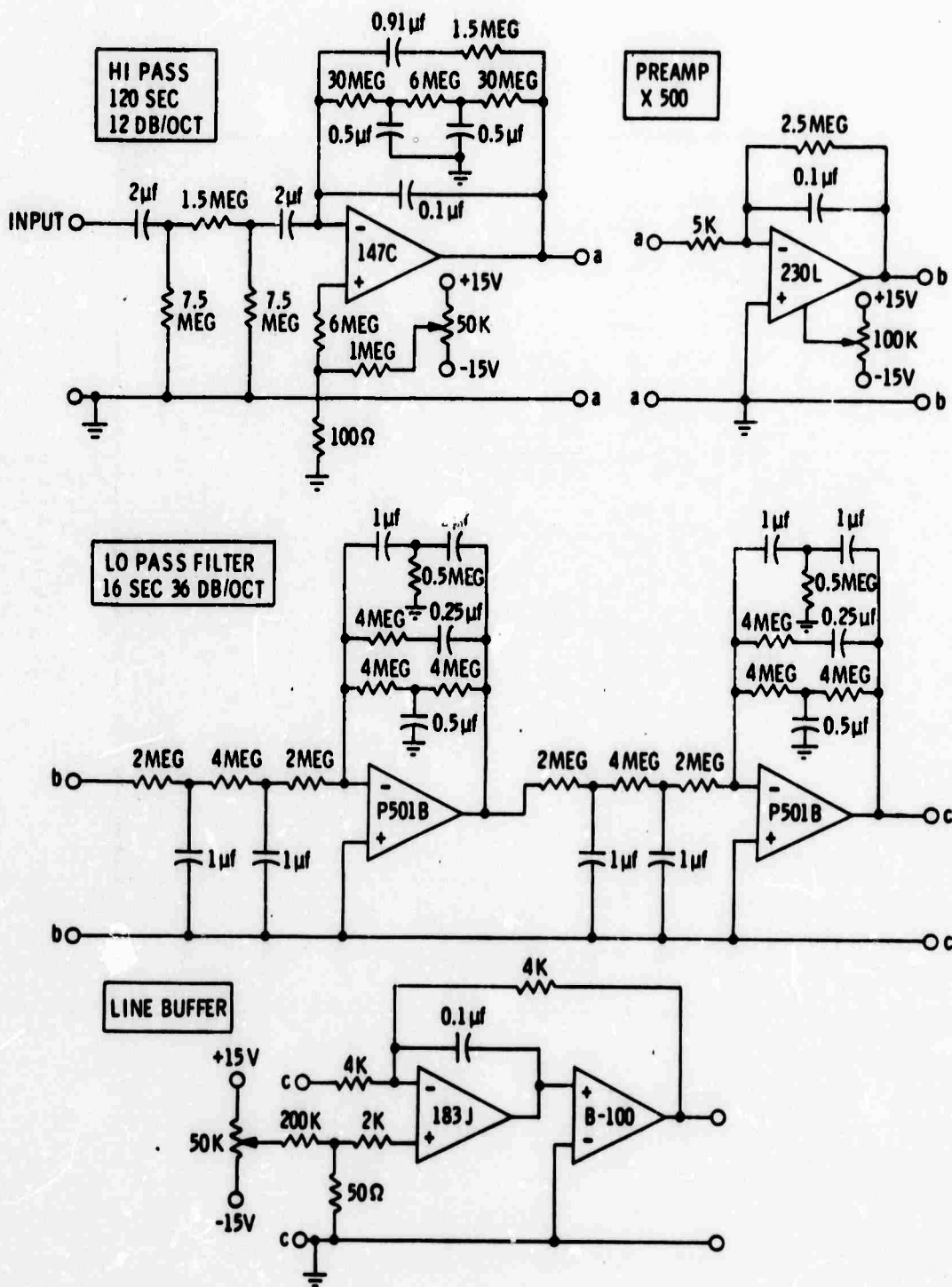
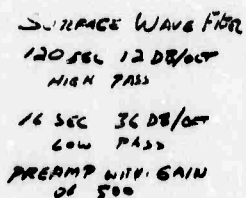
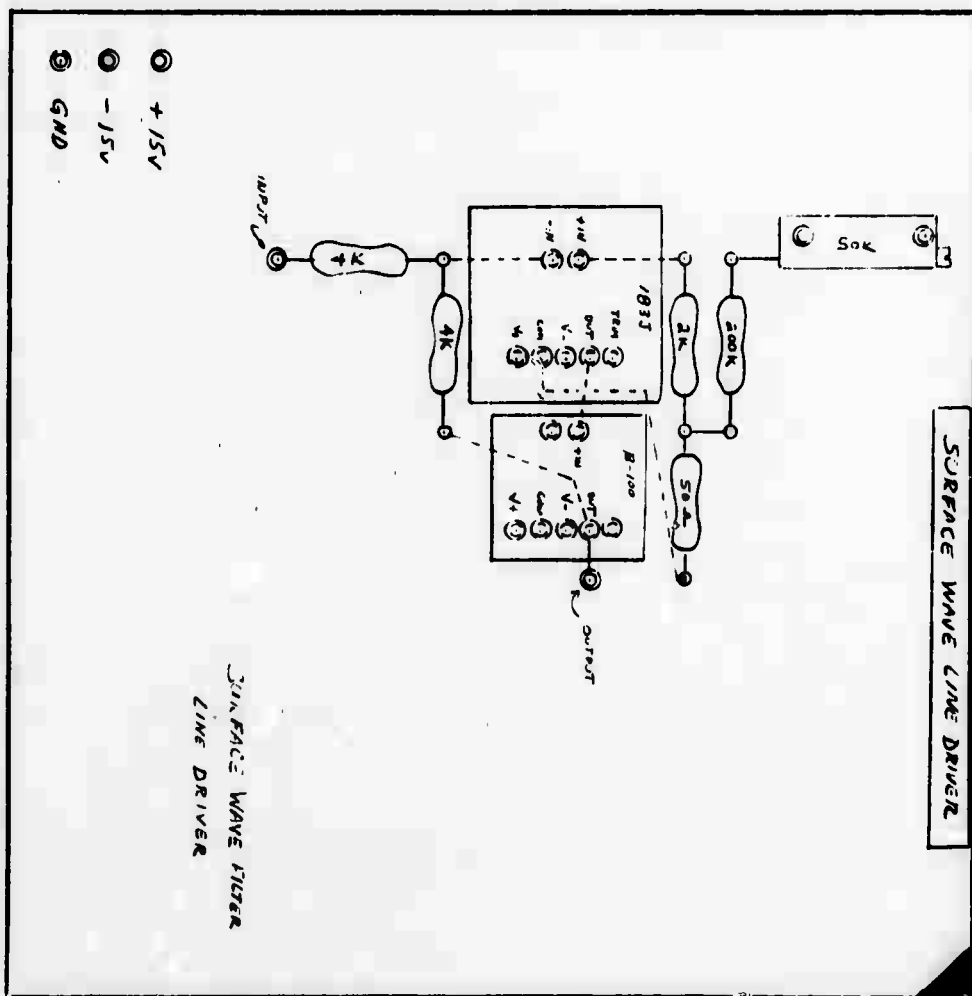


Fig. B.7-8 Surface wave filter.



120



1 - 183J AMP
1 - 8-100 800Ω/A

1 - .1 MFD
STABILIZING CAP

1 - 200 KΩ

2 - 4 K

1 - 2 K

1 - 50 Ω

1 - 50K POT

Fig. B.7-10 Surface wave filter - line driver.

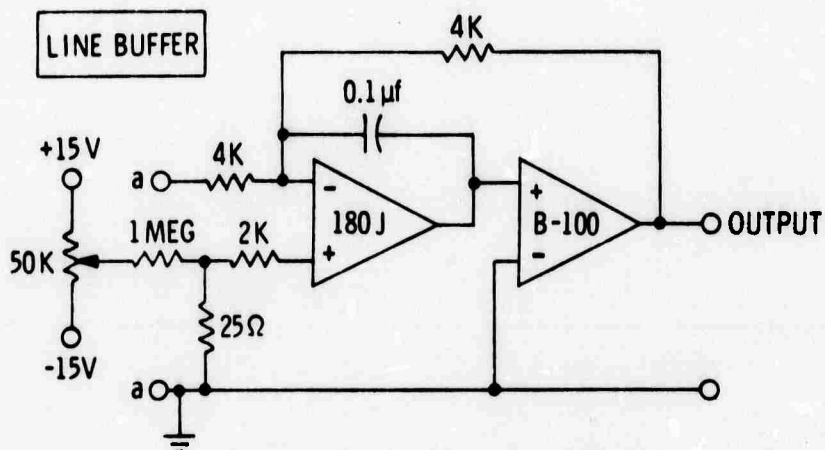
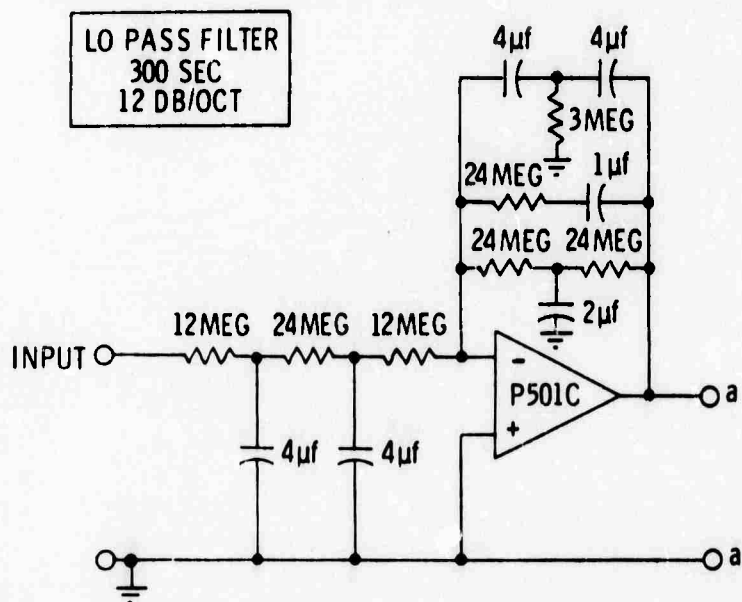


Fig. B.7-11 Tidal filter.



123

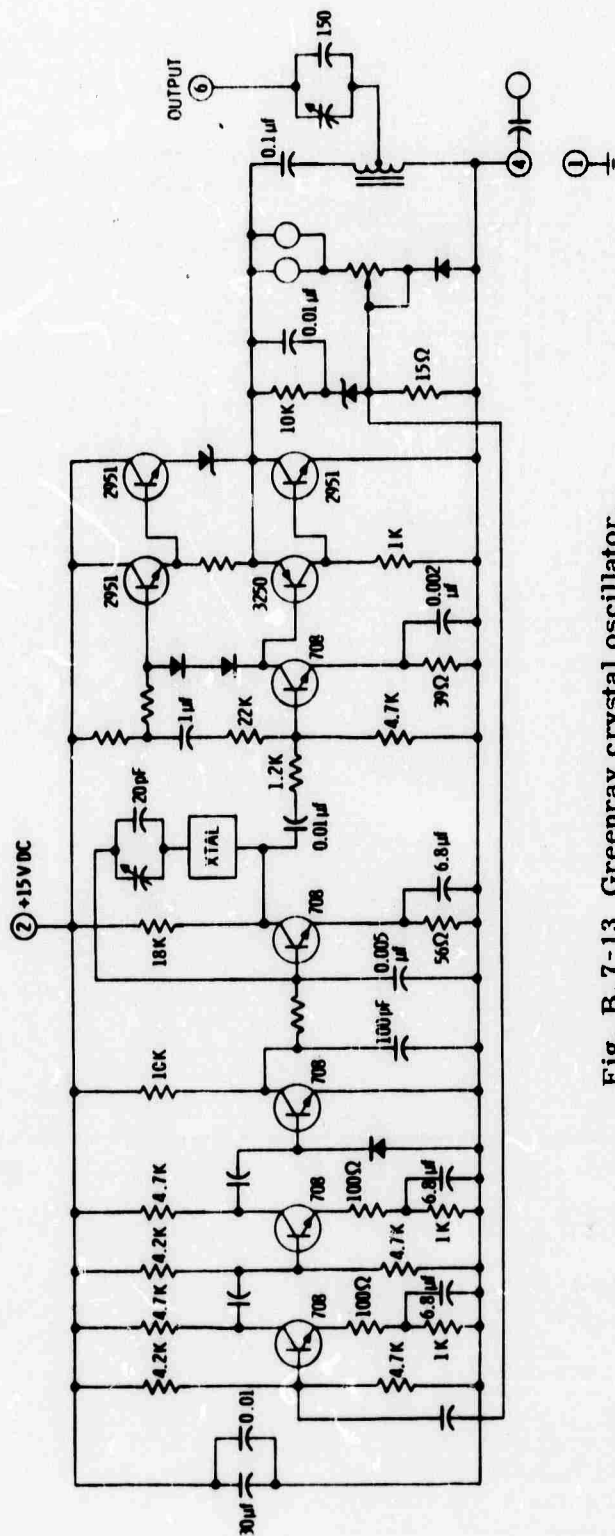


Fig. B.7-13 Greenray crystal oscillator.

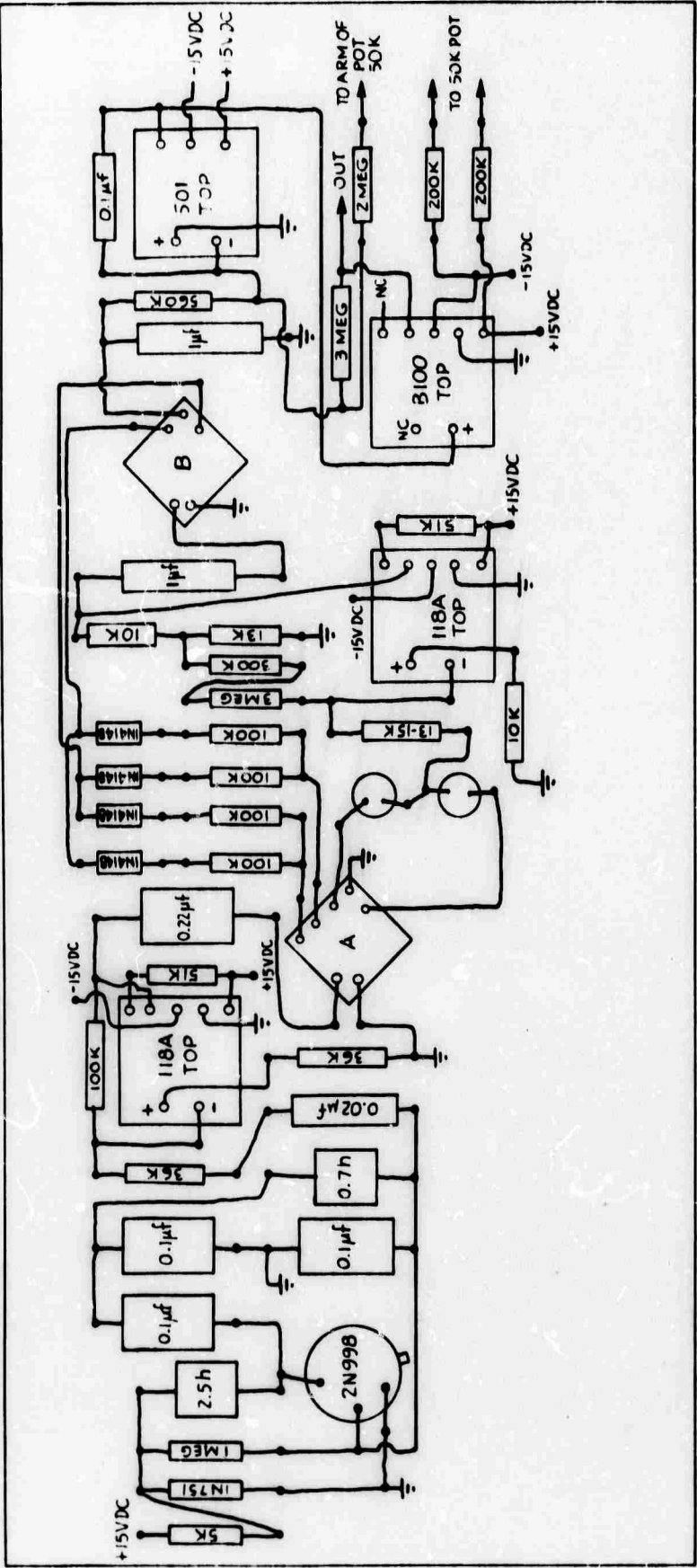


Fig. B. 7-15 Differential thermometer — layout.